



Title: Mathematical Modeling for Marine Crane Operations	Delivered:
	Availability:
Student: Christian Fagereng	Number of pages: 96

Description:

Mathematical models for marine vessel dynamics including environmental loads is frequently used in many applications. Extending these models to include propulsion machinery, deck machinery, large cranes or other equipment used for marine operations or in operation simulators it is important for efficient model development to have a clear understanding of how the interfaces have to be designed to facilitate connection of models. The bond graph representation or modeling methodology focuses on the model structure and properties required for connecting sub-models into large hybrid model and therefore may serve as a language for analysis of model structure in such a sense.

Keyword:

Bond Graph
Multibody dynamics

Advisor:

Eilif Pedersen

Assignment

The work description and scope of work for this master thesis has been the same as for the project work in marine machinery carried out in the fall semester 2010, ref. (Fagereng, 2010). Thus the assignment below is a direct quote of the assignment for the project work. The entire text can be viewed in appendix.

Work description

Mathematical models for marine vessel dynamics including environmental loads is frequently used in many applications. Extending these models to include propulsion machinery, deck machinery, large cranes or other equipment used for marine operations or in operation simulators it is important for efficient model development to have a clear understanding of how the interfaces have to be designed to facilitate connection of models. The bond graph representation or modeling methodology focuses on the model structure and properties required for connecting sub-models into large hybrid model and therefore may serve as a language for analysis of model structure in such a sense.

This representation has been used in the Energy Efficient - All Electric Ship project and in a PhD-thesis where a model library was developed. The work here is a continuation of these attempts and the objective is to increase the number and further develop the models in this library.

Scope of work:

1. Review the modeling and models of Marine Vessel Dynamics. Implement a simplified bond graph template model for a surface vessel for crane operations.
2. Review the modeling and models of large marine cranes for marine operations including typical heave compensation systems, the hydraulic winches and the control of this equipment. Discuss the structure or modular design of these hybrid models and suggest a method or implementation of these model into a modular component model library.
3. Combine the crane model developed and the vessel dynamic model into a complete model of a barge with a large crane for marine operations. Suggest a specific operation and demonstrate the capabilities of the developed model as a software simulator. For demonstration purposes include a Joy-stick for manned operation and develop a simplified animation displaying the motions of the barge and crane.

The report shall be written in English and edited as a research report including literature survey, description of mathematical models, description of control algorithms, simulations results, discussion and conclusion including a proposal for further work. Source code in Matlab/Simulink or equivalent shall be provided on a CD with code listing enclosed in appendix.

Abstract

As mathematical models for marine vessel dynamics are frequently used for several different purposes there is a need for finding ways of facilitating connection of sub models to extend these models to include various equipment of interest which affects the vessel dynamics. The bond graph modeling language is a natural platform for this since it can be used to describe several different disciplines or energy domains using the same basic system elements. Thus for example electrical systems affecting mechanical systems can easily be modeled and connected.

However the basic bond graph modeling concept has to be extended for use in multi-dimensional problems since standard procedures soon become difficult or impossible for larger systems. Using rigid body dynamics such systems can easily be created and incorporated with vessel dynamic equations. Rigid body bond graph can also be used to develop models of various other equipment. But when connecting several such systems together rigidly, causality problems will arise. The solution is to use the mathematical equivalent to a stiff spring in between the rigid bodies, thus the connection will not be entirely rigid.

In this thesis the development of such multi-dimensional bond graph has been research. A model for a simplified barge has been developed. It is clear that such models has great potential, but as with all other mathematical models of marine vessel dynamics accurate simulation results rely on accurate hydrodynamic coefficients which can be hard to derive.

Using the same procedure for multi-dimensional bond graph as for vessel modeling it is possible derive a model representing a pendulum. Which with some modification such as actuators represent a crane beam. Using three dimensional bond graph joints based on the concept of stiff springs to connect several such models a crane model is developed. The model is tested and it is found that the stiff springs in the connections may induce high vibrational natural frequencies which can affect simulation time. For such problems damping in the joint may be adopted.

The barge model and the crane model are interfaced using bond graph joints and it is shown that the movement of the crane indeed will induce forces on the barge as expected. This proves that 6DOF systems (six degrees of freedom) for several different mechanical component can be interfaced and facilitate the modeling of marine vessel dynamics and the connection of sub systems. Thus an efficient way of modeling such systems has been achieved.

To demonstrate the simulation result of the models developed in the thesis animations have been generated and is included in the attached CD.

Acknowledgments

This master thesis is the result of the studies in the spring semester 2011 at the Norwegian University of Science and Technology, Department of Marine Technology. The work represents the entire student work load this semester.

I would like to thank associate professor Eilif Pedersen for formulating the thesis and for guidance and support during this semester. I have found the task given challenging, hard and almost impossible at times. Yet surprisingly comprehensible as theory, models and model code finally came together and worked as intended. Thus proving that modeling really is an art best learned through experience.

The master thesis has been a continuation of a project work in marine machinery fall 2010 which accounted for $\frac{1}{4}$ of the work load last semester. The work description and scope of work has been similar for the two projects. Last semester suggestion for a vessel model and a two dimensional simplified crane was derived, the models where not functional as intended and the connection between them only briefly discussed. This semester the research done has been more thorough, the theory better understood and all models built up from the ground up to function in a three dimensional environment using new background material. The facilitation of the connection of the models has also been solved.

The original scope has been slightly narrowed down. Since modeling of hydraulic actuator where discussed in the previous assignment this has been omitted and only the connection of such models discussed. The demonstration of the complete model as a software simulator with joystick has also been omitted. This has been done in consultation with Eilif Pedersen.

Christian Fagereng

Trondheim, June 29, 2011

Contents

Assignment	i
Abstract	iii
Acknowledgments	v
Contents	vii
Table of figures	xi
Table of simulation plots	xiii
Table of tables	xv
1. Introduction.....	1
1.1 Problem and motivation.....	1
1.2 Organization of thesis.....	1
1.3 Literature	2
2. Mechanical Bond graph modeling.....	3
2.1 Bond graphs.....	3
2.2 Multibody dynamics	3
2.2.1 A basic procedure.....	4
2.2.2 Lagrange/Hamilton IC-field modeling	6
3. Rigid Body and multidimensional dynamics.....	11
3.1 Rigid body equations	11
3.2 The concept of rigid body position and rotation.....	15
3.2.1 Rotational matrixes	15
3.2.2 Euler Angles	18
3.2.3 Implementation in vector bond graphs.....	19
4 The crane model.....	21
4.1 Rigid body beam.....	21
4.2 Connection of rigid body bond graph models.....	23
4.2.1 Causality problem.....	23
4.2.2 Joints.....	24
Spherical joints	24
Revolute joints.....	25
Prismatic joints	26
4.3 Constructing a multi rigid body bond graph model	27
4.3.1 Rigid body beam with revolute joint and rotation around y-axis	27

4.3.2	Rigid body beam with spherical joint	31
4.3.3	Two link planar arm	34
4.4	The realistic crane beam	37
4.4.1	Control and actuators.....	37
4.4.2	Energy dissipation	40
4.4.3	Actuators and energy dissipation in the two link planar arm	41
4.5	Discussion of high vibrational natural frequencies	42
4.5.1	Simulation time and model behavior	42
4.5.2	Experimentation on damping in joint.....	48
5	Vessel model	53
5.1	Motion equation	53
5.2	Added mass and inertia.....	54
5.3	Hydrodynamic damping	55
5.4	Restoring forces.....	55
5.5	Implementation in general rigid body bond graph model	57
5.6	Simulation demonstration with rigid body vessel model.....	58
	Comment on vessel model	59
6	Barge with two link planar arm, a complete model	63
7	Conclusion and further work.....	67
7.1	conclusion.....	67
7.2	Crane model	67
7.3	Vessel model	67
7.4	The Crane Barge	68
7.5	Further work.....	68
	Bibliography.....	69
	Appendix A	71
	Contents of attached CD	71
	Appendix B	73
	20-sim code	73
	Lagrange/Hamilton IC-field	73
	Vector IC-field.....	74
	Transformer element	75
	Appendix C.....	77
	Added mass coefficients, DNV-RP-H103, April 2009.....	77

Appendix D 81
Project assignment fall 2010 81

Table of figures

Figure 1: Mass-spring example.....	4
Figure 2: Mass-spring 1-junctions	6
Figure 3: Mass-spring bond graph.....	6
Figure 4: Two link planar arm.....	8
Figure 5: Two variable IC-field.....	10
Figure 6: Two link planar arm bond graph	10
Figure 7: Rigid body in space	11
Figure 8: Vector IC-field.....	15
Figure 9: Rigid Body position and rotation	15
Figure 10: Euler angle XYZ transformation.....	19
Figure 11: Rigid Body bond graph	20
Figure 12: Beam with local coordinate system	21
Figure 13: Crane beam bond graph.....	22
Figure 14: Derivative causality	23
Figure 15: Complete causality	24
Figure 16: Spherical joint.....	24
Figure 17: Spherical joint bond graph	25
Figure 18: Revolute joint	25
Figure 19: Revolute Joint bond graph	26
Figure 20: Prismatic joint.....	26
Figure 21: Prismatic joint bond graph	27
Figure 22: Pendulum bond graph.....	28
Figure 23: Pendulum animation	30
Figure 24: Beam with spherical joint.....	31
Figure 25: Animation of beam with spherical joint and force in two directions.....	33
Figure 26: Two link planar arm bond graph	34
Figure 27: Animation two link planar arm.....	36
Figure 28: Actuators on crane beam	37
Figure 29: Joint actuator bond graph	38
Figure 30: Animation of joint actuator	38
Figure 31: Perpendicular actuator bond graph	39
Figure 32: Global actuator bond graph	39
Figure 33: Real actuator bond graph.....	40
Figure 34: Energy dissipation in joint bond graph.....	40
Figure 35: Energy dissipation in actuator bond graph	41
Figure 36: Two link planar arm with actuator and energy dissipation.....	41
Figure 37: Simulation time vs. beams connected	43
Figure 38: Simulation time vs. spring constant	47
Figure 39: Time step vs. spring constant	47
Figure 40: Two link planar arm with damping in joints.....	48
Figure 41: Simulation time vs. spring constant (damping in joint)	52
Figure 42: Vessel stability (Fossen, 1994).....	56

Figure 43: Vessel bond graph 57
Figure 44: Barge animation 61
Figure 45: Complete crane barge bond graph..... 63
Figure 46: Complete crane barge bond graph..... 64
Figure 47: Barge animation under influence of crane..... 65

Table of simulation plots

Simulation plot 1: : Pendulum, constrained end.....	29
Simulation plot 2: Pendulum, unconstrained end	29
Simulation plot 3: Beam with spherical joint, constrained end	31
Simulation plot 4: Beam with spherical joint, unconstrained end	32
Simulation plot 5: Beam with spherical joint and force in two directions, constained end	32
Simulation plot 6: Beam with spherical joint and force in two directions, unconstrained end	33
Simulation plot 7: Two link planar arm, arm one, constrained end.....	35
Simulation plot 8: Two link planar arm, arm one, unconstrained end	35
Simulation plot 9: Two link planar arm, arm two, constrained end.....	36
Simulation plot 10: High vibrational natural frequencies	42
Simulation plot 11: High vibrational natural frequencies zoomed in	42
Simulation plot 12: Two link planar arm and spring constant 10^4	44
Simulation plot 13: Two link planar arm and spring constant 10^5	44
Simulation plot 14: Two link planar arm and spring constant 10^6	45
Simulation plot 15: Two link planar arm and spring constant 10^7	45
Simulation plot 16: Two link planar arm and spring constant 10^8	46
Simulation plot 17: Two link planar arm and spring constant 10^9	46
Simulation plot 18: Two link planar arm and spring constant 10^4 and damping	49
Simulation plot 19: Two link planar arm and spring constant 10^5 and damping	49
Simulation plot 20: Two link planar arm and spring constant 10^6 and damping	50
Simulation plot 21: Two link planar arm and spring constant 10^7 and damping	50
Simulation plot 22: Two link planar arm and spring constant 10^8 and damping	51
Simulation plot 23: Two link planar arm and spring constant 10^9 and damping	51
Simulation plot 24: Barge motion	59
Simulation plot 25: Barge motion with torque and low hydrodynamic damping	60
Simulation plot 26: Barge motion with torque and high hydrodynamic damping	60
Simulation plot 27: Barge motion under influece of crane.....	64
Simulation plot 28: Barge motion under influece of crane and load	65

Table of tables

Table 1: Simulation data for increasing number of beams 43
Table 2: Simulation data for increasing spring constant 47
Table 3: Simulation data with damping in joint 51
Table 4: Vessel notation 54
Table 5: Vessel data 58

1. Introduction

1.1 Problem and motivation

The bond graph language is a powerful way of creating models over several different energy domains alone or in a combination. With the implementation of modern computer software as 20-sim the user has an efficient way of designing and analyzing the dynamic behavior of a bond graph system. However for large systems, which include several different sub systems, it is clear that one has to have some understanding on how to facilitate connection of models for efficient model development. As with most large problems the most efficient way of solving them is dividing the problem into several different sub problems. When it is time to solve the large overall problem all sub problems has to be developed in such a way that they can easily be interfaced together. This is especially true in mathematical models of marine vessel dynamics where a large number sub systems as deck machinery, cranes and other equipment is to be considered in the overall model.

The focus in this thesis has been to research and develop efficient ways of modeling marine crane operations using bond graphs. Such problems are complicated in that they have a large number of degrees of freedom and a large number of rigidly connected parts; both difficult to handle efficiently in mathematical problems. Often such systems may be modeled using equations and matrixes taken into account all the degrees of freedom of an overall system, as in (Nielsen, 2007) where the result is large matrix systems which do not facilitate implementation of other sub systems at a later stage. In basic bond graph modeling only a few degrees of freedom may compromise the ease of model development, however by combining rigid body dynamics and multi-dimensional power bonds a relatively easy and graphical neat solution for a 6DOF system (six degrees of freedom) presents itself. It turns out that also the rigid connection of several such models can be solved, thus opening up possibilities for efficiently creating systems with a large number of sub systems attached and a large overall number of degrees of freedom.

1.2 Organization of thesis

To demonstrate such modeling procedures and in line with the assignment basic models for marine vessels and cranes are developed in this report. First the classic ways of modeling multi-dimensional systems are presented and the problems with such procedures discussed and demonstrated. Then the theory behind rigid body dynamics and the implementation into easy graphical bond graphs will be introduced and a step by step process of modeling marine crane vessel follows. Presentations of simulations and animations results to confirm the feasibility of the models are done after each sub model development. Also presented are discussions on simulation time and the rigid connection between models. For some of the more complicated models interpreting the simulation results from simulation plots are almost impossible, and the reader is referred to the animations attached on CD.

The thesis can be interpreted as a continuation or as an academic exercise following the multibody chapters in both (Pedersen & Engja, 2008) and (Karnopp, Margolis, & Rosenberg, 2006) where rigid body dynamics are presented and the connection of these briefly discussed but not demonstrated. As one advantage of bond graph modeling using computers is the ability to produce mathematical models with a minimum usage of code the models developed in this thesis tries to follow this concept.

1.3 Literature

Material for rigid body bond graphs has mainly been taken from (Pedersen & Engja, 2008) and (Karnopp, Margolis, & Rosenberg, 2006). Additional inspiration and understanding of translation and rotation of rigid bodies has been found in (Sciavicco & Siciliano, 1999). Material for vessel dynamics has been found in (Fossen, 1994) with support from (Pedersen, Bond Graph Modelling of Marine Vehicle Dynamics). Material on bond graph joints has been found in (Filippini, Delarmelina, Pagano, Alianak, Junco, & Nigro, 2007) and in (Karnopp, Margolis, & Rosenberg, 2006). In addition inspiration has been found in (Zied & Chung, 1992), (Gilberto & Padilla, 2010), (Nielsen, 2007) and (Berg, 2007).

2. Mechanical Bond graph modeling

2.1 Bond graphs

In this thesis the tool for mathematical modeling of marine crane operation is the bond graph language or method. The bond graph method can be defined as *a unified conceptual and operational framework for the study of a very wide variety of system types and thus provides a general paradigm for modeling of dynamic systems based upon energy and power flow* (Pedersen & Engja, 2008).

It is assumed that the reader has some basic knowledge of the bond graph concept, still it may be useful to list the main advantages which makes this method so useful. As described in (Pedersen & Engja, 2008):

- The same symbolism is used to represent the power interaction in a large selection of physical systems.
- On a graphical form bond graphs display the energetic structure of complex systems with several energy domains in a way which is close to what we may call the physics of the system.
- A physical based sign convention can be shown directly on the graph, which is important when interpreting numerical results from simulations.
- The method is equally applicable for linear and non-linear systems.
- A unique feature of bond graphs is the display of causality on the graph. That is, it indicates which variable for an element is the independent variable or input and which variable is dependent or output variable.
- The bond graph method gives an algorithmic procedure for converting the graph into mathematical equations
- It can be directly entered and processed by a computer.

It follows that bond graphs combined with computer implementation is a very powerful tool for modeling and simulation of dynamic systems, especially for modeling of marine related topics where so many different engineering subjects are combined to make up a complete system. It be electrical, mechanical, hydraulic or even thermodynamic. In the next chapters the focus will be on researching and developing the mechanical side of large marine systems. The building blocks for larger mechanical 6DOF (six degrees of freedom) systems will be established as the modeling of such systems can be quite challenging using basic modeling procedures. The goal is to show how bond graphs can be used for modeling marine vessels coupled with different systems affecting the total dynamics.

2.2 Multibody dynamics

While there in general exists simple procedures to guide one through the modeling of systems in several different energy domains, some subjects needs further investigation and development to make them applicable to modeling of real world systems. Mechanical systems are one of them. The mechanical system often involves a large number of different parts moving relative to one another introducing several different efforts, flows, momentums and displacements.

This complicates the model, especially if the system operates in a 3D world where each velocity has a x , y and z component. We know that even small problems can experience differential causality and algebraic loops which can be solved fairly easy. However for large systems these methods are not practical and it is often better to avoid the problems in the first place. All in all both complexity and general bond graph modeling problems make the standard modeling approach to mechanical systems practically impossible to employ.

In the following chapter the concept of rigid body dynamics will be introduced. This concept enables the modeling of larger multidimensional mechanical systems with relative ease. First I will demonstrate a standard procedure for modeling multidimensional mechanics presented both in (Pedersen & Engja, 2008) and (Karnopp, Margolis, & Rosenberg, 2006). Then I will introduce the Lagrange/Hamilton IC-field modeling concept which offers a potential easier way of achieving mechanical models. Then I will introduce the general rigid body equations in 6DOF and show how these equations actually can be represented in a modified IC-field.

2.2.1 A basic procedure

For the general bond graph the aim is to create first order differential equations representing the dynamics of the system. Though it is possible to derive bond graphs for simple mechanical systems by inspection or using a basic system construction method, the modeling of more complex and realistic systems without a more thorough procedure soon becomes difficult. Skipping the some background equations and discussions a basic procedure for development of such mechanical bond graph systems follows. To illustrate the procedure it will be presented with a standard mass-spring example also presented in (Pedersen & Engja, 2008) and (Karnopp, Margolis, & Rosenberg, 2006). The example concerns a mass in one end of a pendulum suspended from a spring.

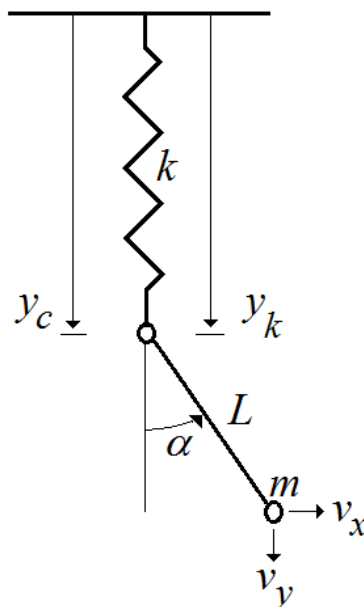


Figure 1: Mass-spring example

Start by defining a set of generalized variables and their derivatives:

$$\mathbf{q}_k = [y_k, \alpha]^T$$

$$\dot{\mathbf{q}}_k = [\dot{y}_k, \dot{\alpha}]^T.$$

\mathbf{q}_k is called the kinematic displacement vector or generalized coordinate vector. This is a vector preferable containing as few coordinate variables as possible to describe the position of the inertia elements.

Define potential energy variables, i.e. variables in the system that changes the potential energy. In this case the spring.

$$\mathbf{q}_c = [y_c - y_0]^T,$$

$$\dot{\mathbf{q}}_c = [\dot{y}_c]^T.$$

Define the inertia variables i.e. variables defining the movement of the inertia element.

$$\mathbf{q}_I = [x, y]^T = [L \sin \alpha, y + L \cos \alpha]^T,$$

$$\mathbf{v}_I = [\dot{x}, \dot{y}]^T.$$

The next step is to establish the transformation relationship between the generalized variables. For general \mathbf{q}_k and \mathbf{q}_c the relation is

$$\mathbf{q}_c = \phi_{Ck}(\mathbf{q}_k),$$

$$\dot{\mathbf{q}}_c = \frac{\partial \phi_{Ck}(\mathbf{q}_k)}{\partial \mathbf{q}_k} \dot{\mathbf{q}}_k = \mathbf{T}_{Ck}(\mathbf{q}_k) \dot{\mathbf{q}}_k,$$

and the i th relation is

$$\dot{q}_{Ci} = \sum_{j=1}^N \frac{\partial \phi_{Cki}}{\partial q_{kj}} \dot{q}_{kj}.$$

This gives the relation

$$y_c = (1)y_k + (0)\alpha,$$

$$\dot{y}_c = (1)\dot{y}_k + (0)\dot{\alpha},$$

and

$$\mathbf{T}_{Ck} = [1, 0].$$

A similar relation is established between \mathbf{q}_k , $\dot{\mathbf{q}}_k$ and \mathbf{v}_I . Now we define $\mathbf{v}_I = \dot{\mathbf{q}}_I$, which gives

$$\mathbf{v}_I = \dot{\mathbf{q}}_I = \frac{\partial \phi_{Ik}(\mathbf{q}_k)}{\partial \mathbf{q}_k} \dot{\mathbf{q}}_k = \mathbf{T}_{Ik}(\mathbf{q}_k) \dot{\mathbf{q}}_k,$$

and the i th relation

$$v_{Ii} = \sum_{j=1}^N \frac{\partial \phi_{Iki}}{\partial q_{kj}} \dot{q}_{kj}.$$

Which leads to

$$\dot{x} = (0)\dot{y}_k + (L \cos \alpha) \dot{\alpha},$$

$$\dot{y} = (1)\dot{y}_k + (-L \sin \alpha) \dot{\alpha},$$

and

$$\mathbf{T}_{Ik} = \begin{bmatrix} 0 & L \cos \alpha \\ 1 & -L \sin \alpha \end{bmatrix}.$$

Now that all the variables are stated and the relationships between them have been established, the bond graph can be drawn. Write down the 1-junctions corresponding to $\dot{\mathbf{q}}_C$, $\dot{\mathbf{q}}_k$ and \mathbf{v}_J .

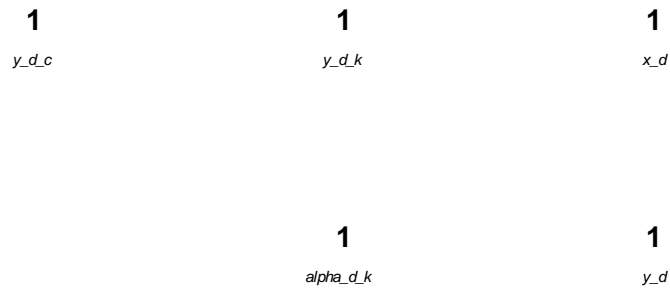


Figure 2: Mass-spring 1-junctions

We now write down the transformations using MTF- elements and 1-junctions. An R-element representing friction and an Se- element representing gravity is also added.

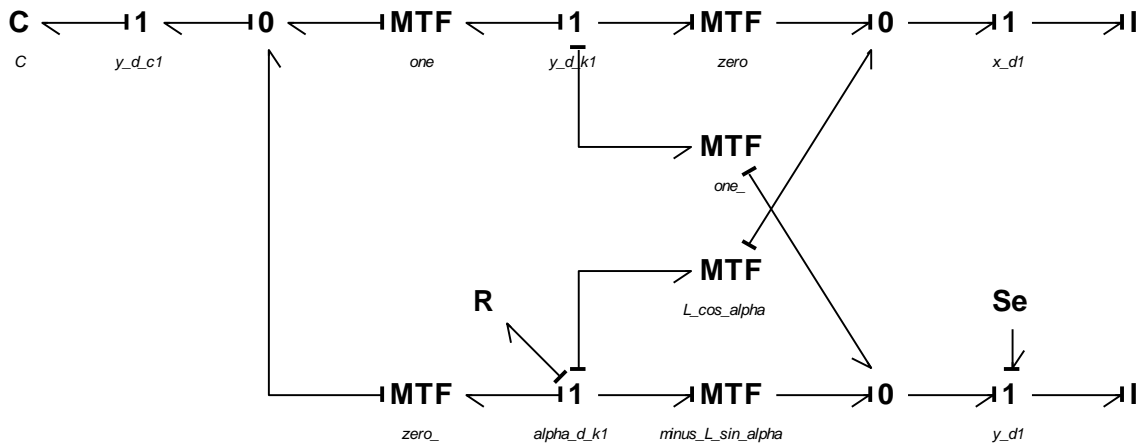


Figure 3: Mass-spring bond graph

This concludes the short walkthrough of the standard procedure.

2.2.2 Lagrange/Hamilton IC-field modeling

Though the procedure above works for solving multidimensional mechanical problems it offers no solution to algebraic loops and differential causality problems which will appear if the problems involve more than one rigidly connected inertia. It is left to the engineer to solve these in the traditional way.

An alternative is to use Lagrange formulation to generate the equations of motions for the coupled displacements in the system and then implementing these into the bond graph using an IC-field. Since the bond graph method actually is about generating equations of motions the Lagrange/Hamilton IC-field procedure can be interpreted as writing down the motion equations for the difficult part of the system, i.e. the part generating the causal problems, and then solving them with bond graphs.

As for the general method presented the Lagrange/Hamilton is based on a set of generalized coordinates defined in the system. The goal is to express the kinetic energy $T(\dot{q}_i, q_i)$ and the potential energy $V(q_i)$ of the system. These can be used to write the equation of motion using the Lagrange equation

$$\frac{d}{dt} \left(\frac{dT}{d\dot{q}_i} \right) - \left(\frac{dT}{dq_i} - \frac{dV}{dq_i} \right) = E_i \quad i = 1, 2, \dots, N.$$

Where q_i is the generalized coordinate, \dot{q}_i is the derivative and N is the number of generalized coordinates.

For implementation in bond graphs we define the generalized momentums as

$$p_i = \frac{dT}{d\dot{q}_i} \quad i = 1, 2, \dots, N.$$

When writing out the generalized momentums it will always take the following general form (matrix notation)

$$\mathbf{p} = \mathbf{M}(\mathbf{q}, \mathbf{t})\dot{\mathbf{q}} + \mathbf{a}(\mathbf{q}, \mathbf{t}).$$

Solving for $\dot{\mathbf{q}}$ gives the expression for the rate of change of generalized displacement.

$$\dot{\mathbf{q}} = \mathbf{M}^{-1}(\mathbf{q}, \mathbf{t})(\mathbf{p} - \mathbf{a}).$$

The $\mathbf{a}(\mathbf{q}, \mathbf{t})$ term is zero unless we have time varying velocity sources. We can rewrite the Lagrange equation with regard to the derivative of the momentum as

$$\frac{d}{dt} \left(\frac{dT}{d\dot{q}_i} \right) = \dot{p}_i = \frac{dT}{dq_i} - \frac{dV}{dq_i} + E_i \quad i = 1, 2, \dots, N.$$

Then define

$$e_i = \frac{dT}{dq_i} - \frac{dV}{dq_i},$$

and we get

$$\dot{p}_i = e_i + E_i.$$

Which in matrix form is written

$$\dot{\mathbf{p}} = \mathbf{e}(\dot{\mathbf{q}}, \mathbf{q}, \mathbf{t}) + \mathbf{F}.$$

Now observe that the rate of change of generalized momentum and displacement is the same quantities which we search for when writing state equations from bond graphs, i.e. we have found the state equations for the part of the system we wanted to avoid modeling with the standard approach.

For implementation in bond graphs we define the IC element with $2N$ ports. One power-in port $p\{i\}I$ corresponding to the generalized displacement and one power-out port $p\{i\}C$ corresponding to the generalized momentum. Causality is preferred to be flow out in the I -port and flow in on the C -port. The displacements rates are assigned in the IC-field to the *flow*. In the same way the momentum rate are assigned to the *effort*.

$$p\{i\}I.f = \dot{q}_i$$

$$p\{i\}C.e = e'_i$$

$$i = 1, 2, \dots, N.$$

As always theory and procedure are best illustrated with an example. The following example was originally solved for the project thesis written fall 2010, (Fagereng, 2010). Consider the two-link planar arm with center of mass in the geometrical center of each arm. The two arms rigidly connected results in differential causality when the standard modeling approach is used. We want to describe the motion of the systems with as few variables as possible and it is convenient to use the two angles between the ground and arm one, and between arm one and arm two.

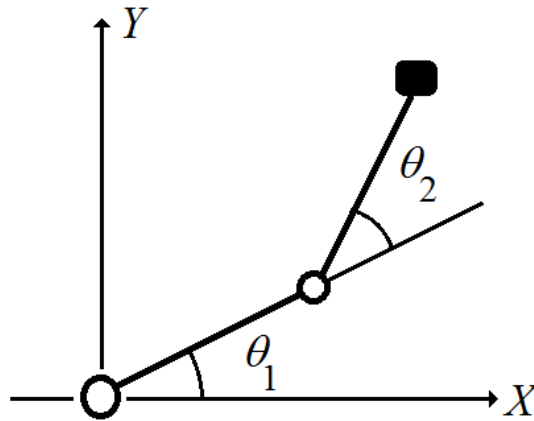


Figure 4: Two link planar arm

First we derive the expression for the kinetic and potential energy of the system with respect to $\dot{\theta}_1$ and $\dot{\theta}_2$ by inspection.

$$T = \frac{1}{2}I\dot{\theta}_1^2 + \frac{1}{2}I\dot{\theta}_2^2 + \frac{1}{2}m(\dot{x}_2^2 + \dot{y}_2^2)$$

$$V = mg\frac{l}{2}\sin\theta_1 + mg(l\sin\theta_1 + \frac{l}{2}\sin\theta_2)$$

Where

$$\dot{x}_2 = -l \sin\theta_1 \dot{\theta}_1 - \frac{l}{2} \sin\theta_2 \dot{\theta}_2 ,$$

$$\dot{y}_2 = l \cos\theta_1 \dot{\theta}_1 + \frac{l}{2} \cos\theta_2 \dot{\theta}_2 ,$$

$$\dot{I} = \frac{1}{3} ml^2 ,$$

$$I = \frac{1}{12} ml^2 .$$

We then differentiate the kinetic energy with respect to $\dot{\theta}_1$ and $\dot{\theta}_2$.

$$p_1 = \frac{dT}{d\dot{\theta}_1} = \frac{1}{3} l^2 [4m \dot{\theta}_1 - 3 \cos^2(\theta_1) m \dot{\theta}_1 - 3 \sin(\theta_1) \sin(\theta_2) \dot{\theta}_2 + 6 \cos^2(\theta_1) \dot{\theta}_1 + 3 \cos(\theta_1) \cos(\theta_2) \dot{\theta}_2]$$

$$p_2 = \frac{dT}{d\dot{\theta}_2} = \frac{1}{12} m l \dot{\theta}_2 - l^2 \sin(\theta_1) \sin(\theta_2) \dot{\theta}_1 + \frac{1}{2} \dot{\theta}_1 - \frac{1}{2} \dot{\theta}_2 \cos^2(\theta_2) + l^2 \cos(\theta_1) \cos(\theta_2) \dot{\theta}_1 + \frac{1}{2} l^2 \cos^2(\theta_2) \dot{\theta}_2$$

Then differentiate both kinetic- and potential- energy with respect to θ_1 and θ_2 .

$$\frac{dT}{d\theta_1} = -l^2 \dot{\theta}_1 [-m \sin(\theta_1) \cos(\theta_1) + \cos(\theta_1) \sin(\theta_2) \dot{\theta}_2 + 2 \cos(\theta_1) \dot{\theta}_1 \sin(\theta_1) + \sin(\theta_1) \cos(\theta_2) \dot{\theta}_2]$$

$$\frac{dT}{d\theta_2} = -\frac{1}{2} \dot{\theta}_2 [2l^2 \sin(\theta_1) \cos(\theta_2) \dot{\theta}_1 - \sin(\theta_1) \dot{\theta}_2 \cos(\theta_2) + 2l^2 \cos(\theta_1) \sin(\theta_2) \dot{\theta}_1 + l^2 \cos(\theta_2) \dot{\theta}_2 \sin(\theta_2)]$$

$$\frac{dV}{d\theta_1} = \frac{3}{2} mgl \cos(\theta_1)$$

$$\frac{dV}{d\theta_2} = \frac{1}{2} mgl \cos(\theta_2)$$

We can now generate the system matrixes.

$$\begin{bmatrix} p_{\theta_1} \\ p_{\theta_2} \end{bmatrix} = \begin{bmatrix} \frac{1}{3} l^2 [4m - 3 \cos^2(\theta_1) m + 6 \cos^2(\theta_1)] & \frac{1}{3} l^2 [-3 \sin(\theta_1) \sin(\theta_2) + 3 \cos(\theta_1) \cos(\theta_2)] \\ -l^2 \sin(\theta_1) \sin(\theta_2) + \frac{1}{2} + l^2 \cos(\theta_1) \cos(\theta_2) & \frac{1}{12} m l - \frac{1}{2} \cos^2(\theta_2) + \frac{1}{2} l^2 \cos^2(\theta_2) \end{bmatrix} \begin{bmatrix} \dot{\theta}_1 \\ \dot{\theta}_2 \end{bmatrix} + \begin{bmatrix} 0 \\ 0 \end{bmatrix}$$

Which gives

$$\begin{bmatrix} \dot{\theta}_1 \\ \dot{\theta}_2 \end{bmatrix} = \mathbf{M}^{-1} \begin{bmatrix} p_{\theta_1} \\ p_{\theta_2} \end{bmatrix}$$

and

$$\begin{bmatrix} \dot{p}_{\theta_1} \\ \dot{p}_{\theta_2} \end{bmatrix} = \begin{bmatrix} \frac{dT}{d\theta_1} - \frac{dV}{d\theta_1} \\ \frac{dT}{d\theta_2} - \frac{dV}{d\theta_2} \end{bmatrix} .$$

The system Lagrange/Hamilton equations can then be programmed in an IC field with two sets of in- and out- ports from two one-junctions representing each generalized coordinate. The IC-field code can be viewed in appendix.

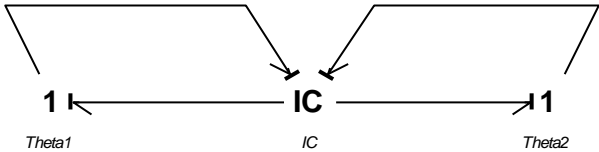


Figure 5: Two variable IC-field

In this case there are no external forces acting on the two arms. Though such forces can be written in to the IC-field, as stated by the above equations, such forces are much easier added to the bond graph at a later stage by simply adding them to the one-junctions. Example on such forces may be the actuators moving the two arms. The potential energy may also be added on a later stage. It is the I-field we want to get rid of, spring forces and resistance can simply be put on their respective one junction as C- and R- elements.

For completing the bond graph and finding the displacements of the crane tip, the IC-field can be used to generate the value of θ_1 and θ_2 . These values can then be sent to MTF-elements with power connections to the two one-junctions. The MTF-elements calculate the transformation modulus for the power with respect to θ_1 and θ_2 , giving the power in x- and y direction. The simple bond graph is presented in fig. 6.

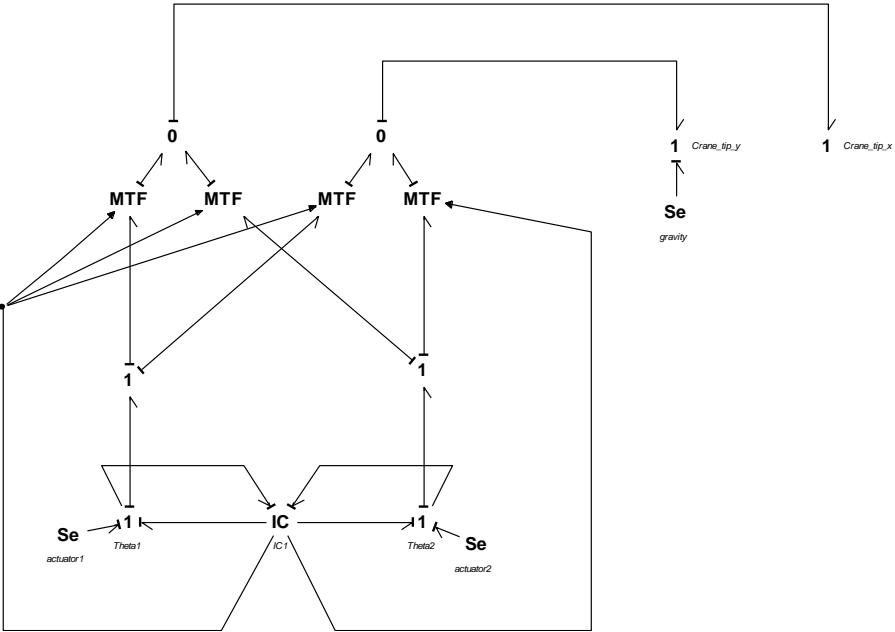


Figure 6: Two link planar arm bond graph

Though it may seem like an extensive procedure to carry out, the Lagrange/Hamilton equations can easily be derived with the help of symbolic mathematical computer software like Maple. The real challenge it to derive the correct expressions for kinetic and potential energy.

3. Rigid Body and multidimensional dynamics

This chapter is written on the basis of material presented (Pedersen & Engja, 2008), (Fossen, 1994) and (Sciavicco & Siciliano, 1999).

3.1 Rigid body equations

Consider an idealized body in space, i.e. a body with defined size where all non-linear effects such as deformation is neglected. This is called a rigid body, and has a special and important role in multidimensional dynamics and the bond graph modeling of such systems. The fact is that once a mechanical problem becomes multidimensional, with velocities in more than two degrees of freedom, the bond graph modeling of such systems becomes increasingly difficult in a way that compromises the simplicity and ease of use that the bond graph method is known for.

A rigid body in space is free to move around and thus have one absolute velocity \mathbf{v} and one absolute angular velocity $\boldsymbol{\omega}$. These velocities are denoted on a local coordinate system with origin \mathcal{O}' and axis x' , y' , and z' attached to the rigid body and are $\mathbf{v} = [u, v, w]^T$ and $\boldsymbol{\omega} = [\omega_x, \omega_y, \omega_z]^T$. Let another coordinate system x , y , and z with origin \mathcal{O} be a global coordinate system acting as a system of reference or observation. The trick is to use this system to describe the motion of the rigid body.

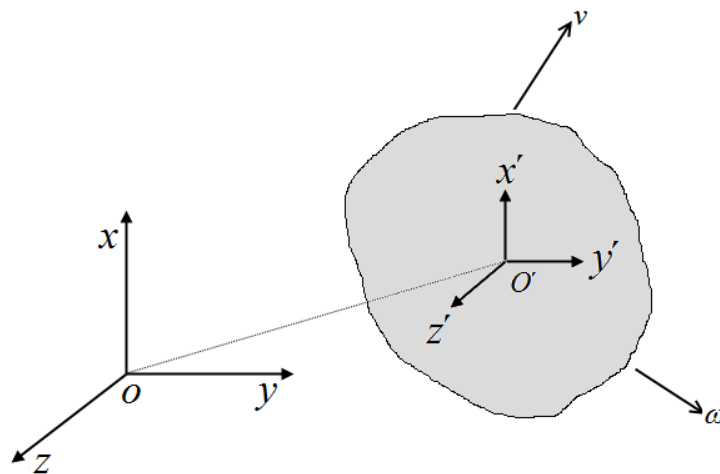


Figure 7: Rigid body in space

Now we want to develop the equation of motion for this rigid body and we start with the simple Newton law which states that net force \mathbf{F} action on a body induces a change of linear momentum.

$$\sum_{i=1}^n \mathbf{F}_i = \frac{d}{dt} \mathbf{p},$$

where

$$\mathbf{p} = m\mathbf{v}_0.$$

Expressing \mathbf{v} in with respect to the rotating frame i.e. putting the equations together

$$\sum_{i=1}^n \mathbf{F}_i = \left. \frac{\partial \mathbf{p}}{\partial t} \right|_{rel} + \boldsymbol{\omega} \times \mathbf{p} ,$$

where $\left. \frac{d\mathbf{p}}{dx} \right|_{rel}$ indicates the rate of change of momentum relative to the moving frame.

Same procedure can be applied to expressing that the net torque $\boldsymbol{\tau}$ acting on a body is the time rate of change of the angular momentum \mathbf{L} .

$$\sum_{i=1}^n \boldsymbol{\tau}_{o,i} = \frac{d}{dt} \mathbf{L}_o ,$$

where

$$\mathbf{L}_o = \mathbf{I} \boldsymbol{\omega} .$$

\mathbf{I} is the diagonal matrix of moment of inertias of the rigid body. Expressing $\boldsymbol{\omega}$ with respect to the rotating frame gives

$$\sum_{i=1}^n \boldsymbol{\tau}_{o,i} = \left. \frac{\partial \mathbf{L}_o}{\partial t} \right|_{rel} + \boldsymbol{\omega} \times \mathbf{L}_o .$$

Using the right hand rule it is possible to write down the component equations for the net force and torque.

$$F_x = m\dot{u} + m\omega_y w - m\omega_z v ,$$

$$F_y = m\dot{v} + m\omega_z u - m\omega_x w ,$$

$$F_z = m\dot{w} + m\omega_x v - m\omega_y u ,$$

$$\tau_x = I_x \dot{\omega}_x + \omega_y I_z \omega_z - \omega_z I_y \omega_y ,$$

$$\tau_y = I_y \dot{\omega}_y + \omega_z I_x \omega_x - \omega_x I_z \omega_z ,$$

$$\tau_z = I_z \dot{\omega}_z + \omega_x I_y \omega_y - \omega_y I_x \omega_x .$$

Now these equations are only valid if the if the origin of the local frame is the same point as the center of mass of the rigid body. However it is possible derive more general equations where the local origin can be positioned anywhere on the rigid body. By redefining the linear- and angular-momentum to include this we get

$$\mathbf{p} = m\mathbf{v}_c = m(\mathbf{v}_0 + \boldsymbol{\omega} \times \mathbf{r}_c) ,$$

$$\mathbf{L}_o = \{\mathbf{I}\} \boldsymbol{\omega} + \mathbf{r}_c \times \mathbf{p} .$$

Where $\mathbf{r}_c = [x_G \ y_G \ z_G]$ is the vector between the local origin and the center of mass and $\{\mathbf{I}\}$ is called the inertia tensor and is defined as

$$\{\mathbf{I}\} = \begin{bmatrix} I_{xx} & -I_{xy} & -I_{xz} \\ -I_{xy} & I_{yy} & -I_{yz} \\ -I_{xz} & -I_{yz} & I_{zz} \end{bmatrix},$$

and

$$\begin{aligned} I_{xx} &= \int_V \rho(y^2 + z^2) dV, & I_{xy} &= I_{yx} = \int_V \rho xy dV, \\ I_{yy} &= \int_V \rho(z^2 + x^2) dV, & I_{xz} &= I_{zx} = \int_V \rho xz dV, \\ I_{zz} &= \int_V \rho(x^2 + y^2) dV, & I_{yz} &= I_{zy} = \int_V \rho yz dV. \end{aligned}$$

Using the same Newton law as previous the equations for the system can be written in matrix form as

$$\mathbf{M}\dot{\mathbf{v}} + \mathbf{C}(\mathbf{v}, \mathbf{r}_c)\mathbf{v} = \boldsymbol{\tau},$$

which we recognize as an equation of motion. \mathbf{M} is the mass matrix

$$\mathbf{M} = \begin{bmatrix} m & 0 & 0 & 0 & mz_G & -my_G \\ 0 & m & 0 & -mz_G & 0 & mx_G \\ 0 & 0 & m & mx_G & -mx_G & 0 \\ 0 & -mz_G & my_G & I_{xx} & -I_{xy} & -I_{xz} \\ mz_G & 0 & -mx_G & -I_{yx} & I_{yy} & -I_{yz} \\ -my_G & mx_G & 0 & -I_{zx} & -I_{zy} & I_{zz} \end{bmatrix},$$

and $\mathbf{C}(\mathbf{v})$ is called the Coriolis-centrifugal matrix

$$\mathbf{C}(\mathbf{v}) = \begin{bmatrix} 0 & 0 & 0 & m(y_G\omega_y + z_G\omega_z) & -m(x_G\omega_y - w) & m(x_G\omega_z + v) \\ 0 & 0 & 0 & -m(y_G\omega_x + w) & m(z_G\omega_z + x_G\omega_x) & -m(y_G\omega_z - u) \\ 0 & 0 & 0 & -m(z_G\omega_x - v) & -m(z_G\omega_z + u) & m(x_G\omega_x + y_G\omega_y) \\ m(y_G\omega_y + z_G\omega_z) & -m(y_G\omega_x + w) & -m(z_G\omega_x - v) & 0 & -I_{yz}\omega_y - I_{xz}\omega_x - I_{zz}\omega_z & I_{yz}\omega_z + I_{xy}\omega_x - I_{zz}\omega_y \\ -m(x_G\omega_y - w) & m(z_G\omega_z + x_G\omega_x) & -m(z_G\omega_z + u) & I_{yz}\omega_y + I_{xz}\omega_x - I_{zz}\omega_z & 0 & -I_{xz}\omega_z - I_{xy}\omega_y + I_{xx}\omega_x \\ m(x_G\omega_z + v) & -m(y_G\omega_z - u) & m(x_G\omega_x + y_G\omega_y) & -I_{yz}\omega_z - I_{xy}\omega_x + I_{zz}\omega_y & I_{xz}\omega_z + I_{xy}\omega_y - I_{xx}\omega_x & 0 \end{bmatrix}$$

Note that \mathbf{v} in this case represents both the linear and rotational velocities,

$\mathbf{v} = [u, v, w, \omega_x, \omega_y, \omega_z]^T$, and $\boldsymbol{\tau}$ is a vector representing the external forces and moments,

$\boldsymbol{\tau} = [F_x, F_y, F_z, M_x, M_y, M_z]^T$.

We now have the general motion equation for a rigid body in 6DOF. The question now is how we can implement this in to bond graphs. It turns out that these equations can be derived from analyzing kinetic energy of a body in space and thus be implemented in a vector IC-field.

The kinetic energy of a body in space can be expressed like

$$T = \frac{1}{2} \iiint \rho (\mathbf{v} + \boldsymbol{\omega} \times \mathbf{r})^T (\mathbf{v} + \boldsymbol{\omega} \times \mathbf{r}) dV,$$

where again $\mathbf{v} = [u, v, w]^T$ and $\boldsymbol{\omega} = [\omega_x, \omega_y, \omega_z]^T$. The velocities are assumed to be the velocities of the local or moving reference frame origin and thus

$$\begin{aligned} T &= \frac{1}{2} m \mathbf{v}_o \cdot \mathbf{v}_o + \mathbf{v}_o \cdot \left(\boldsymbol{\omega} \times \int \rho \mathbf{r} dV \right) + \frac{1}{2} \int \rho (\boldsymbol{\omega} \times \mathbf{r}) \cdot (\boldsymbol{\omega} \times \mathbf{r}) dV \\ &= \frac{1}{2} m \mathbf{v}_o \cdot \mathbf{v}_o + \mathbf{v}_o \cdot (\boldsymbol{\omega} \times m \mathbf{r}_c) + \frac{1}{2} \boldsymbol{\omega}^T \{I\} \boldsymbol{\omega}. \end{aligned}$$

Now that we have the kinetic energy the motion equation can be written using quasi-Lagrange equations

$$\begin{aligned} \frac{d}{dt} \left(\frac{dT}{d\mathbf{v}} \right) + \boldsymbol{\omega} \times \frac{dT}{d\mathbf{v}} &= \boldsymbol{\tau}_v, \\ \frac{d}{dt} \left(\frac{dT}{d\boldsymbol{\omega}} \right) + \boldsymbol{\omega} \times \frac{dT}{d\boldsymbol{\omega}} + \mathbf{v} \times \frac{dT}{d\mathbf{v}} &= \boldsymbol{\tau}_\omega. \end{aligned}$$

From the Lagrange/Hamilton IC-field we know that we can write the equations for the generalized momentum using the Lagrange equation. Thus

$$\begin{aligned} P_v &= \frac{dT}{d\mathbf{v}}, \\ P_\omega &= \frac{dT}{d\boldsymbol{\omega}}. \end{aligned}$$

Writing the motion equation in momentum form

$$\begin{aligned} \frac{dP_v}{dt} + \boldsymbol{\omega} \times \frac{dT}{d\mathbf{v}} &= \boldsymbol{\tau}_v, \\ \frac{dP_\omega}{dt} + \boldsymbol{\omega} \times \frac{dT}{d\boldsymbol{\omega}} + \mathbf{v} \times \frac{dT}{d\mathbf{v}} &= \boldsymbol{\tau}_\omega, \end{aligned}$$

and using the fact that the generalized momentums always takes the same general form we get the equation for generalized momentum for a body in space.

$$\begin{aligned} \mathbf{P} &= \mathbf{M}(q, t) \mathbf{v} + \mathbf{a}(q, t), \\ \mathbf{v} &= [u, v, w, \omega_x, \omega_y, \omega_z]^T, \end{aligned}$$

which can be rewritten to get the rate of change of the generalized displacement

$$\dot{\mathbf{q}} = \mathbf{M}^{-1}(q, t) \mathbf{P}.$$

We recognize that this equation can be written into the previously derived IC-field approach where we in this case use the Coriolis-centrifugal matrix for the \mathbf{e}' term.

$$\mathbf{e}' = \mathbf{C}(\mathbf{v}, \mathbf{r}_c) \mathbf{v}.$$

Note that the potential energy has been neglected for now. However elements creating potential energy can easily be added to the IC-field bond graph at a later stage.

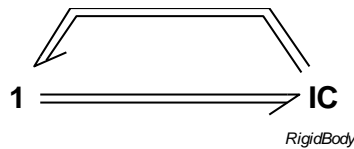


Figure 8: Vector IC-field

Using vector bond graphs the rigid body equations can be programmed in a IC field connected to only one one-junction representing the motion in 6DOF, i.e. each bond is carrying six different efforts and flows. The constitutive relation for the IC-field is

$$f = M^{-1}p,$$

$$e = C(\mathbf{v})\mathbf{v}.$$

3.2 The concept of rigid body position and rotation

Until now we have only discussed rigid body equations and how to implement them in to a bond graph system or IC-field. However the bond graph for a rigid body is still missing one key element. This is the relation between the local coordinate frame for the rigid body and the global coordinate frame from which all motion is observed. As for now the derived bond graph has little or no practical meaning.

3.2.1 Rotational matrixes

When deriving a complete description of the position of an object in space one generally needs the concept of relative distance and orientation. For example if you were to give a description of the book on your desk you might say that it lies at an angle to the left and down, and that it is lying upside-down. Such a description is given with your position and orientation as a reference. A person located on the other side of the room will give a different description. Hence position and orientation of an object is only valid in relation to a reference. The same concept applies when describing motion.

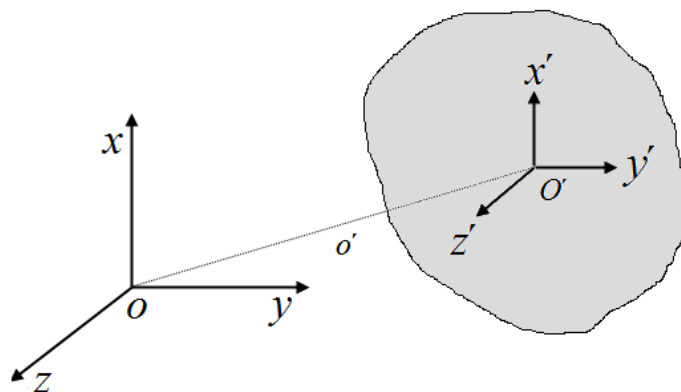


Figure 9: Rigid Body position and roation

The position and orientation of a rigid body in space can be described using two coordinate frames. One attached to the body called the body-fixed or local coordinate system, and one reference system called the earth-fixed coordinate system.

The position of the local frame is given by the vector o' between the two frame origins and with respect to the earth-fixed system. The vector o' can be expressed mathematically

$$o' = o'_x \mathbf{x} + o'_y \mathbf{y} + o'_z \mathbf{z}.$$

Where \mathbf{x} , \mathbf{y} and \mathbf{z} are the unit vectors of the global frame. In compact form the vector can be written

$$o' = \begin{bmatrix} o'_x \\ o'_y \\ o'_z \end{bmatrix}.$$

Let x' , y' and z' be the unit vector of the local coordinate frame of the body. Then the orientation of the local frame in relation to the global frame can be denoted

$$x' = x'_x \mathbf{x} + x'_y \mathbf{y} + x'_z \mathbf{z}$$

$$y' = y'_x \mathbf{x} + y'_y \mathbf{y} + y'_z \mathbf{z}$$

$$z' = z'_x \mathbf{x} + z'_y \mathbf{y} + z'_z \mathbf{z}$$

This can conveniently be written in compact form as a rotation matrix that is valid anywhere in the global system

$$R = [x' \quad y' \quad z'] = \begin{bmatrix} x'_x & y'_x & z'_x \\ x'_y & y'_y & z'_y \\ x'_z & y'_z & z'_z \end{bmatrix} = \begin{bmatrix} x'^T x & y'^T x & z'^T x \\ x'^T y & y'^T y & z'^T y \\ x'^T z & y'^T z & z'^T z \end{bmatrix}$$

For now forget the rotation of the body fixed frame and only concentrate rotation of the earth fixed system, i.e. rotation around global origin. Consider a rotation of the global frame around its own origin. The rotation results in a new frame which origin coincides with the global. The rotation rules apply here to. Consider a rotation α of the frame in positive direction (right hand rule) about the z axis. The unit vectors of the new frame with respect to the reference frame are

$$x' = \begin{bmatrix} \cos \alpha \\ \sin \alpha \\ 0 \end{bmatrix} \quad y' = \begin{bmatrix} -\sin \alpha \\ \cos \alpha \\ 0 \end{bmatrix} \quad z' = \begin{bmatrix} 0 \\ 0 \\ 1 \end{bmatrix}.$$

Applying compact notation we get the rotation matrix as described earlier

$$R_z(\alpha) = \begin{bmatrix} \cos \alpha & -\sin \alpha & 0 \\ \sin \alpha & \cos \alpha & 0 \\ 0 & 0 & 1 \end{bmatrix}.$$

We get similar results for a rotation β about y -axis and γ about x -axis.

$$R_y(\beta) = \begin{bmatrix} \cos \beta & 0 & \sin \beta \\ 0 & 1 & 0 \\ -\sin \beta & 0 & \cos \beta \end{bmatrix}.$$

$$R_x(\gamma) = \begin{bmatrix} 1 & 0 & 0 \\ 0 & \cos \gamma & -\sin \gamma \\ 0 & \sin \gamma & \cos \gamma \end{bmatrix}.$$

These are called elementary rotations. The rotation matrix concept has some valuable properties. The R matrix is orthogonal giving

$$R^T R = I, \quad R^T = R^{-1},$$

where I is the 3x3 identity matrix.

If we consider a case where the origin of a local frame coincides with the origin of the global frame, then a point P in space can be described by the global frame as

$$p = \begin{bmatrix} p_x \\ p_y \\ p_z \end{bmatrix}.$$

The same point P can be described by the local frame as

$$p' = \begin{bmatrix} p'_x \\ p'_y \\ p'_z \end{bmatrix}.$$

This gives that

$$p = p'_x \mathbf{x}' + p'_y \mathbf{y}' + p'_z \mathbf{z}' = [x' \quad y' \quad z'] p'.$$

Thus we get

$$p = R p', \quad p' = R^T p.$$

Where both p and p' is a representation of the same point in space. The rotation matrix can also be used to describe the rotation of a vector about an arbitrary axis in space i.e. using the same relations as just stated. This gives us some useful results.

Remembering the velocity vector from the rigid body chapter denoted

$$\mathbf{v} = [u, v, w]^T.$$

Assuming this is the velocity of the local frame moving in space the velocity in relation to the global frame here denoted \mathbf{v}' is

$$\mathbf{v}' = R \mathbf{v}.$$

Integrate with respect to time and we get the position of the local frame in relation to the global.

Remembering the rotational velocity vector from the rigid body chapter denoted

$$\boldsymbol{\omega} = [\omega_x, \omega_y, \omega_z]^T.$$

Assuming this is the velocity of the local frame rotating in space the rotation velocity in relation to the global frame here denoted $\boldsymbol{\omega}'$ is

$$\boldsymbol{\omega}' = R \boldsymbol{\omega}.$$

Integrate with respect to time and we get the orientation of the local frame in relation to the global.

I.e given a rotation of a local frame about the global the rotation matrix describes the new position of the local frame in relation to the global. Given a rotation of a local frame about its own origin and the rotation matrix describes the new orientation of the local frame in relation to the global.

It turns out that given several rotations of a local frame the new orientation or position can be described by multiplying several rotation matrixes together, one for each rotation. Consider a vector p going through two rotations. Denote p^0 as the initial condition, p^1 is the vector after one rotation and p^2 after two rotations. We denote the rotation matrixes as R_1^0 describing the first rotation and R_2^1 describing the second rotation. Then

$$p^0 = R_1^0 R_2^1 p^2$$

This means that by composing elementary rotations given earlier in this chapter we can completely describe the position and orientation of a rigid body in space. In fact using only three elementary rotations given that no successive rotations are made about parallel axis will be enough. The sequence of orientation matrixes is however not to be taken arbitrary i.e.

$$p^0 \neq R_2^1 R_1^0 p^2$$

3.2.2 Euler Angles

When generating a set of rotation matrixes for describing position and orientation of a body in space there are several sets of three successive rotations possible. In fact there are 12 of them, ref.(Sciavicco & Siciliano, 1999). One of the most common ones and the one we are going to use here is the XYZ convention.

- First rotate the reference frame by the angle ψ about the z axis (yaw). The rotation is described by the elementary rotation matrix R_z .
- Then rotate the reference frame by the angle θ about the new y axis (roll). The rotation is described by the elementary rotation matrix R_y .
- Finally rotate the reference frame by the angle ϕ about the new x axis (pitch). The rotation is described by the elementary rotation matrix R_x .

Thus the complete rotation

$$R_{tot} = R_{z,\psi} R_{y,\theta} R_{x,\phi} .$$

However this is not useful if we do not know the values of the Euler angles. The relation between the body-fixed rotational velocities and the rate of change of the Euler angles gives the solution.

$$\omega_x = \dot{\phi} - \dot{\psi} \sin(\theta),$$

$$\omega_y = \dot{\theta} \cos(\phi) + \dot{\psi} \cos(\theta) \sin(\phi),$$

$$\omega_z = -\dot{\theta} \sin(\phi) + \dot{\psi} \cos(\theta) \cos(\phi).$$

Solving these equations with respect to the Euler angles we get

$$\dot{\theta} = \cos(\phi) \omega_y - \sin(\phi) \omega_z ,$$

$$\dot{\psi} = \frac{\sin(\phi)}{\cos(\theta)} \omega_y + \frac{\sin(\phi)}{\cos(\theta)} \omega_z$$

and finally

$$\dot{\phi} = \omega_x + \sin(\phi) \tan(\theta) \omega_y + \cos(\phi) \tan(\theta) \omega_z .$$

3.2.3 Implementation in vector bond graphs

We have now derived the necessary equations needed to evaluate the position and orientation of our rigid body bond graph system in 6DOF. In such a system, using vector bond graphs, we have the flows equal to $\mathbf{v} = [u, v, w, \omega_x, \omega_y, \omega_z]^T$ flowing in one direction and the efforts equal to $\boldsymbol{\tau} = [F_x, F_y, F_z, M_x, M_y, M_z]^T$ flowing in the other direction. Using our causality knowledge with the orthogonal property of the rotation matrix we get that

$$\begin{bmatrix} \omega_x \\ \omega_y \\ \omega_z \end{bmatrix}_{(global)} = R_{tot} \begin{bmatrix} \omega_x \\ \omega_y \\ \omega_z \end{bmatrix}_{(local)} ,$$

$$\begin{bmatrix} u \\ v \\ w \end{bmatrix}_{(global)} = R_{tot} \begin{bmatrix} u \\ v \\ w \end{bmatrix}_{(local)} ,$$

$$\begin{bmatrix} F_x \\ F_y \\ F_z \end{bmatrix}_{(global)} = R_{tot}^T \begin{bmatrix} F_x \\ F_y \\ F_z \end{bmatrix}_{(local)} ,$$

$$\begin{bmatrix} M_x \\ M_y \\ M_z \end{bmatrix}_{(global)} = R_{tot}^T \begin{bmatrix} M_x \\ M_y \\ M_z \end{bmatrix}_{(local)} .$$

Using these relations we can implement these transformations in MTF-elements. There are several ways of doing this, but one weary easy-to-understand way is to use one MTF-element for each sub transformation (i.e. $R_{z,\psi}$, $R_{y,\theta}$ and $R_{x,\phi}$) connected in the correct successive order.

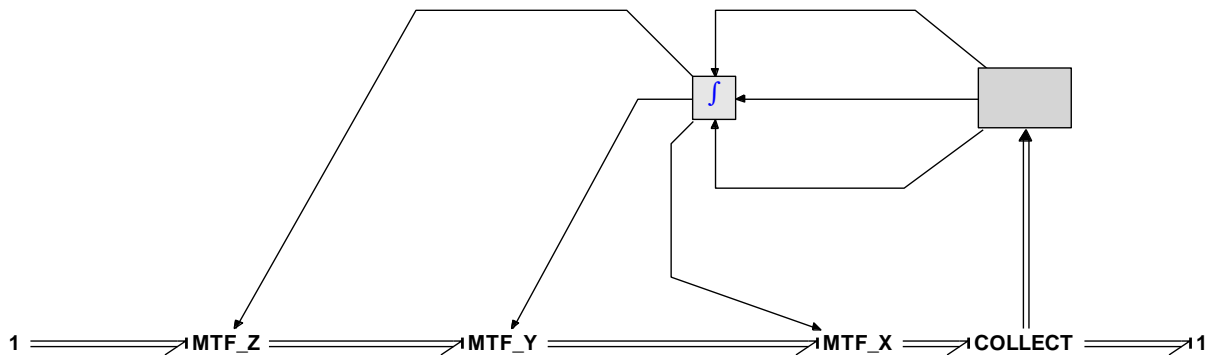


Figure 10: Euler angle XYZ transformation

Here the collect element collects the rotational velocities and sends them to a box containing the rate-of-change Euler angles. The solved rate-of-change Euler angles are then integrated to obtain the angles and send to their respective transformation element.

Since the vector power bonds have six flows and efforts (translation and rotation) we extend the matrixes in the MTF-elements to account for this. Thus the transformation modulus in the MTF_Z element will look like

$$m_{z,\psi} = \begin{bmatrix} \cos(\psi) & -\sin(\psi) & 0 & 0 & 0 & 0 \\ \sin(\psi) & \cos(\psi) & 0 & 0 & 0 & 0 \\ 0 & 0 & 1 & 0 & 0 & 0 \\ 0 & 0 & 0 & \cos(\psi) & -\sin(\psi) & 0 \\ 0 & 0 & 0 & \sin(\psi) & \cos(\psi) & 0 \\ 0 & 0 & 0 & 0 & 0 & 1 \end{bmatrix}$$

and similar for the other transformation modulus.

We now have the relation between the local and global coordinates our system. Thus we can describe motion and forces in our rigid body system by connecting the whole transformation element to our IC-field model. Here all the transformations are collected in one sub-model called MTF_to_global.

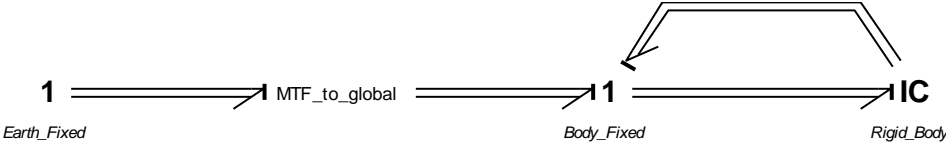


Figure 11: Rigid Body bond graph

Fig.11 represents the general rigid body bond graph for motion in six degrees of freedom. This model can easily be extended a later stage to include different physical phenomena unique to the respective system being modeled. Examples on this will be demonstrated in the next chapters.

4 The crane model

4.1 Rigid body beam

The basic simple light load crane consists of two crane arms or beams connected together. Neglecting deformation and bending each beam can be considered a rigid body. The goal is to build a model where for each step in time the location of the crane tip is known. This implies knowing the location of each end of the crane arms and the forces and momentums acting in these locations. Consider the general rigid body bond graph model where the coordinate transformation enables us to locate the position of the rigid body and the forces acting in the chosen center of gravity. Using bond graph transformer elements it is possible to transform the forces acting in the center of gravity out to the rigid end of the crane beam.

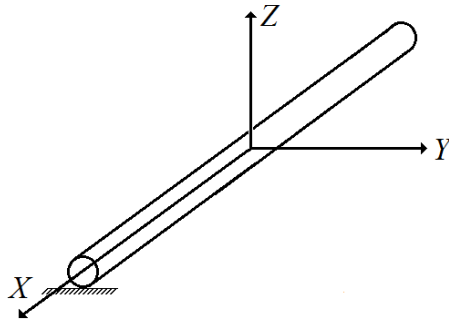


Figure 12: Beam with local coordinate system

A transformation matrix for the efforts and flows can be derived by inspection. Picture a beam where one end is constrained in x-, y- and z- direction but allowed to rotate around one global axis. Then a translational velocity in the opposite end, perpendicular to the beam, will create a rotational velocity proportional to the beam length. Also any initial rotational velocities will be the same throughout the beam length. Defining the local coordinate system as in the figure, the transformation matrix for effort and flow in the local origin to the beam end can be written

$$m = \begin{bmatrix} 1 & 0 & 0 & 0 & Z_g & -Y_g \\ 0 & 1 & 0 & -Z_g & 0 & X_g \\ 0 & 0 & 1 & Y_g & -X_g & 0 \\ 0 & 0 & 0 & 1 & 0 & 0 \\ 0 & 0 & 0 & 0 & 1 & 0 \\ 0 & 0 & 0 & 0 & 0 & 1 \end{bmatrix},$$

Where $[X_g, Y_g, Z_g]$ is the local coordinates of the point of interest. I.e. the end coordinate of the beam in the figure would be $[L/2, 0, 0]$ where L is the total length.

For example positive effort in the x- direction gives

$$\begin{aligned} e_{origin}[1] &= e_{beam_end}[1] + Z_g e_{beam_end}[5] - Y_g e_{beam_end}[6] \\ &= e_{beam_end}[1] + 0 \cdot e_{beam_end}[5] - 0 \cdot e_{beam_end}[6] = e_{beam_end}[1]. \end{aligned}$$

And positive effort in y- direction gives

$$e_{origin}[2] = e_{beam_end}[2] - Z_g e_{beam_end}[4] + X_g e_{beam_end}[6]$$

$$= e_{beam_end}[2] - 0 \cdot e_{beam_end}[4] + \left(\frac{L}{2}\right) e_{beam_end}[6] = e_{beam_end}[2] + \left(\frac{L}{2}\right) e_{beam_end}[6].$$

Using the general rigid body bond graph we want to translate the center fixed effort and flows to each end of the crane beam.

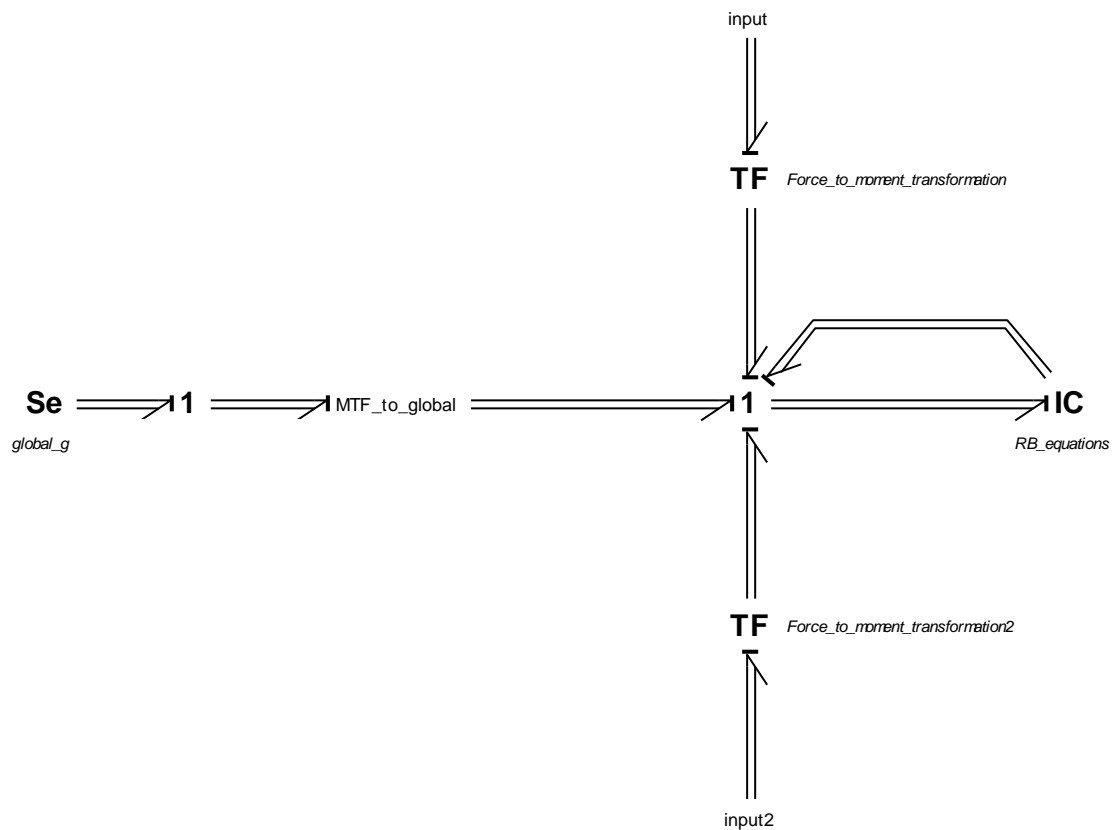


Figure 13: Crane beam bond graph

Noticing the causality for the TF- element (effort flowing with power input to local 1-junction) the constitutive relation is

$$e_2 = m^T e_1,$$

$$f_1 = m f_2.$$

Here the ports “input” and “input2” represents the connection to the next bond graph element. We recognize the Se-element connected to the MTF-element as the gravity forces acting on the body.

4.2 Connection of rigid body bond graph models

4.2.1 Causality problem

In the start of this thesis general procedures for development of mechanical bond graph where discussed. It was found that such procedures where not sufficient when dealing with large multidimensional systems. Increasing complexity of the mechanical system made the procedures time consuming and the kinematic relationships increasingly complex. Such systems are also constantly experiencing derivative causality problems which can be practical impossible to solve. The Lagrange/Hamilton IC-field modeling procedure was introduced considerable simplifying the system modeling and elimination causal problems. It proved possible to use the IC-field formulation for general rigid body bond graph modeling.

The question is now how to connect different rigid body bond graph models. Just as for simpler mechanical systems the connecting two rigid bodies together will result in derivative causality problems.

In three dimensions, a rigid body has six degrees of freedom represented by six inertial elements. When two bodies are connected rigidly, the tree linear and three angular velocities for the two bodies cannot all be independent, meaning that not all the I-elements can have integral causality, ref (Karnopp, Margolis, & Rosenberg, 2006).

In an IC-field all six inertia element are represented in one element, however the same principle applies here. Try to connect two IC-fields together and derivative causality appear.

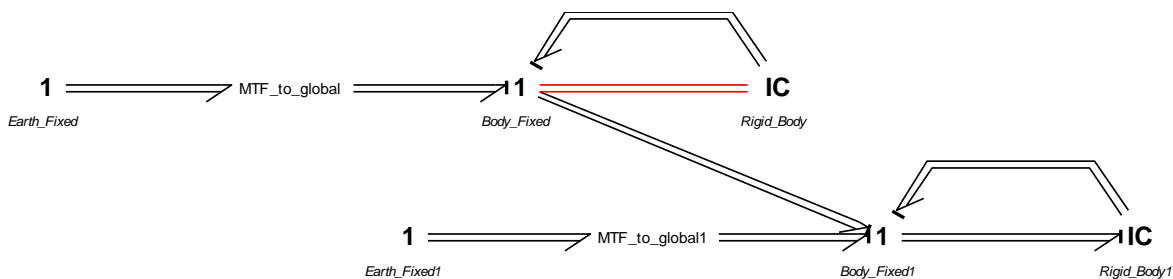


Figure 14: Derivative causality

One solution is to implement all rigid body equations in to one IC-field. However the size of the rigid body matrixes and the vector power bonds are proportional to the total degrees of freedom in the system, i.e. a two rigid body system will give 12x12 matrixes and 12 vector power bonds. A three body system 18x18 matrixes and 18 vector power bonds and so on. Such a solution would make the rigid body bond graph less intuitive to work with, complicate the connection of other elements and complicate the process of getting the desired values. We want to make a model which to a certain degree is graphical and intuitive, i.e. finding a solution for connecting different rigid body bond graphs together with ease. Thus large mechanical systems models can be derived from a library of rigid body bond graph models. Since we know that the source of derivative causality in such elements is the rigid connection, the clue for developing models is to construct flexible connections.

Imagine two rigid bodies connected with an infinite small spring. Thus the gap δ between the two rigid bodies is close to zero ($\delta \approx 0$) in equilibrium state. Whenever forces acting on the two bodies tries to pull them apart, a proportional large spring force will resist separation provided a large enough spring constant. Such imaginary springs can be modeled in every degree of freedom between the two bodies, creating a connection which will dynamically behave close to a rigid connection. Modeling in bond graphs using a 6 DOF C-element eliminates the derivative causality. Note that the C-element automatically gives effort input on power bonds to both rigid body bond graphs.

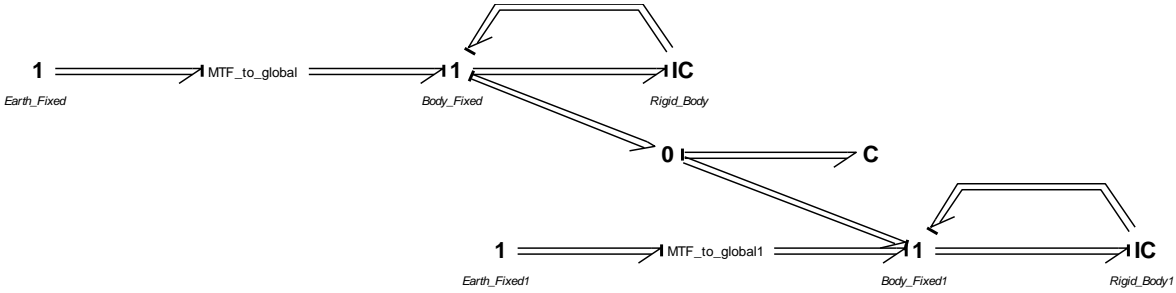


Figure 15: Complete causality

4.2.2 Joints

The models in the next part chapter are derived by inspiration from (Filippini, Delarmelina, Pagano, Alianak, Junco, & Nigro, 2007).

Such spring connections are the basis for the modeling of joints. Joints are couplings allowing freedom to move in some of the directions in a 6 DOF system, making it possible for two bodies to move relative to one another. Such a joints can be found in the typical two link planar arm where arm one needs to rotate around a point to the fixed ground and the other arm needs to rotate around the first arm. There are three basic representations of joints; spherical, revolute and prismatic. They all are modeled after the same principle; spring elements restricting movement in some directions and coordinate transformation for translation of the effort and flow in the desired direction. Using joint modeling theory it is possible to connect the rigid body bond graphs for the vessel and crane beams to get a complete model.

Spherical joints

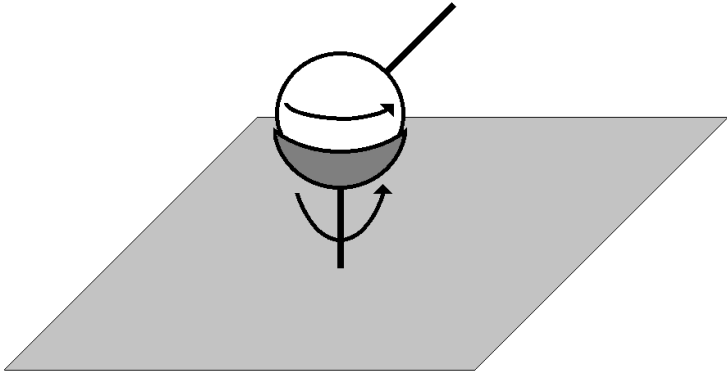


Figure 16: Spherical joint

The spherical joint allows for rotation around all three axes while translation is prohibited making the attached body free to rotate around while connected to ground or another body.

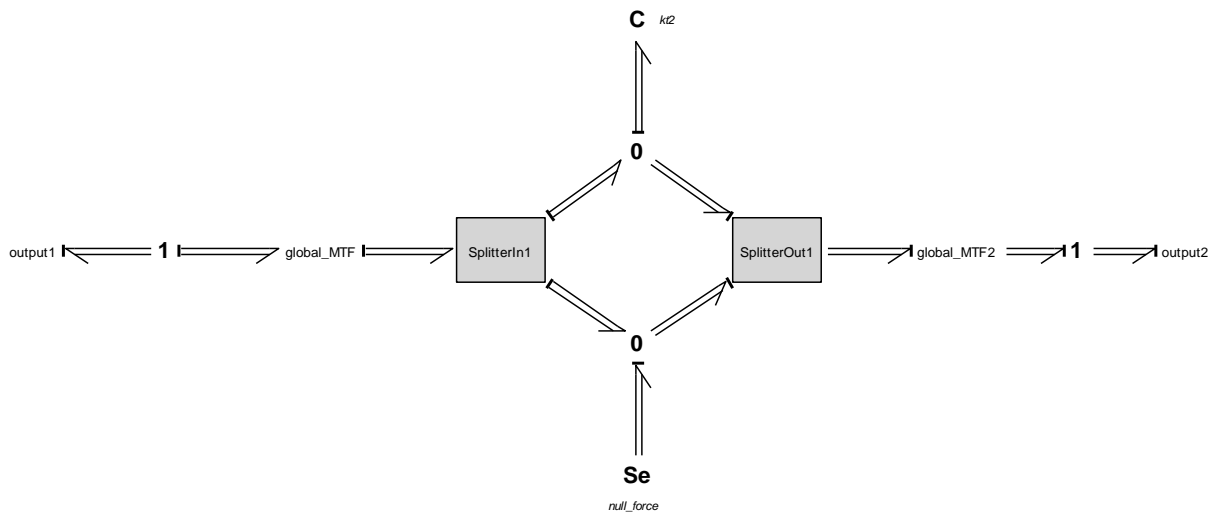


Figure 17: Spherical joint bond graph

Shown in fig. 17 is the sub model called “splitterinn”. The sub model separates the angular and linear effort and flows in the 6ODF input power bond and sends out two power bonds, the top one representing the linear velocities and the bottom one the angular velocities. The linear velocities are then constrained with a C-element with a sufficient high spring constant to resemble $\delta \approx 0$. The Se-element attached to the angular velocities, which are unconstrained, is a zero-torque element meaning the effort value is set to zero representing total freedom to rotate. The “splitterout” sub model collects the angular and linear velocities to one power bond. In each end there is a coordinate transformation sub model. This element is similar to the one used when transforming between global and local coordinates but tuned to only account for the transformations needed in this particular case. These are transformation of linear velocities and forces. However in practice the total local-to-global transformation derived earlier will produce the same results, with some superfluous transformations.

Revolute joints

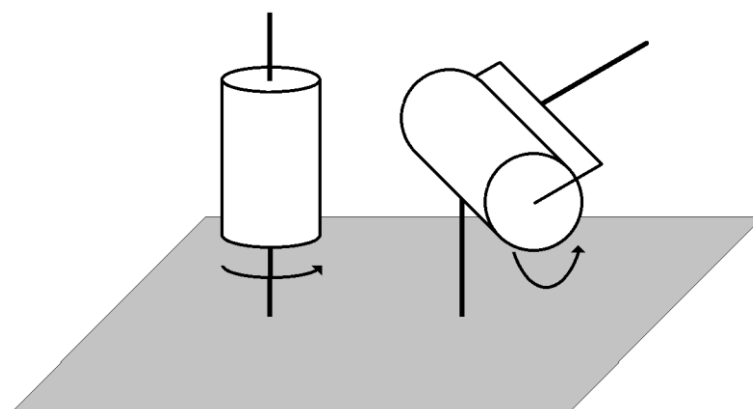


Figure 18: Revolute joint

The revolute joint is similar to the spherical joint but only allows rotation in one angular direction, meaning that the other two is constrained in addition to the translational degrees of freedom.

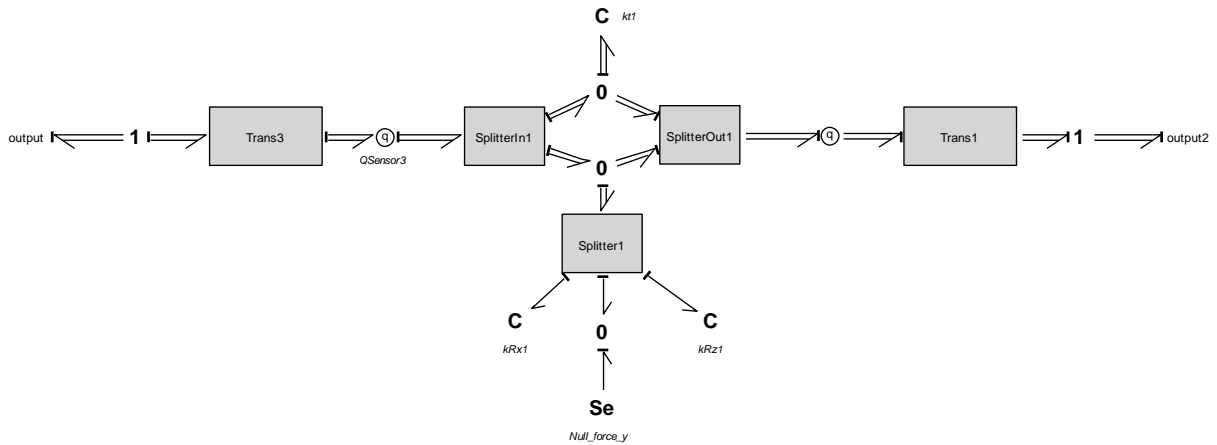


Figure 19: Revolute Joint bond graph

Here this is done by splitting up the rotational degrees of freedom and constraining two of them. The unconstrained power bond has zero effort source imposing no torque.

Prismatic joints

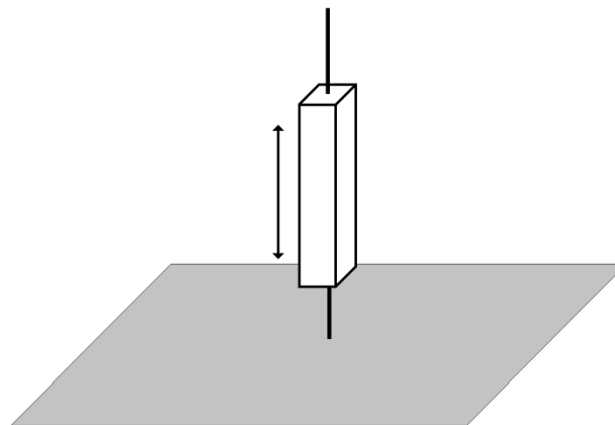


Figure 20: Prismatic joint

A prismatic joint allows for translation in one direction while the other two translational freedoms as well as all three rotational are constrained. Such joints can be used to model elongation of crane beams. Thus an actuator imposing force in the unconstrained direction can be added instead of the zero effort source for control of the extension.

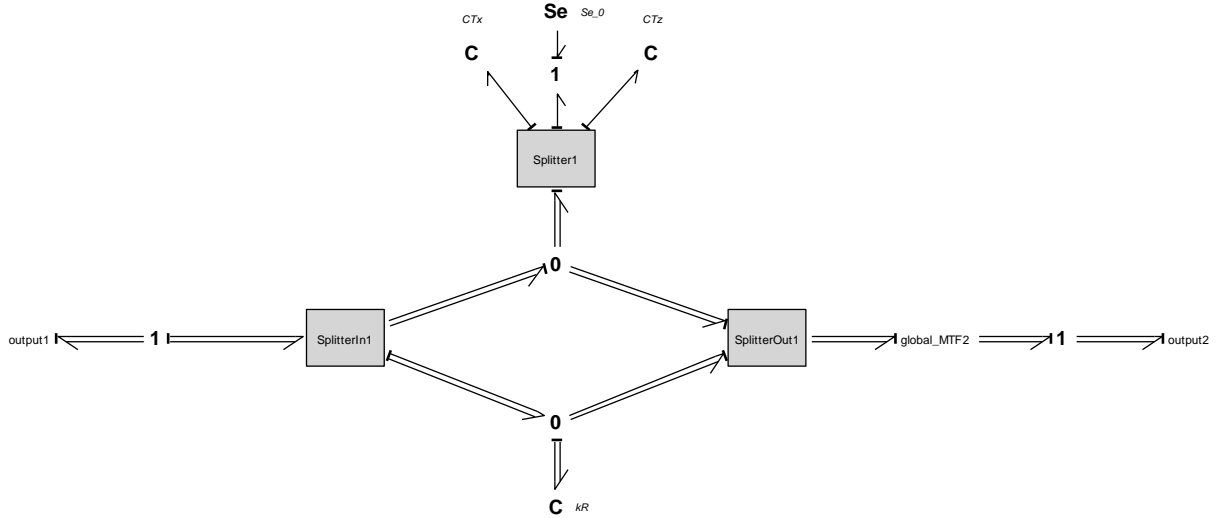


Figure 21: Prismatic joint bond graph

4.3 Constructing a multi rigid body bond graph model

In the previous chapters the basis for rigid body models and the connection of these has been developed. Here the connection between these models will be demonstrated and discussed using different modeling cases. The end goal is a model basis for a marine crane operation. But such a model procedure also opens up for forming models with a large number of rigid body components. However it will be shown that such models also has disadvantages.

4.3.1 Rigid body beam with revolute joint and rotation around y-axis

In this case the rigid body has been coupled with the revolute joint, se “One Arm Revolute Y” on attached CD. The rigid body is programmed with the general rigid body equations with the center of the local coordinate frame located in the center of mass, i.e. the product of the inertias is zero which simplifies the matrixes in the dynamic equation

$$\mathbf{M}\dot{\mathbf{v}} + \mathbf{C}(\mathbf{v})\mathbf{v} = \boldsymbol{\tau}.$$

In short all lines in the equation containing a term from the \mathbf{r}_c vector goes to zero as $\mathbf{r}_c = [x_G, y_G, z_G] = [0, 0, 0]$. Thus the mass matrix simplifies to

$$\mathbf{M} = \begin{bmatrix} m & 0 & 0 & 0 & 0 & 0 \\ 0 & m & 0 & 0 & 0 & 0 \\ 0 & 0 & m & 0 & 0 & 0 \\ 0 & 0 & 0 & I_x & 0 & 0 \\ 0 & 0 & 0 & 0 & I_y & 0 \\ 0 & 0 & 0 & 0 & 0 & I_z \end{bmatrix},$$

with terms only on the diagonal. The same thing happen to the coriolis centrifugal matrix, all terms related to \mathbf{r}_c goes to zero.

$$C(\mathbf{v}) = \begin{bmatrix} 0 & 0 & 0 & 0 & m w & m v \\ 0 & 0 & 0 & -m w & 0 & m u \\ 0 & 0 & 0 & m v & -m u & 0 \\ 0 & -m w & m v & 0 & -I_z \omega_z & -I_z \omega_y \\ m w & 0 & -m u & -I_z \omega_z & 0 & I_x \omega_x \\ m v & m u & 0 & I_z \omega_y & -I_x \omega_x & 0 \end{bmatrix}$$

The rigid body representing a crane beam has a mass of 150 [kg] and an inertia of 120 [kgm²] and a length of 3 [m]. The arm is constrained with spring elements in one end for translation in global x-, y- and z- direction in addition to rotation around global x and z, leaving it free to rotate around global y. Note that there are no energy dissipation in this model.

To get the model to simulate the right coordinates for the arm the initials conditions have to be given. This means setting the q- sensor on the constrained side of the sensor to -1.5 [m] in the x- direction, which is the axis going along the length of the arm. Same applies for the q- sensor in the unconstrained end of the arm, setting it to 1.5 [m] in the x direction giving the total length of the arm (3 [m]). Connected to the 1- junction representing the local coordinate system and center of mass is a coordinate transformer and a Se- element giving a gravity force in the global negative Z- direction.

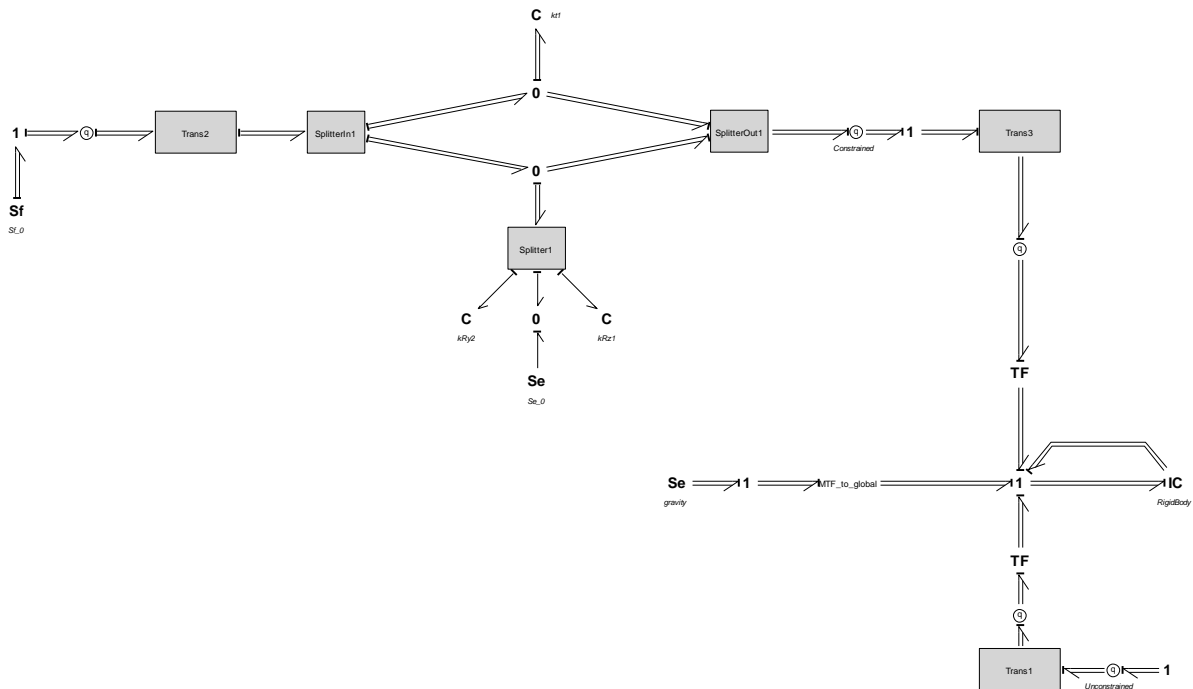
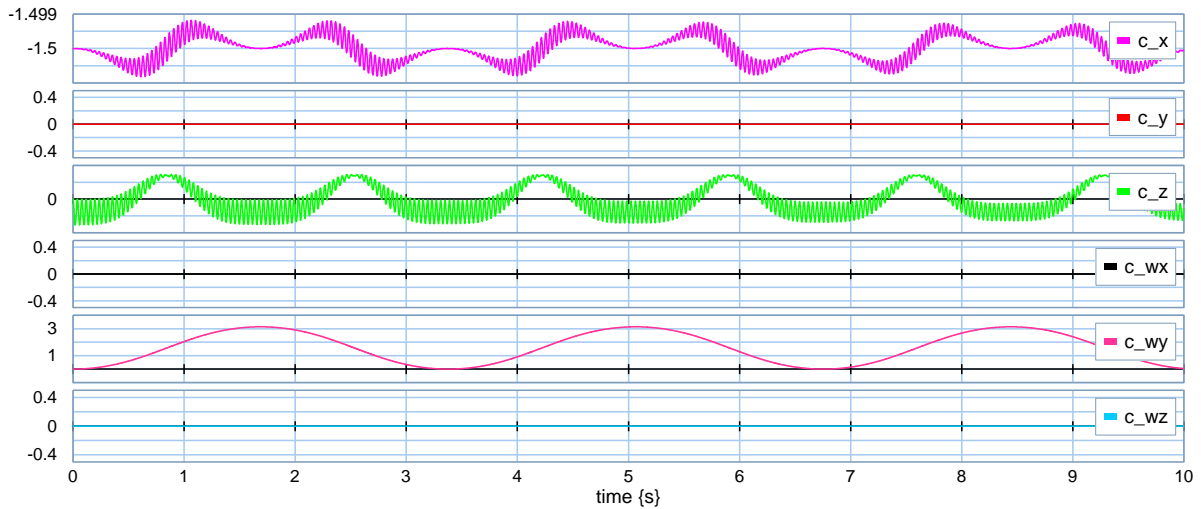


Figure 22: Pendulum bond graph

Running a simulation for 10 second reveals the following results for the q- sensor in the constrained end of the arm:

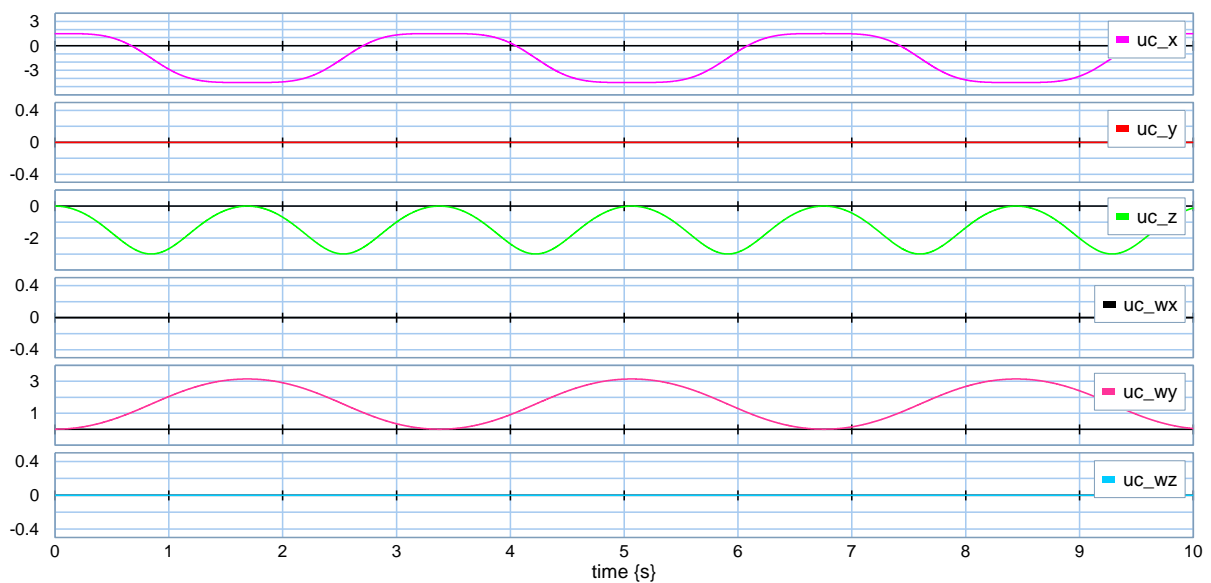


Simulation plot 1: : Pendulum, constrained end

The plot displays displacement in global coordinates where index c indicates constrained and x, y, z, wx, wy, wz translation and rotation in- and around respective coordinate axis.

For rotation around global y one would expect forces in x and z in magnitude depending on the stiffness of the spring elements constraining the arm. In this case the spring constants are set high resulting in high natural vibrational frequencies. Note that the forces in x oscillate around the initial condition -1.5 [m] as expected. The plot displays no rotation around x- and z- axis. Also the oscillations around y is in phase with the small displacement in x and z.

The next plots show the same type of displacements, but now for the unconstrained end of the arm.



Simulation plot 2: Pendulum, unconstrained end

The plot shows the same result as the constrained end for rotation around the axis which is correct as the angle would not change along the length of the arm. The displacement in the x and z direction also seems ok, though it can be hard to determine this from a plot. A simple animation of the arm based on the same values as the plot verifies the motions. The animation can be viewed on the attached CD.

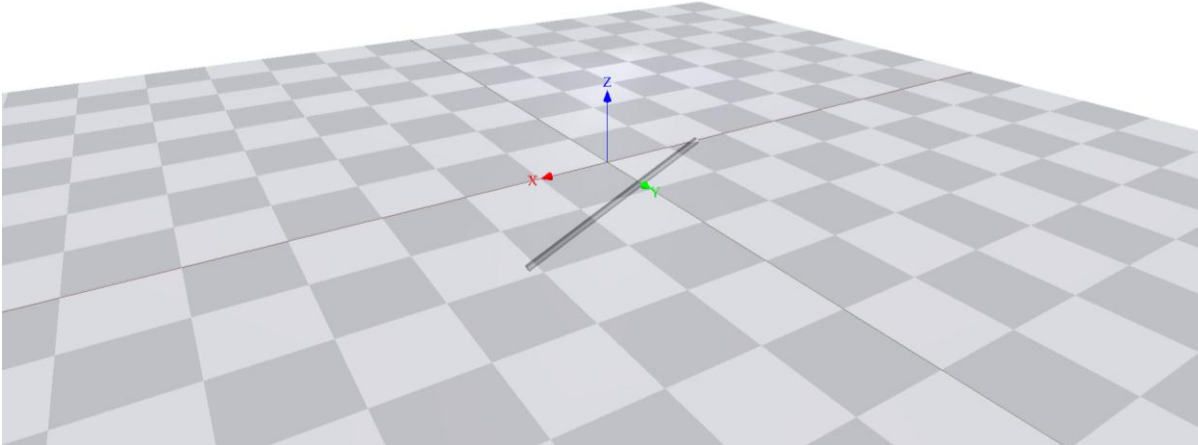


Figure 23: Pendulum animation

4.3.2 Rigid body beam with spherical joint

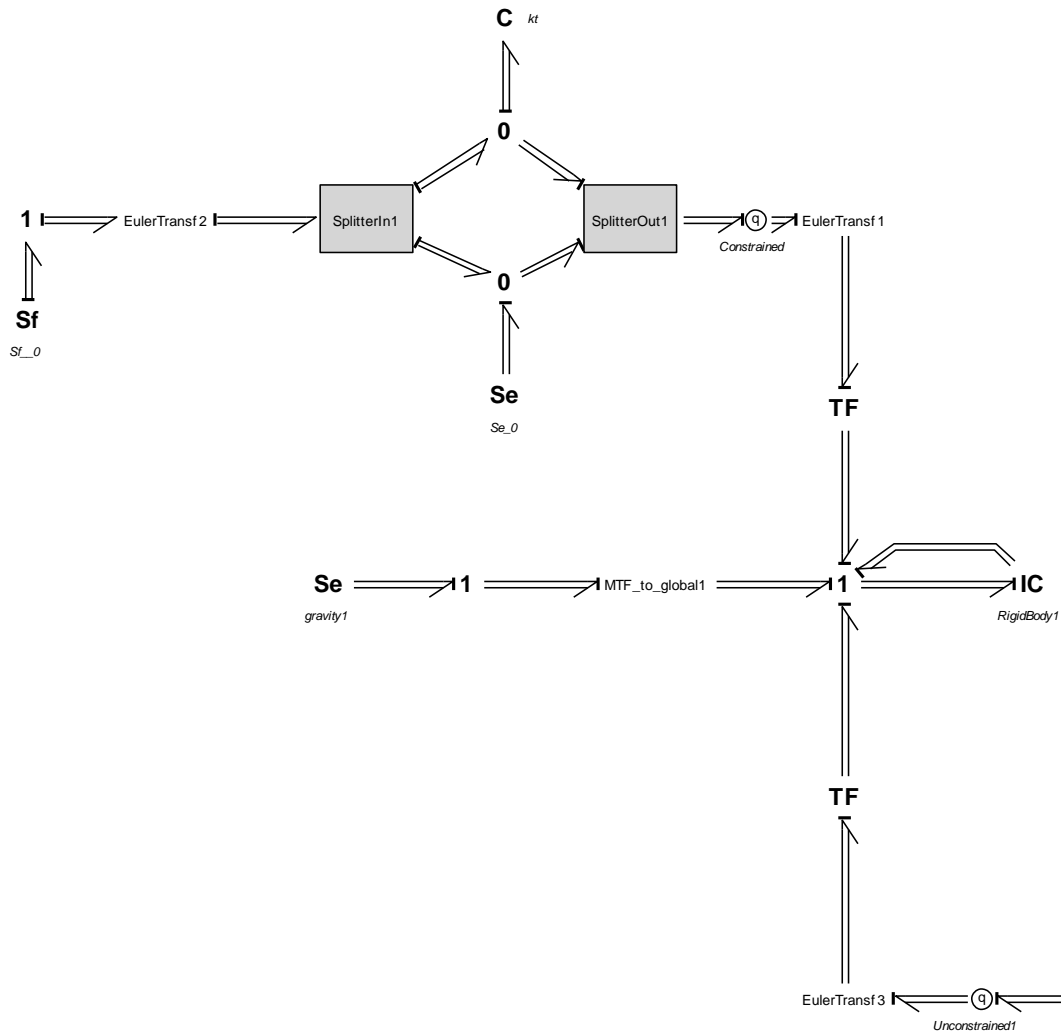
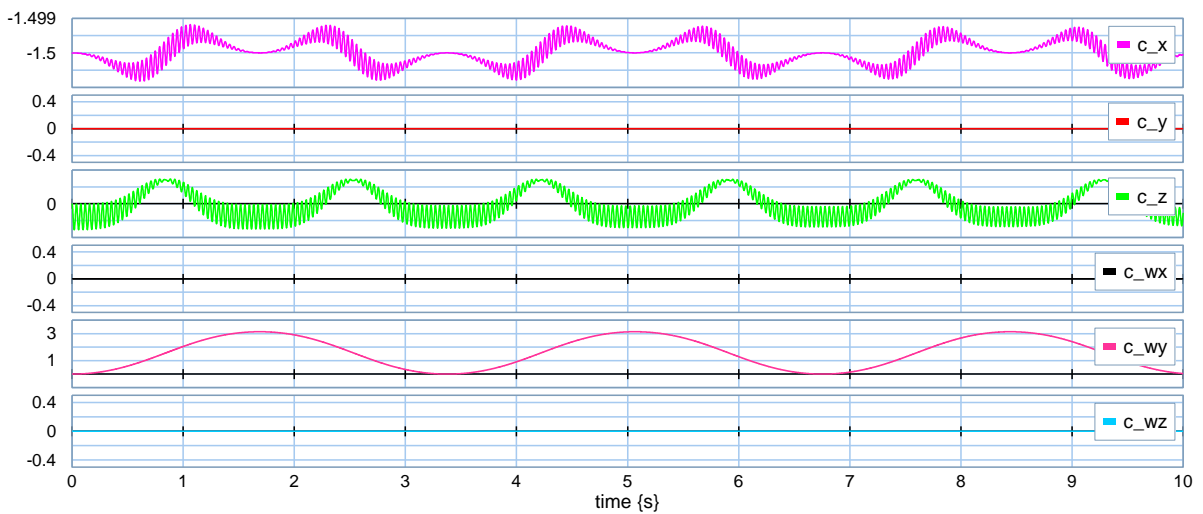
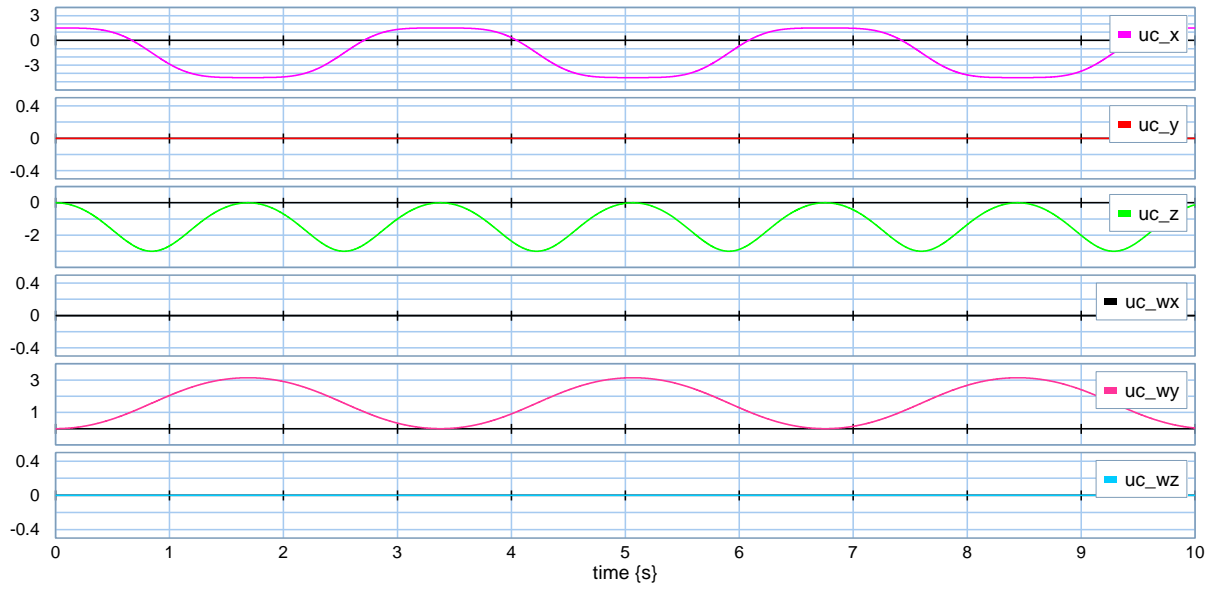


Figure 24: Beam with spherical joint

In this case the rigid body beam model is connected with the spherical joint. The beam data are the same as in the last case. First we put on a gravity force in the global negative z-direction.

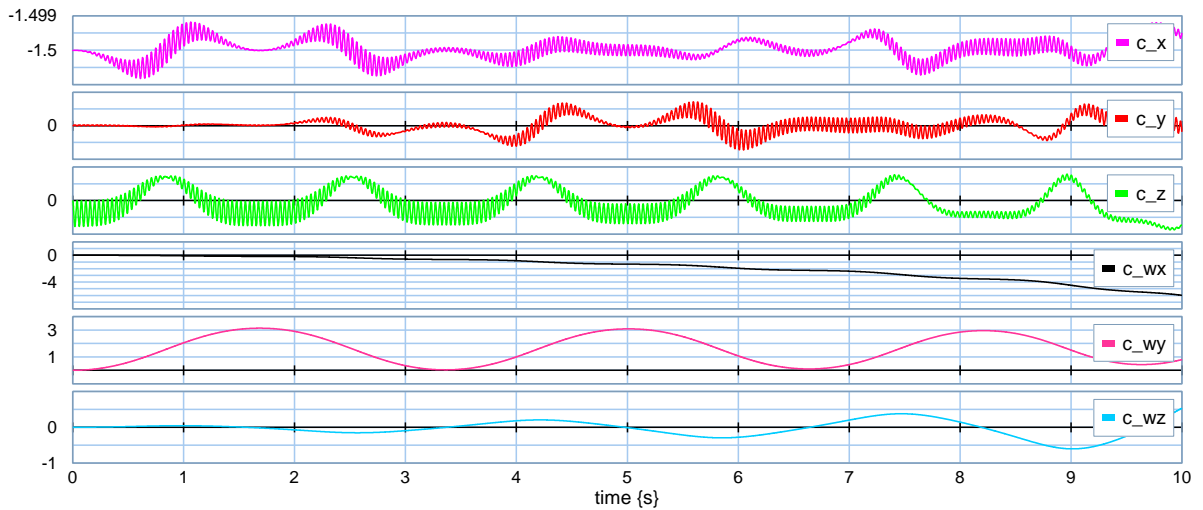


Simulation plot 3: Beam with spherical joint, constrained end

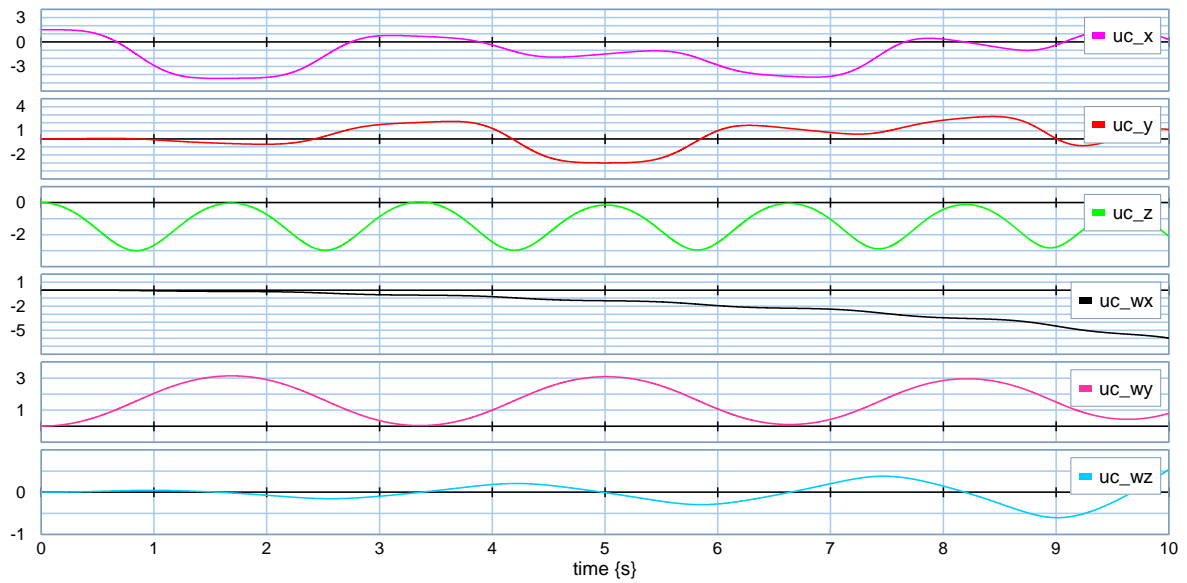


Simulation plot 4: Beam with spherical joint, unconstrained end

As expected the model behaves as in the revolute joint case. In the next trial a force of 50 [N] is put in the global positive y direction.



Simulation plot 5: Beam with spherical joint and force in two directions, constained end



Simulation plot 6: Beam with spherical joint and force in two directions, unconstrained end

Again the plot is difficult to interpret and the reader is referred to the animation on CD (One Arm Spherical). The results and animation confirms the performance of the joint allowing for rotation around the constrained end.

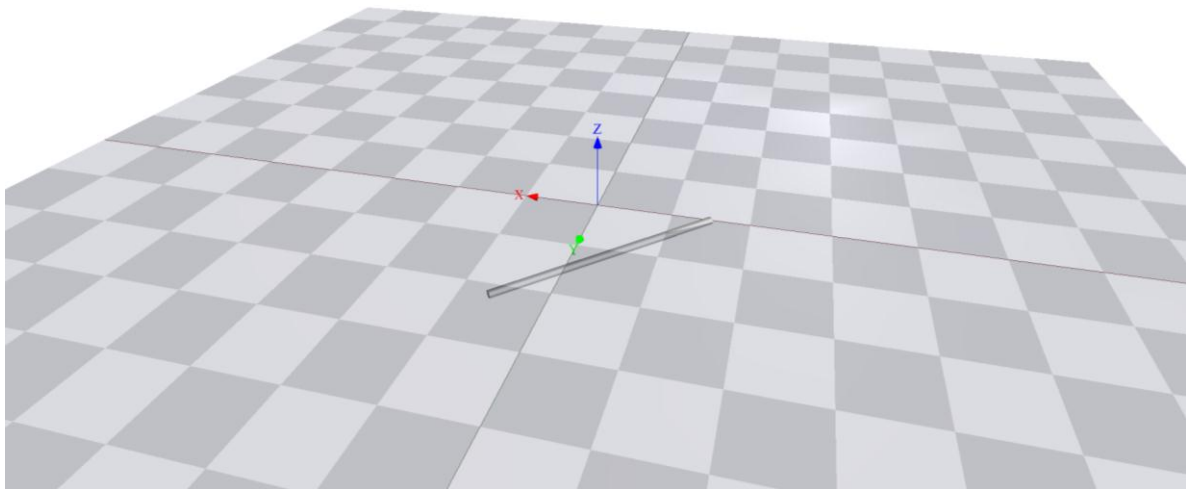


Figure 25: Animation of beam with spherical joint and force in two directions

Note that there are no energy dissipation elements in this model either resulting in continuous oscillation around the global force vector made up of the gravity force and the applied force in the y direction.

4.3.3 Two link planar arm

Serving as the basis for a simple crane is the two link planar arm. This is the same type of arm which was used in the Lagrange equation example for a 2D rigid body. Here the model is built up of the 6DOF rigid body elements. The two link planar arm is assembled using two revolute joints and two rigid body beams. All elements are programmed to rotate around global y. Both beams share the same data as the beams in the previous examples.

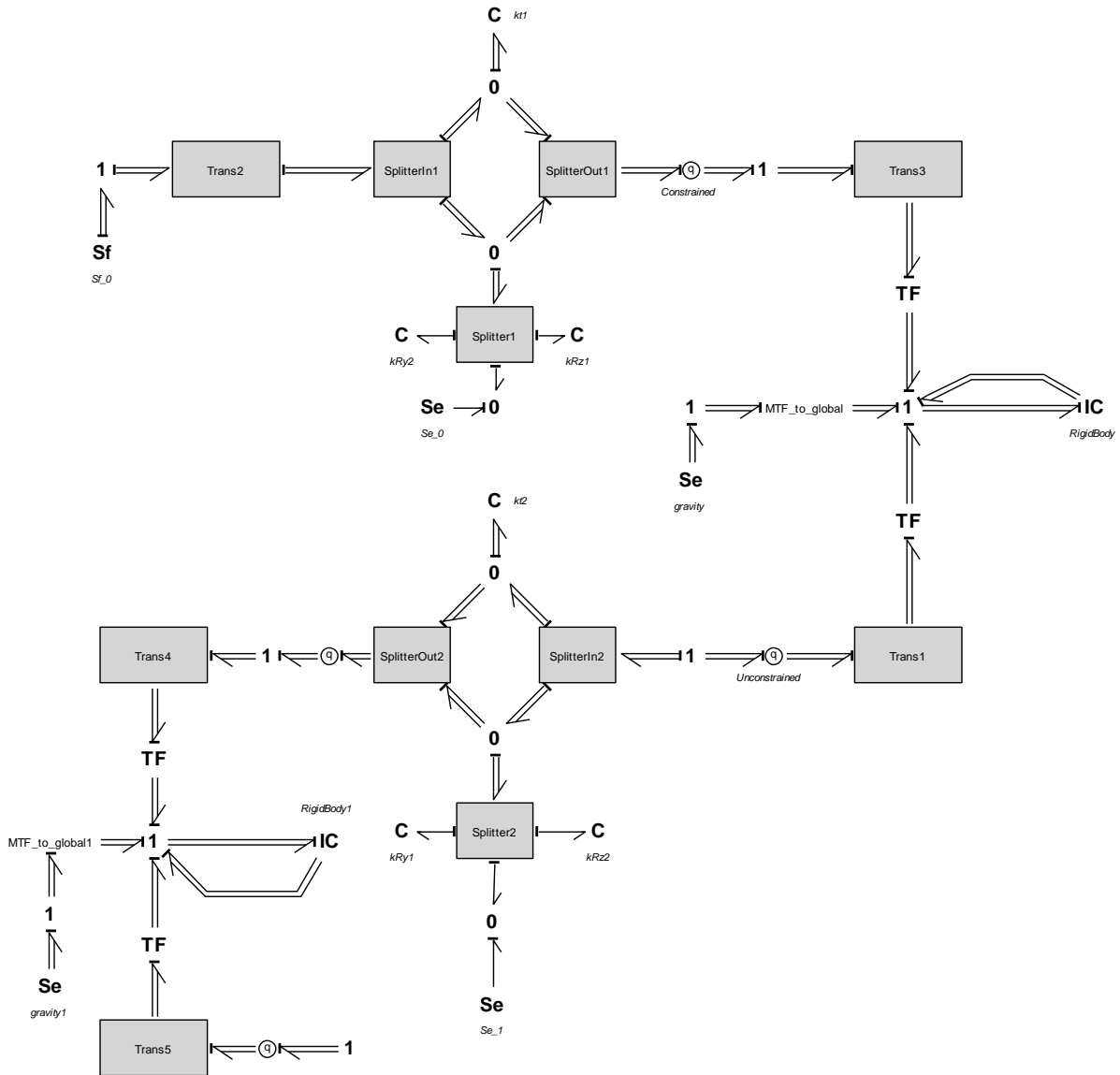
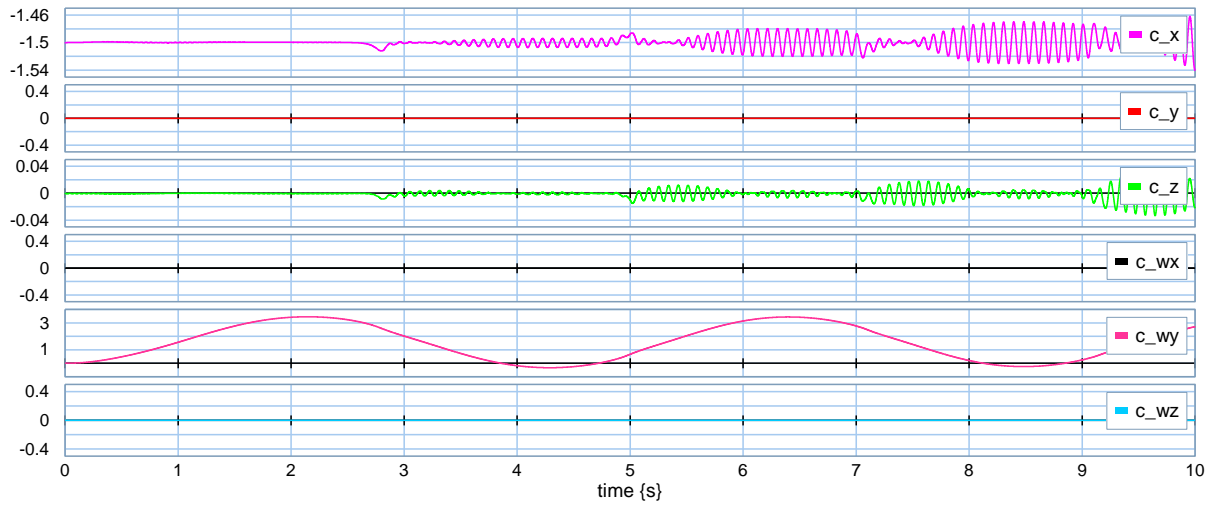
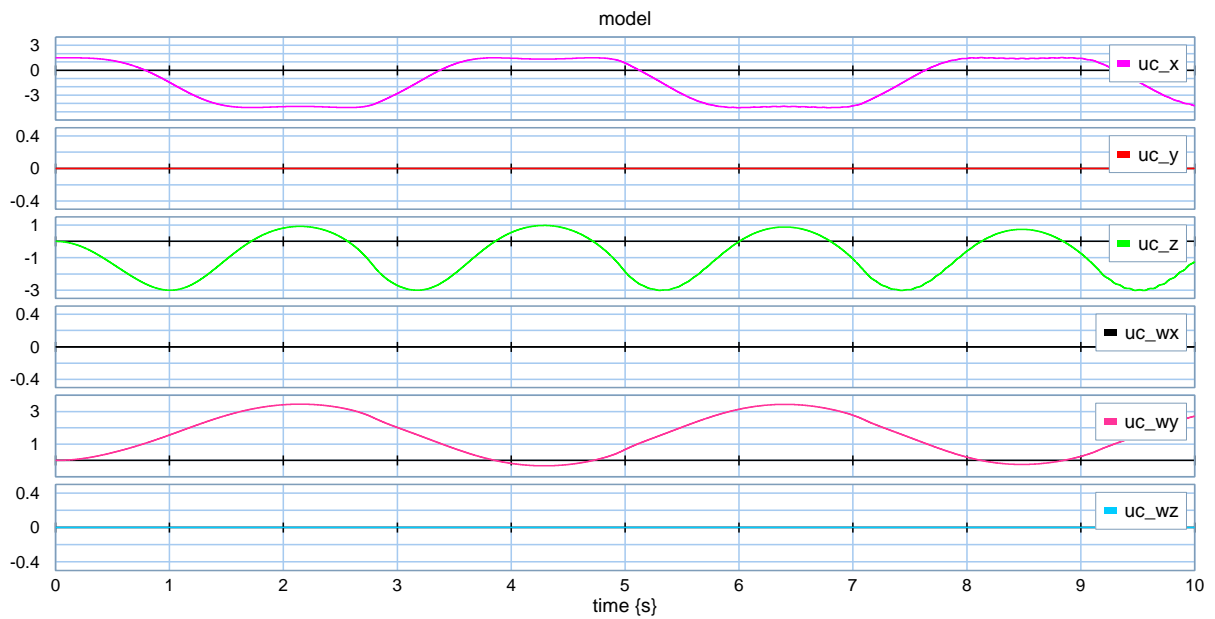


Figure 26: Two link planar arm bond graph

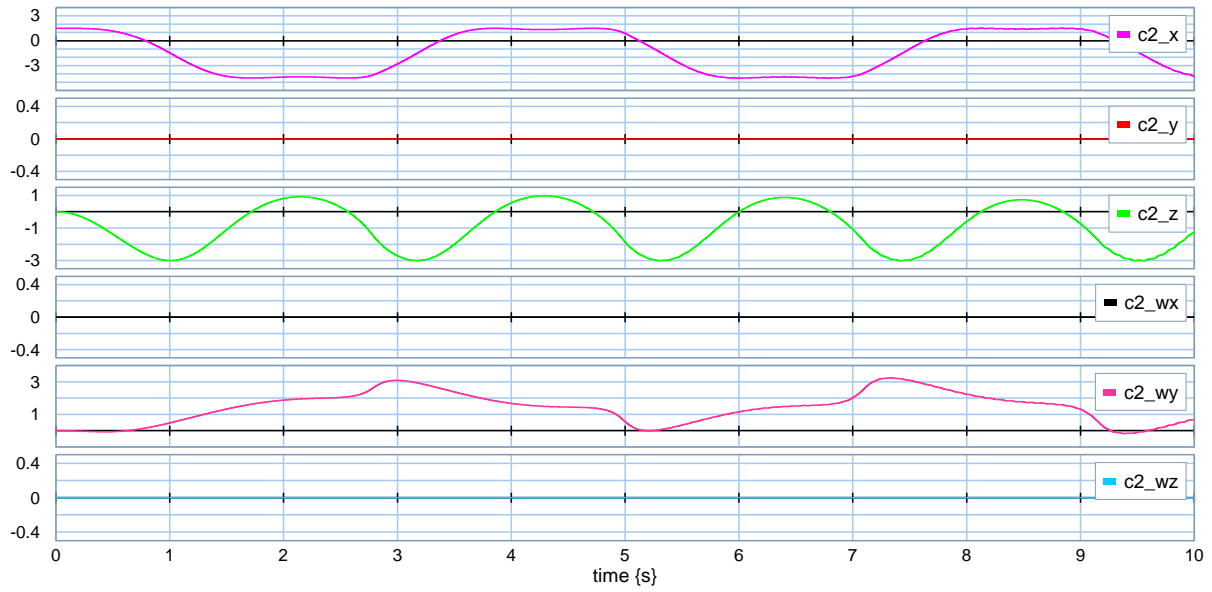


Simulation plot 7: Two link planar arm, arm one, constrained end

The first plot shows the displacement values of the constrained end of beam one. As for the single beam we have rotation about y and high frequency small displacement in the global x- and z-direction.



Simulation plot 8: Two link planar arm, arm one, unconstrained end



Simulation plot 9: Two link planar arm, arm two, constrained end

The two next two plots shows the ends of the beams which are constrained together. The plot shows the same displacement in the global x- and z- direction which confirms the joint ability to create a close to rigid coupling. For demonstration of the movement see animation on CD (Two link planar arm).

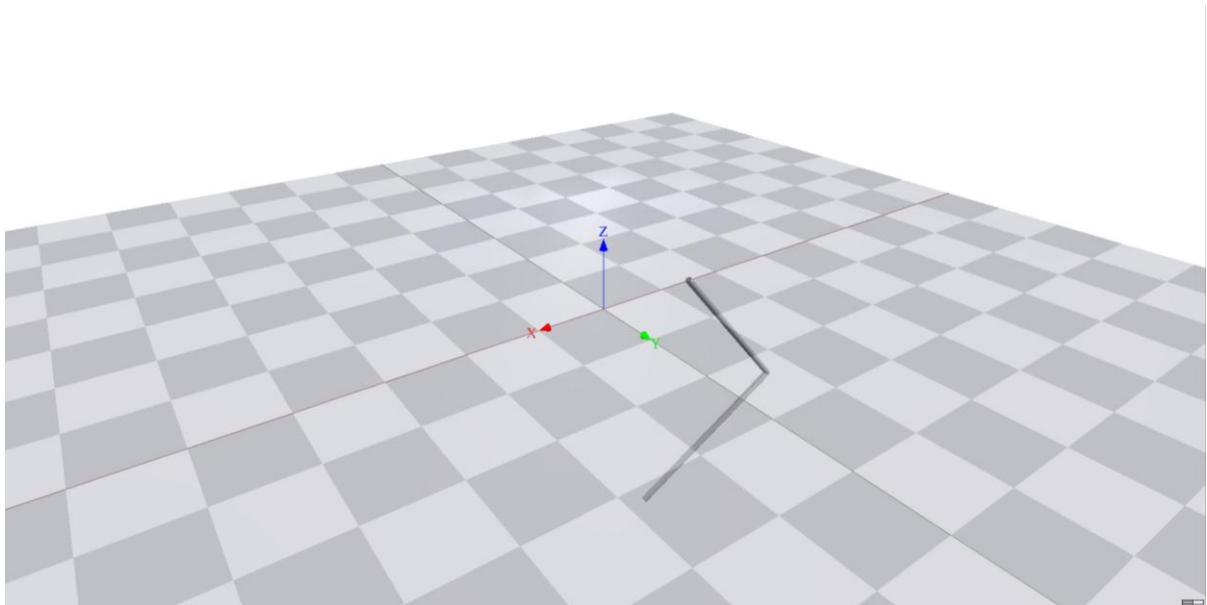


Figure 27: Animation two link planar arm

4.4 The realistic crane beam

Till now we have developed the rigid body crane beam and we have connected two of these to form the two link planar arm. However such models are of no further use without some form of control. They also lack realism since there is no form for damping in the models, thus they only portray free undamped motion. In this chapter these issues will be discussed and some solutions presented.

4.4.1 Control and actuators

Actuators are sources of force which can move around and manipulate an object such as a crane. Typical actuators are electric motors and hydraulic cylinders as often the case with cranes. Here only the connection of such actuators will be discussed and the actual actuator force will be represented by effort sources for simplicity. However as always in the bond graph method the interfacing of more realistic sources of effort such as hydraulics are easily done. The 20sim software also offers the possibility for implementing joystick control, thus making it possible to control the actuator effort live.

Consider the single beam arm. In the previous case presented the arm oscillated around the global gravity force in the negative z-direction. There are several ways of controlling this motion. The first one resembling a hydraulic actuator solution is to apply a counter force with center of attack somewhere along the beam. The second one resembling an electric motor solution is to apply a counter torque in the constrained end of the beam.

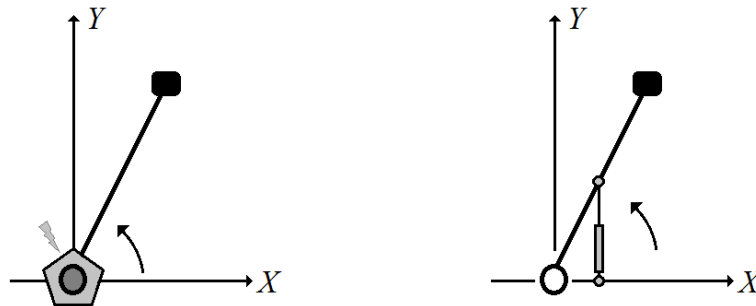


Figure 28: Actuators on crane beam

Applying a counter torque actually requires almost no modification to the bond graph model. One can simply apply effort value in the joint Se-element which before represented zero torque. The gravity force acts on the joint with the positive torque $T = mg \left(\frac{l}{2} \right) = 150 \cdot 9,81 \cdot 1,5 = 2207,25$ [Nm]. By applying the same negative torque in the Se-element the beam will hold still. By applying a more negative torque the beam will rotate in the opposite direction. See animation “Single beam torque ex” in CD. Note that the beam will continue accelerate due to the fact that the torque arm of the gravity force is reduced during the arm elevation while the joint torque is constant.

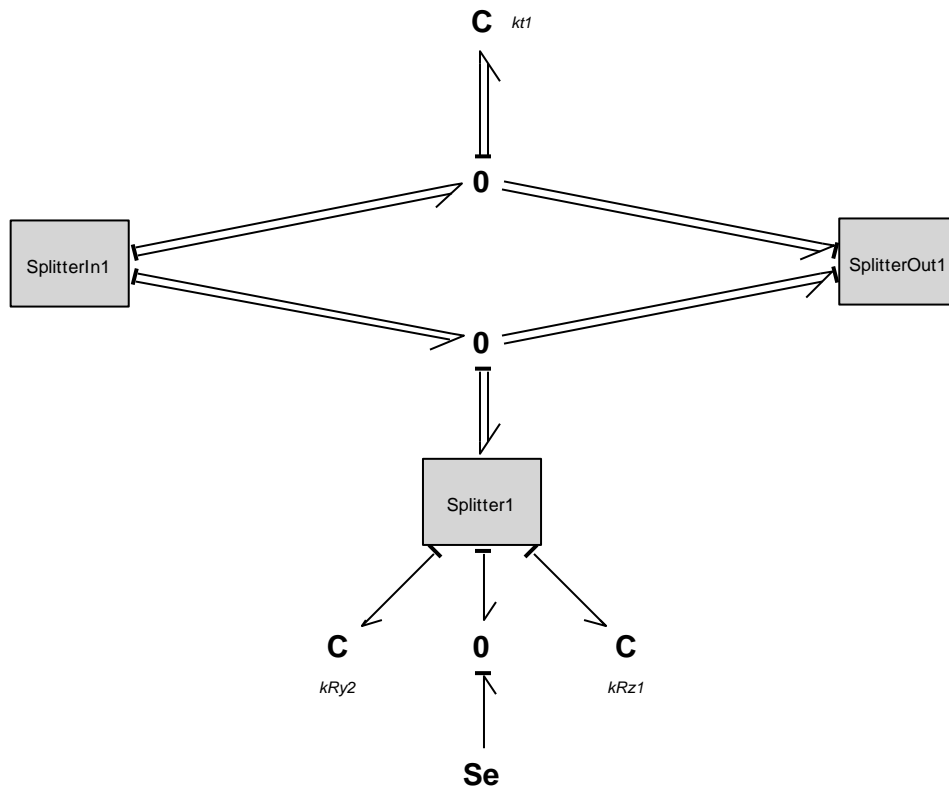


Figure 29: Joint actuator bond graph

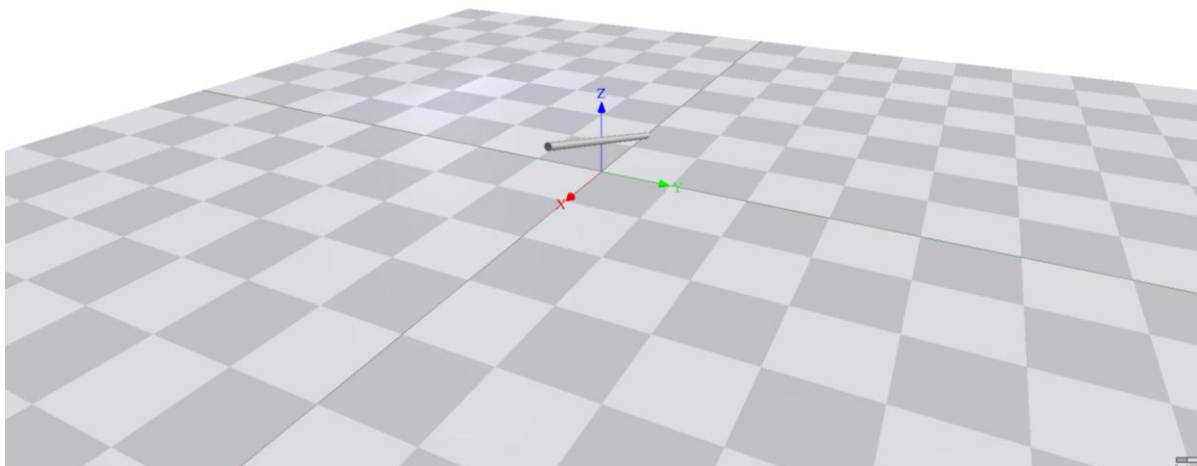


Figure 30: Animation of joint actuator

Linear actuator forces acting on the beam can be added in several different ways. In all cases there is the possibility to use TF-elements to change the point of attach on the beam. Here only forces on the local origin will be considered for simplicity.

- Adding a Se- element in the local one junction representing a perpendicular force on the crane beam. Such a solution will not be not physical correct since the force will always be in the local z direction.
- Using the existing Se (gravity)- element or add a new Se- element to the global one-junction representing a force in the positive global z direction. This solution is closer to representing the physical actuator since the torque arm in the global x direction will decrease as the beam is elevated, thus the torque will decrease. This is more equivalent to what an actual hydraulic actuator will experience.
- A combination. Using an MTF- element connected to the local one-junction programmed with the geometry of the actuator with respect to the angle of the beam. Such a solution gives a realistic view on how the actuator forces affect the beam, but deriving the geometrical relations can be time consuming.

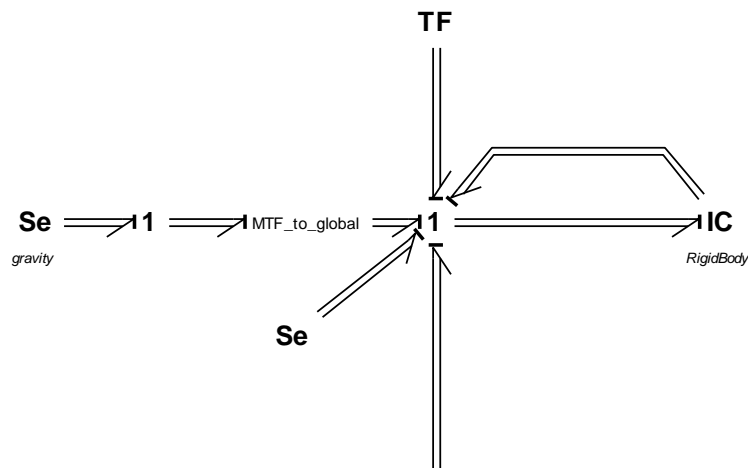


Figure 31: Perpendicular actuator bond graph

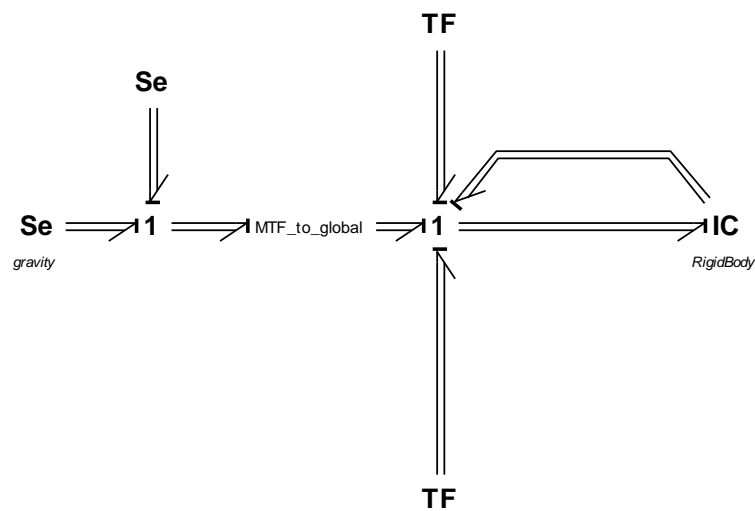


Figure 32: Global actuator bond graph

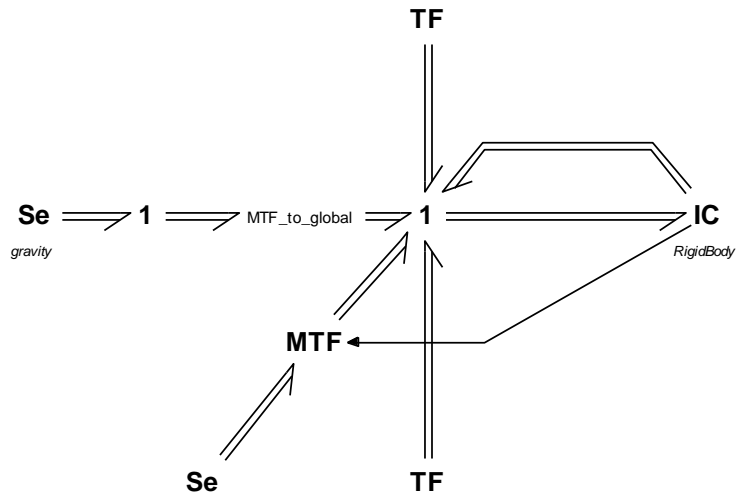


Figure 33: Real actuator bond graph

4.4.2 Energy dissipation

In every mechanical system there is energy dissipation present. This can be friction in joints or friction in actuator among other things. Such energy dissipation represented by R- elements and can be added to the bond graph just as the Se- elements.

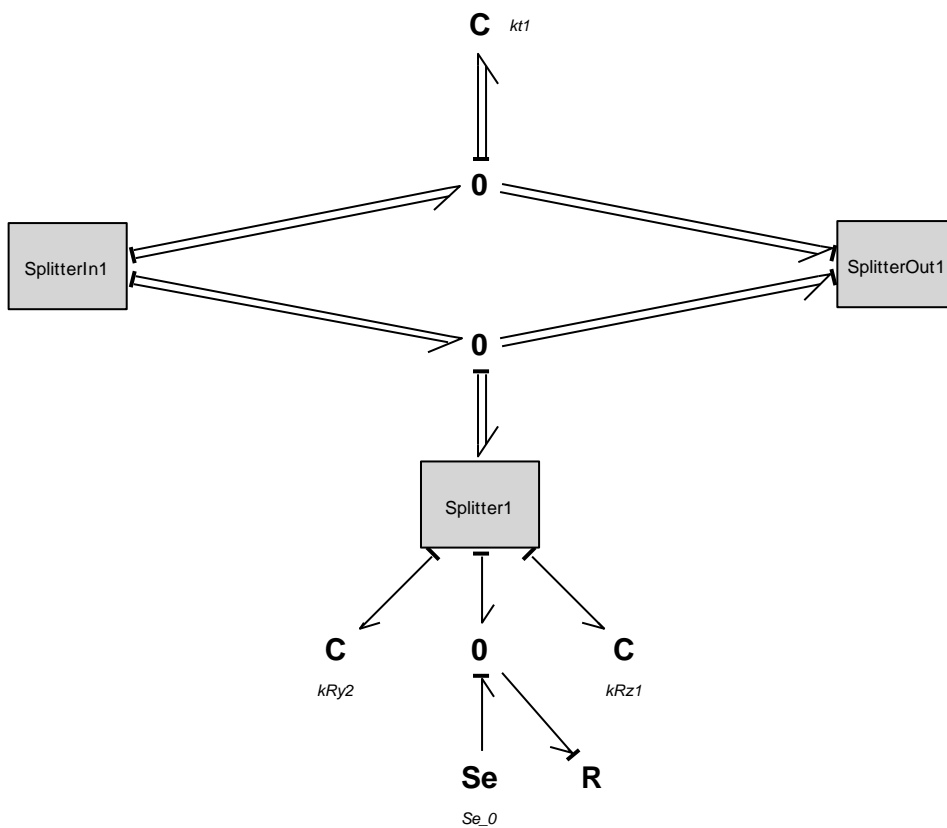


Figure 34: Energy dissipation in joint bond graph

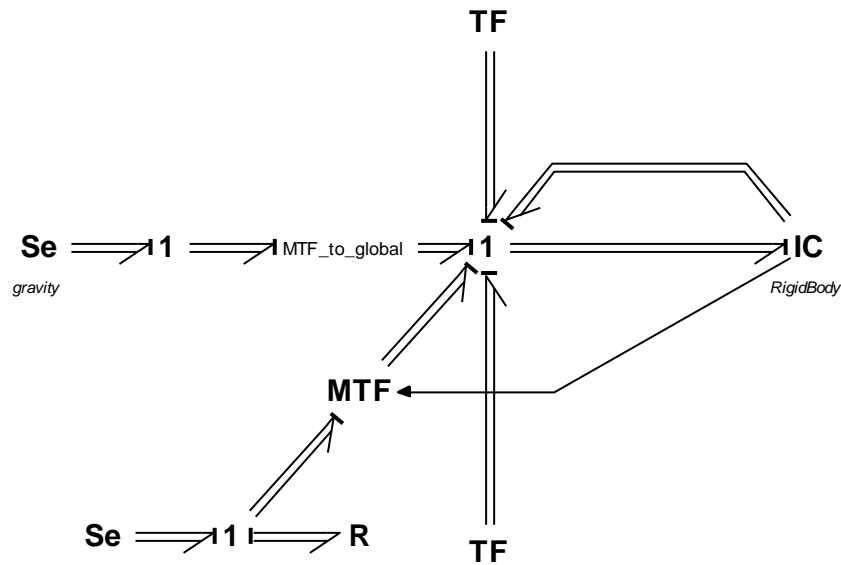


Figure 35: Energy dissipation in actuator bond graph

4.4.3 Actuators and energy dissipation in the two link planar arm

In this example energy dissipation and actuator effort have been applied to the two link planar arm to demonstrate the functionality. The model is tuned for elevation of both arms, however the values for energy dissipation and actuator force are taken arbitrary and may not be realistic. The code in the MTF-elements representing the geometric relation between the beams, actuators and ground are taken from the 2D crane model (Pedersen, ICexampleW3, 2010) The animation “Two link planar arm with actuators” is attached on CD.

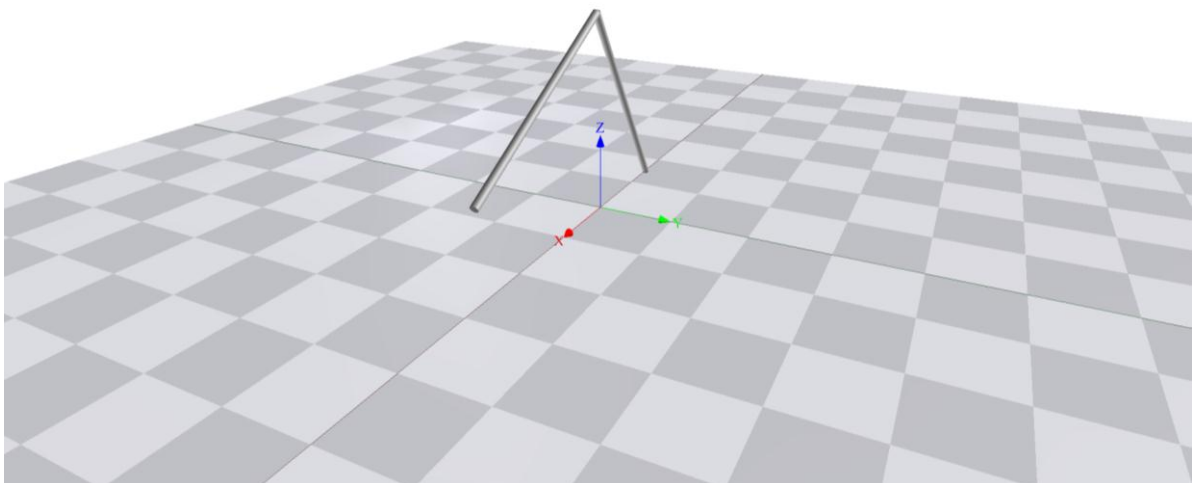


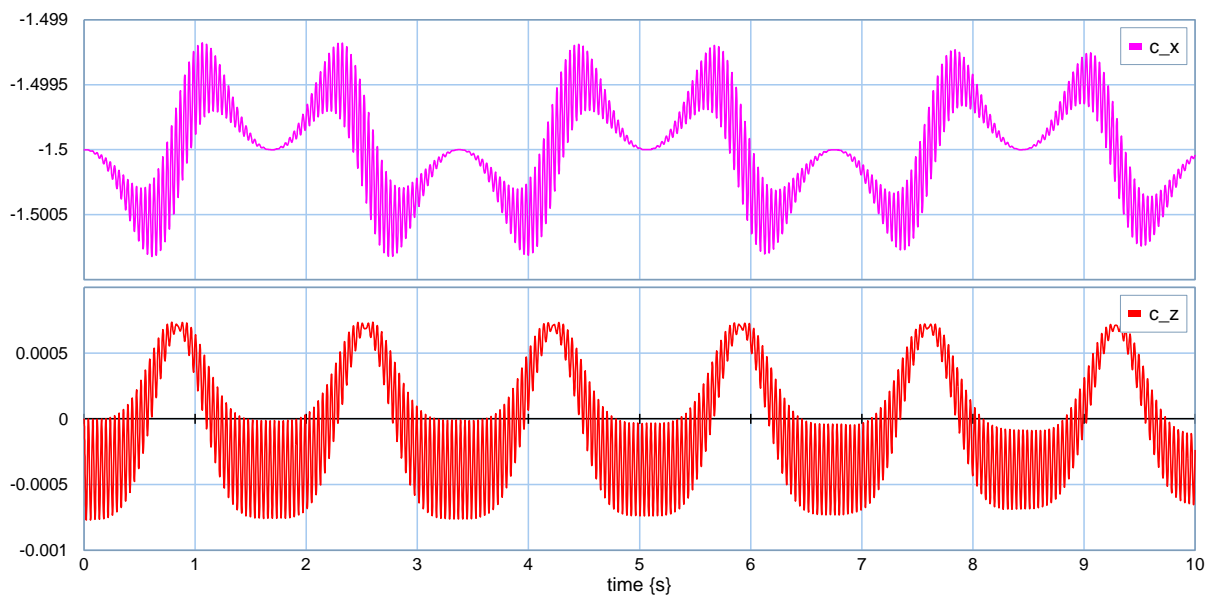
Figure 36: Two link planar arm with actuator and energy dissipation

4.5 Discussion of high vibrational natural frequencies

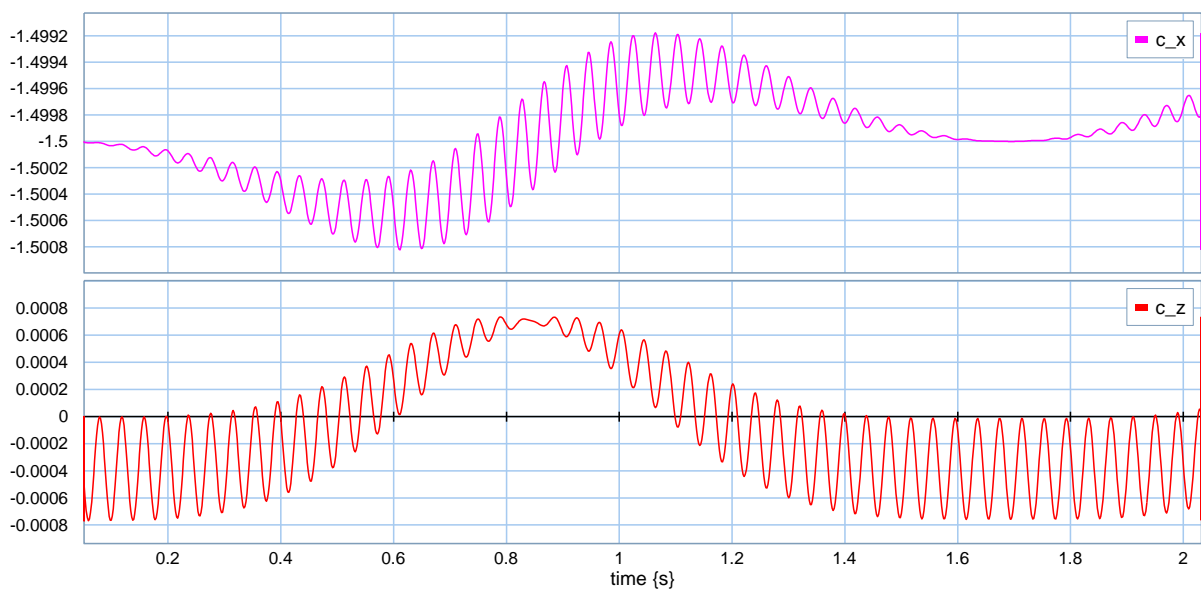
Though the spring c-element offers a solution to the derivative causality problem when connecting rigid bodies, it is far from an optimal solution. The approach requires a high spring constant to realistically model the interaction between the bodies, which in most cases should be as stiff as possible. For example in the joints connecting two crane arms the connection is to be considered close to rigid, or at least have a very high stiffness if the model is to be so realistic that it takes into account the bearing stiffness in the connection. The problem is however that such high spring constants in mathematical terms means creating high vibrational natural frequencies in the system.

4.5.1 Simulation time and model behavior

One place this can be shown is in the constrained end of the single beam model which has been discussed in short earlier.



Simulation plot 10: High vibrational natural frequencies



Simulation plot 11: High vibrational natural frequencies zoomed in

Zooming in on the displacement of in the global x- and z- direction these high frequencies is clearly shown. Though in itself not a problem, such high frequencies pose a problem for the effectiveness of the coupling between the rigid bodies. To calculate these frequencies high time step in the simulation is needed, meaning longer simulation times. As more rigid bodies as connected the simulation time increases.

Number of arms	Simulation time	Model calculations	Output points	Avarage step per second
1	0,555	14260	5732	25693
2	5,207	88835	12155	17060
3	7,395	86541	11710	11702
4	11,73	105421	11960	8987
5	14,899	109280	11859	7334

Table 1: Simulation data for increasing number of beams

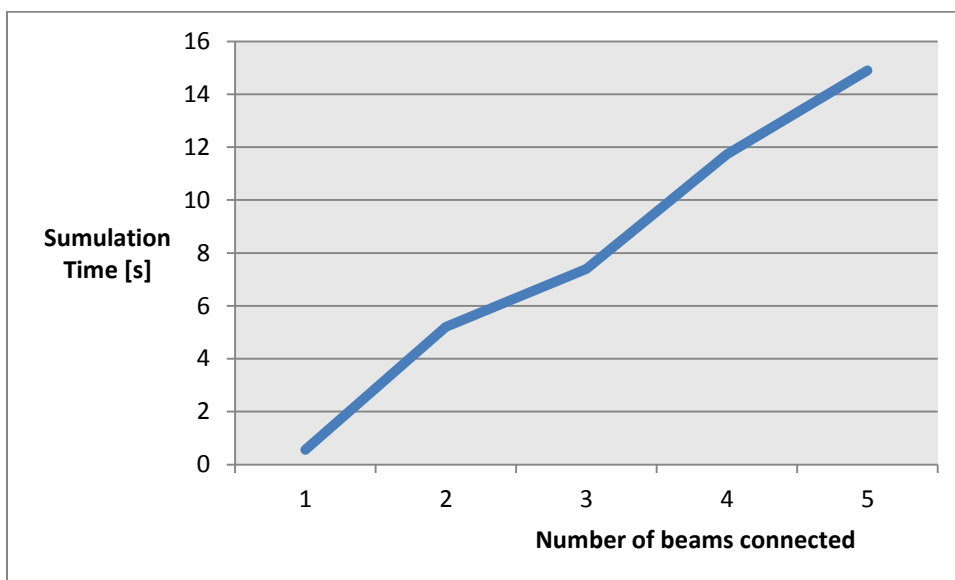
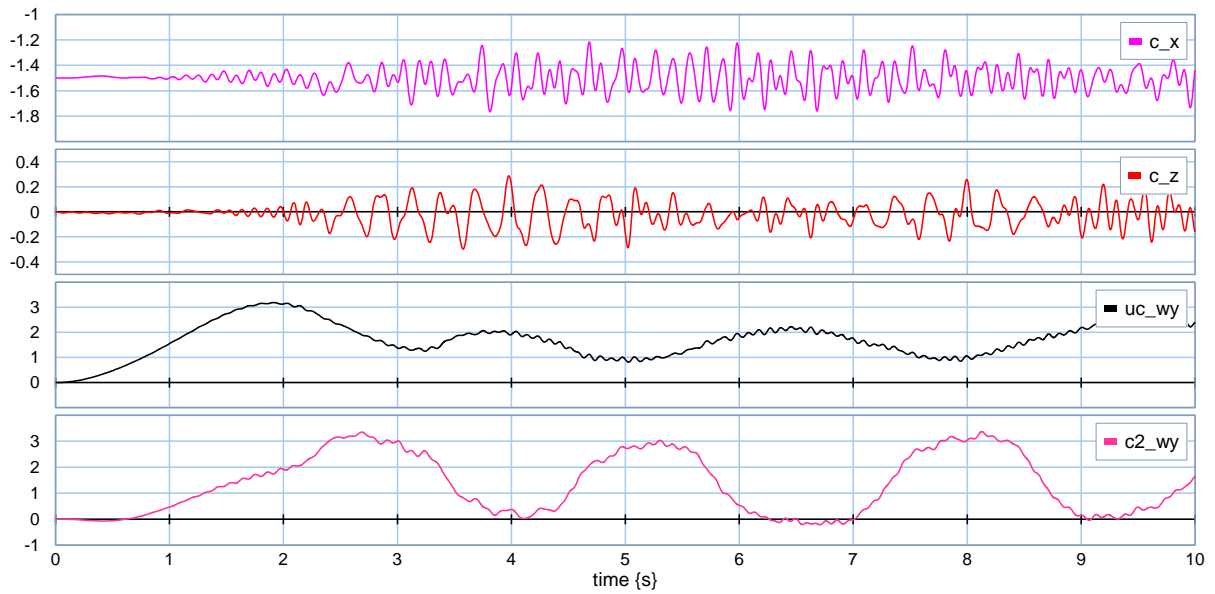


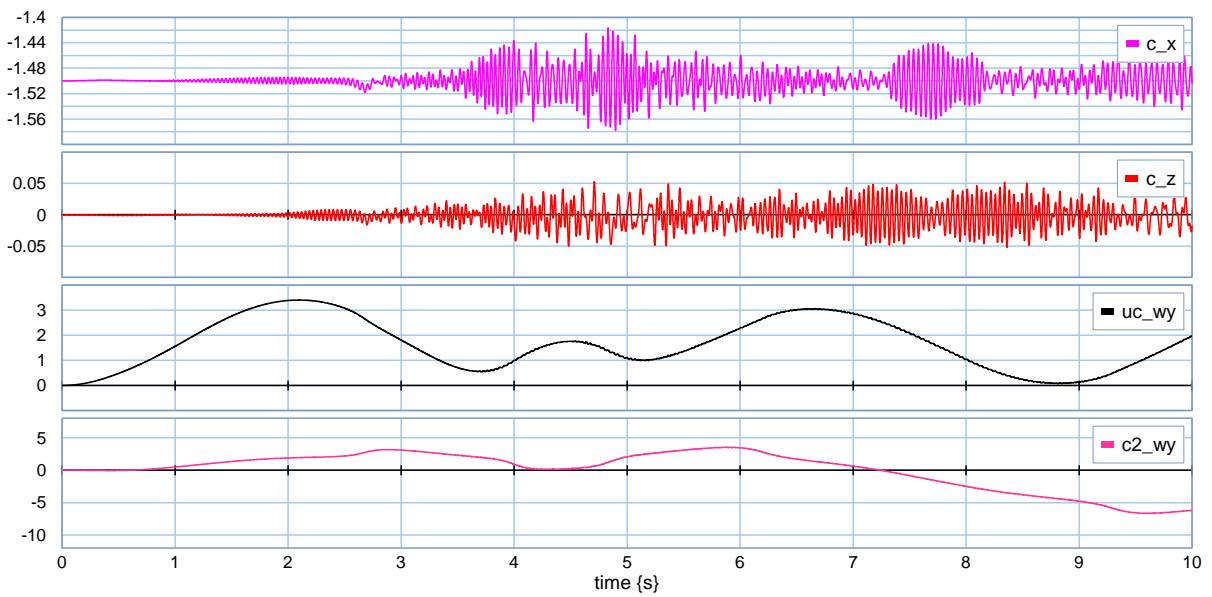
Figure 37: Simulation time vs. beams connected

The table shows the difference between simulations when attaching an increasing number of arms after one another. The simulation was done under the same computer conditions, i.e. the same processor power was available. All spring constants where the same values. The data shows a linear relation between the simulation time and number of rigid bodies connected. However in this simulation the beam displacements where not evaluated. The fact is for each rigid body the beam motion has to be evaluated and the spring constants tuned for realistic behavior. For some cases this will revile the need for modifying spring constants to compensate for the higher forces which may arise when connecting more rigid bodies. In such cases the simulation curve may very well be exponential. This can be tested in a simple experiment with the two link planar arm. First we set both the spring constants constraining beam one to ground and the constants constraining the beams together to a relatively low value (10^4). We plot the displacement in x- and z- direction for the constrained end and the rotational displacement on both sides of the two ends constrained together.

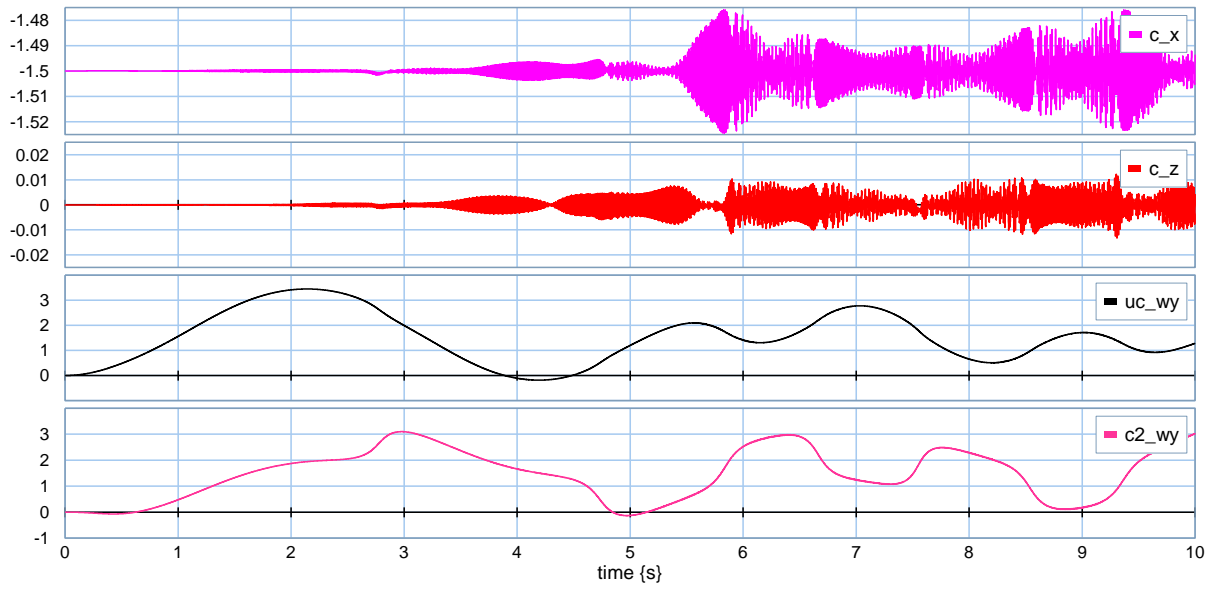


Simulation plot 12: Two link planar arm and spring constant 10^4

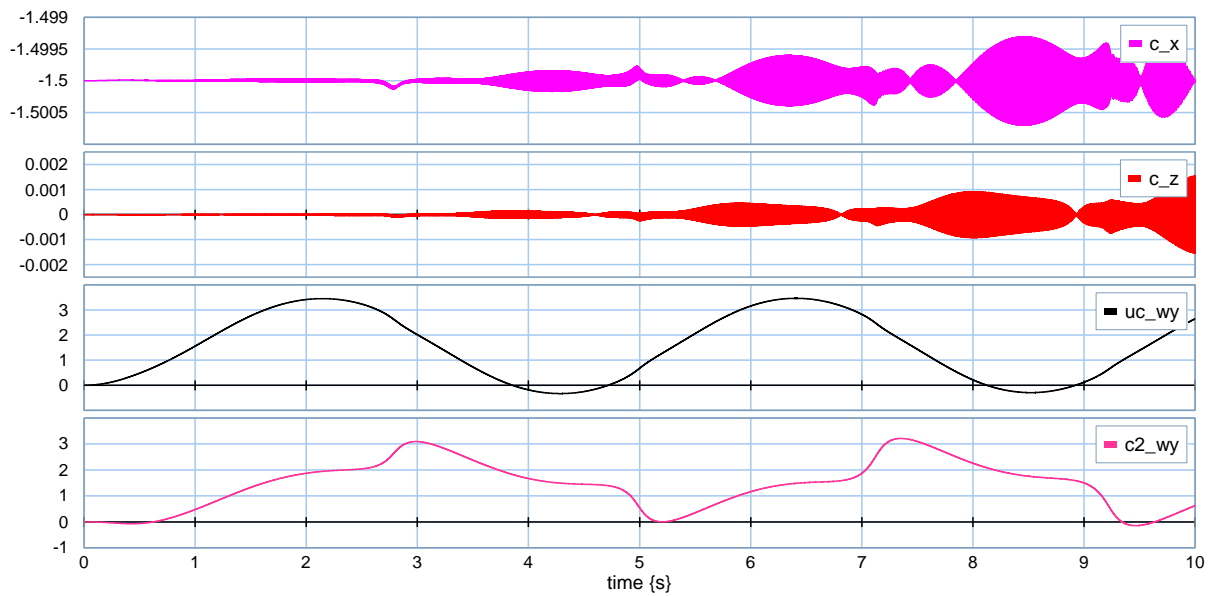
We observe large displacements where beam one is constrained to ground (c_x and c_z), which is unwanted considering a rigid connection. The rotational displacements are experiencing inconsistent behavior. The animation “ 10^4 ” shows the poor model behavior. The model is acting like the joints are springs and not a rigid coupling, which is not surprising considering the low spring constants. The next plot shows the spring constants increased with 10^1 for each time.



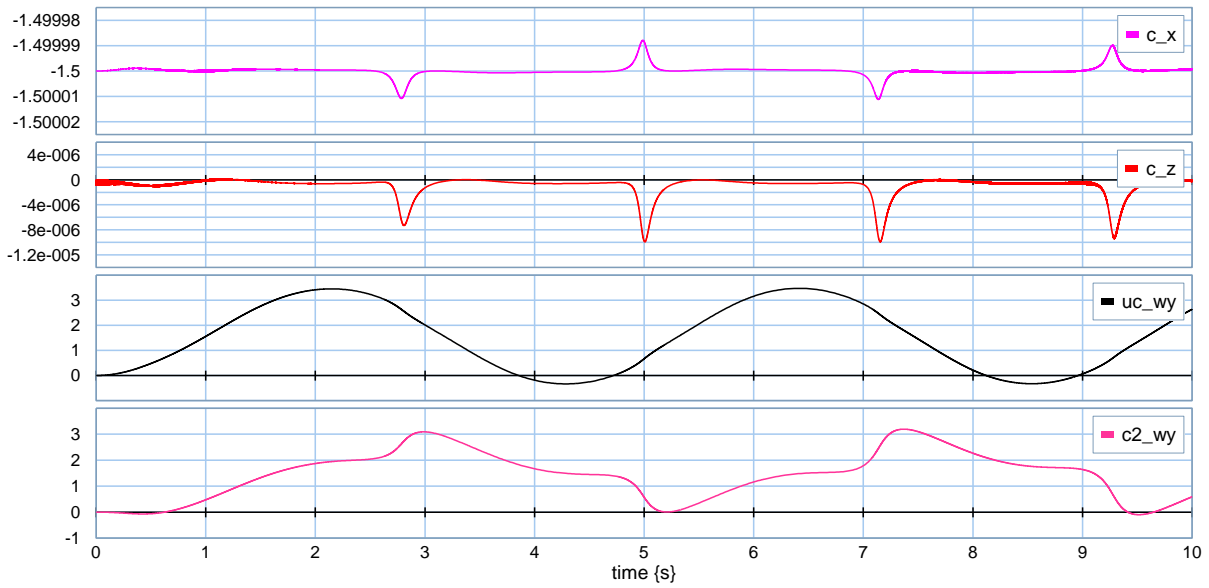
Simulation plot 13: Two link planar arm and spring constant 10^5



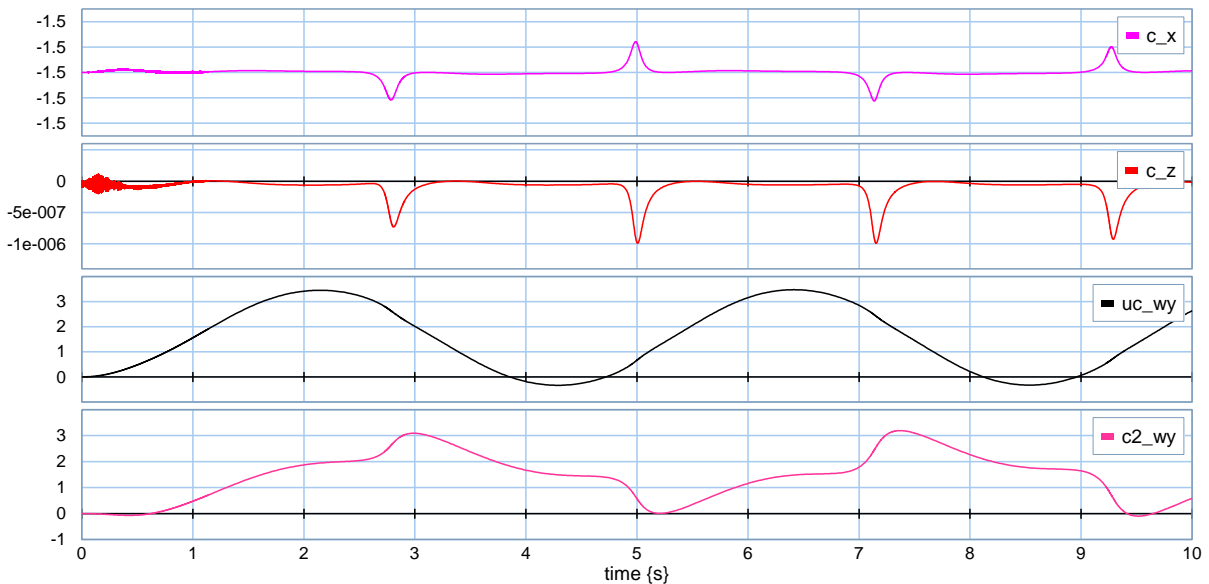
Simulation plot 14: Two link planar arm and spring constant 10^6



Simulation plot 15: Two link planar arm and spring constant 10^7



Simulation plot 16: Two link planar arm and spring constant 10^8



Simulation plot 17: Two link planar arm and spring constant 10^9

The plot shows that for high spring constants the vibrational frequencies for the displacement in x- and z- direction get higher. There is also a buildup of amplitude which may cause problems for longer simulations. At the same time the rotational displacements become more consistent. This can also be seen in the animation if the highest spring constant where the model behaves nicely. An unexpected result for the two highest spring constants are that the high frequencies for the linear displacement seem to disappear, only a small hint of the in the beginning of the simulation remains. This is consistent with the simulation time suddenly dropping at for higher values of k , which until $k = 10^7$ displays the expected exponential curve.

Spring konstant	Simulation time	Model calculations	Output points	Avarage step per second
10 ⁴	4,119	35432	4597	8602
10 ⁵	6,786	88835	12155	13090
10 ⁶	19,609	263186	35281	13421
10 ⁷	49,125	486600	89801	9905
10 ⁸	42,931	437490	71503	10190
10 ⁹	29,593	294697	52582	9958

Table 2: Simulation data for increasing spring constant

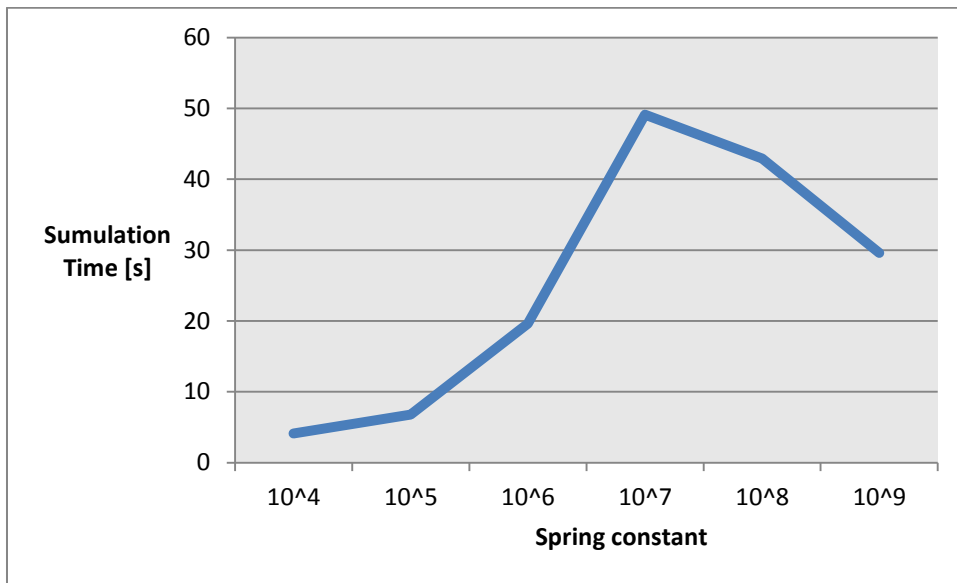


Figure 38: Simulation time vs. spring constant

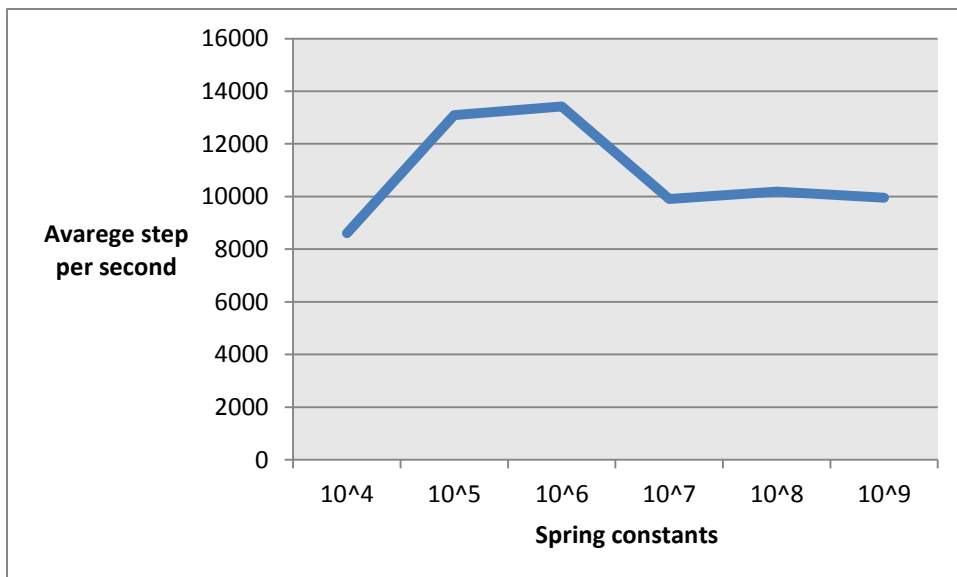


Figure 39: Time step vs. spring constant

Inspecting the data for the model calculations and the number of output points they display the same type of curve as the simulation time. Inspecting the data for the average time step per second it drops between $k = 10^6$ and $k = 10^7$ which is consistent with more data being processed at $k = 10^7$. However it does not go up for $k = 10^9$ where there are a lot less calculations being done, but this could maybe be a consequence of computer power being allocated to other tasks at that time. Finding an answer for why it is easier to do time simulations of the system with wary high values for k is more difficult. We know that the amplitude of the natural frequency of a vibrating system decreases with a higher value, i.e. as $k \rightarrow \infty$ amplitude goes to zero. However what is to be considered infinite here is unknown. The numerical integration method (default: Backward differentiation formula) is off course also one possible answer. However it is clear that forming a definite conclusion on the basis of so few tests cannot be done. It is stressed that simulation data are dependent on the computer used and may be different for other computers. The general trend should however be the same.

4.5.2 Experimentation on damping in joint

In both (Karnopp, Margolis, & Rosenberg, 2006) and (Zied & Chung, 1992) it is suggested to use damping elements in joints. Such a solution makes sense since the damping parameter should reduce high frequencies and thus shorten the simulation time. The following simulations is done with the same setup as previous and with $k = 10^4$ as the start spring constant which revealed poor results without damping. Here a damping- element is added in each joint to the rotational power bonds. The damping parameter value is set to $r = 1000$ in all simulations.

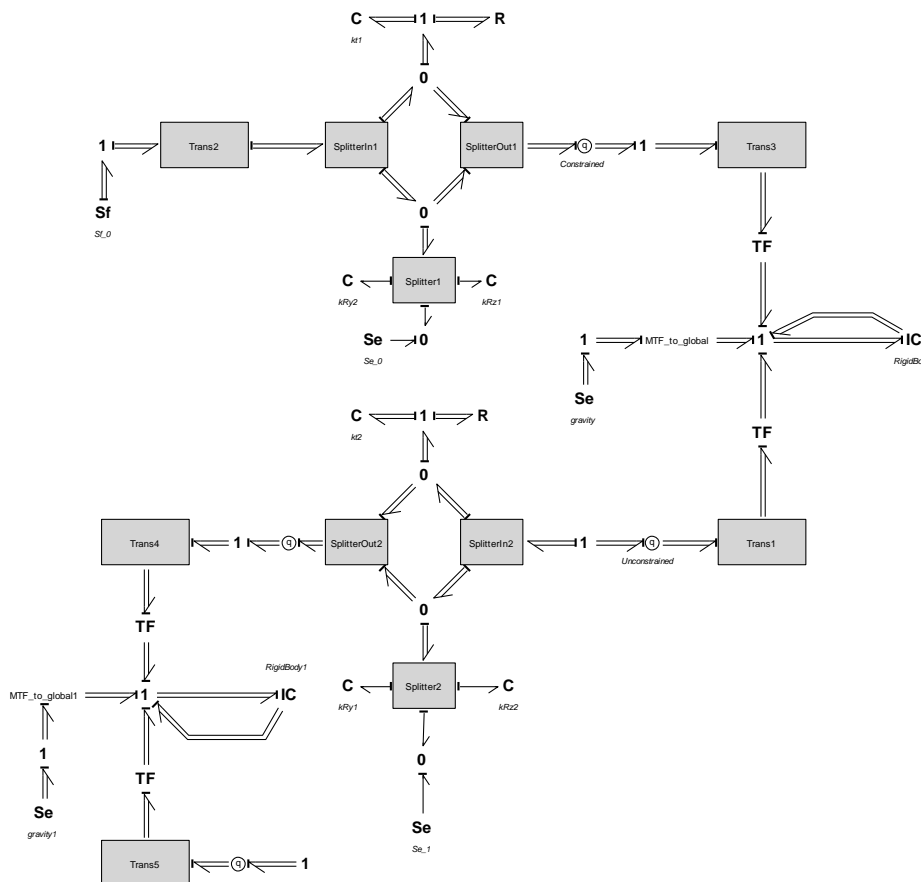
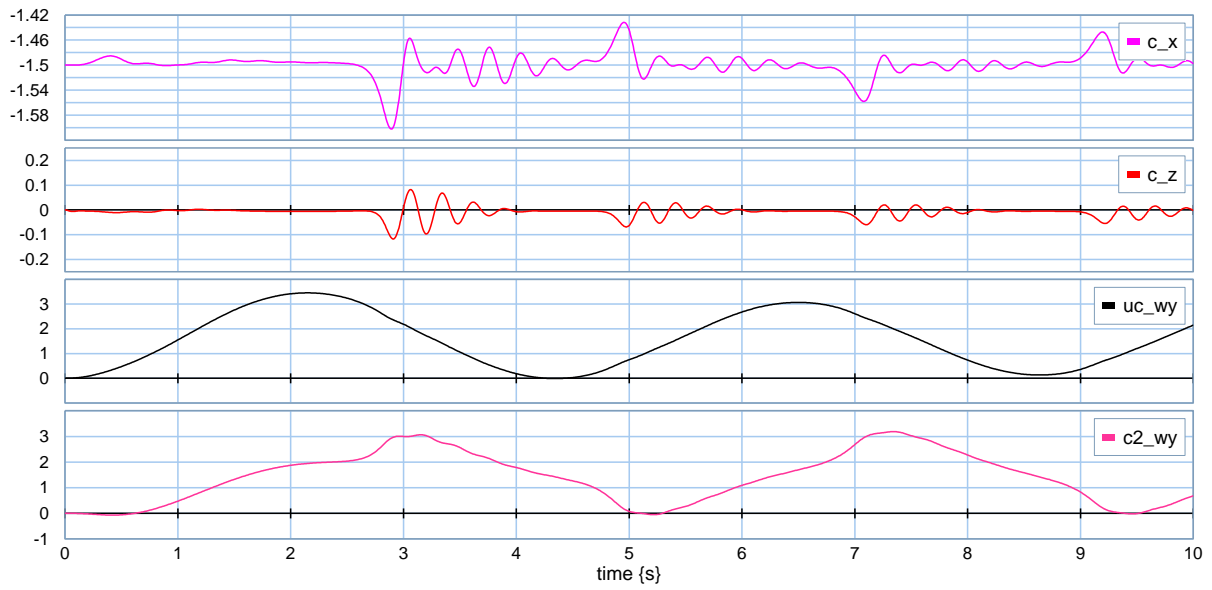
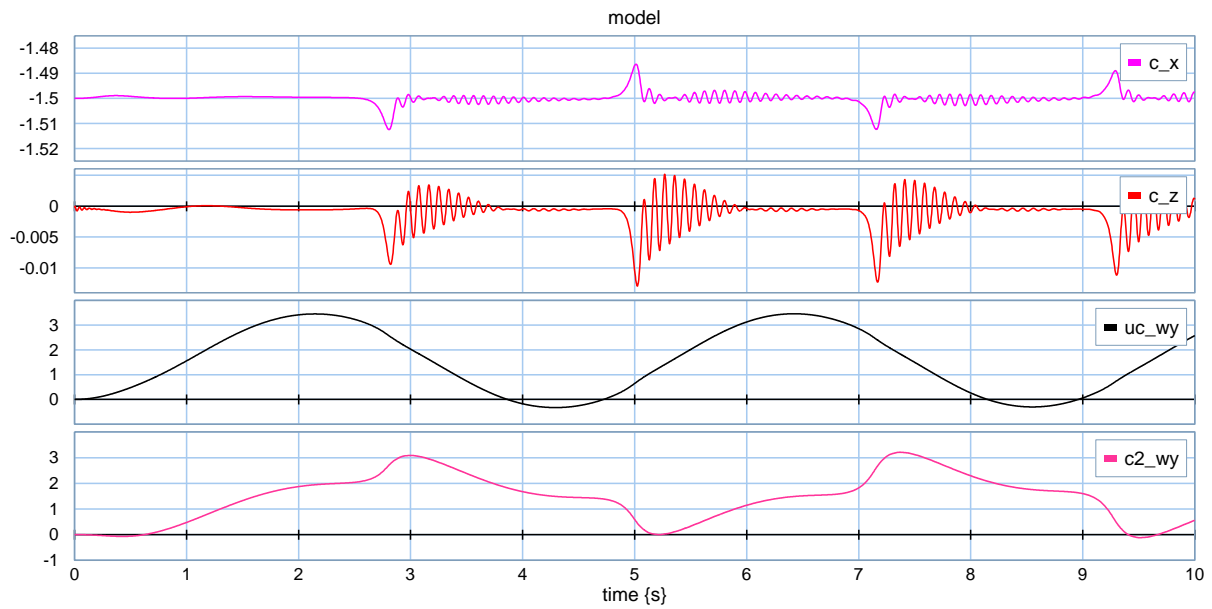


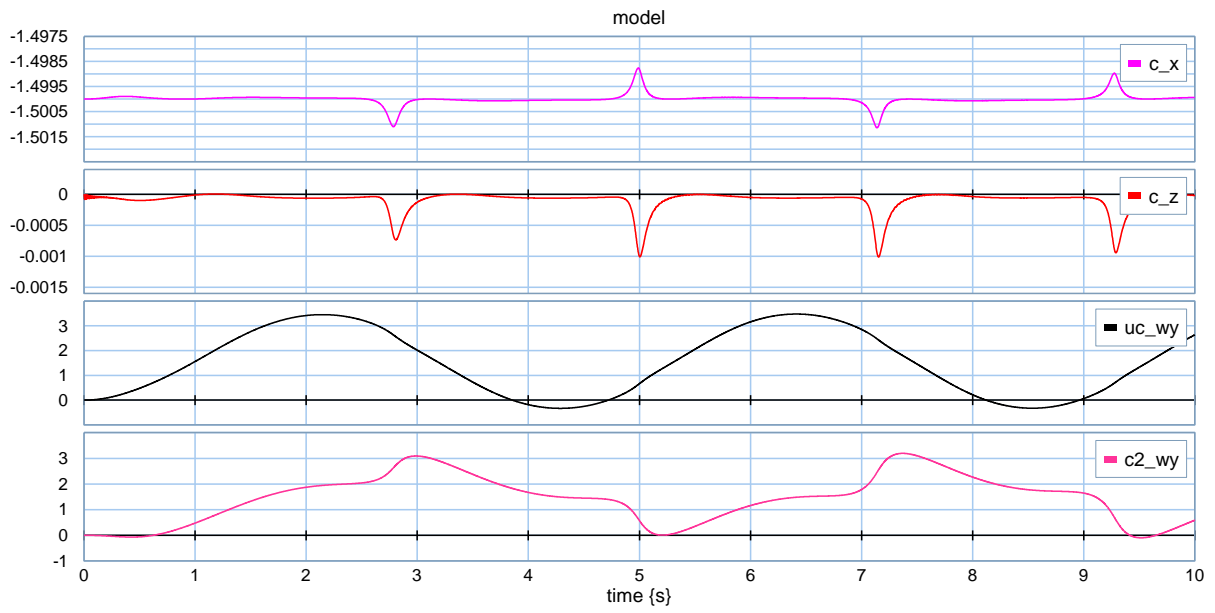
Figure 40: Two link planar arm with damping in joints



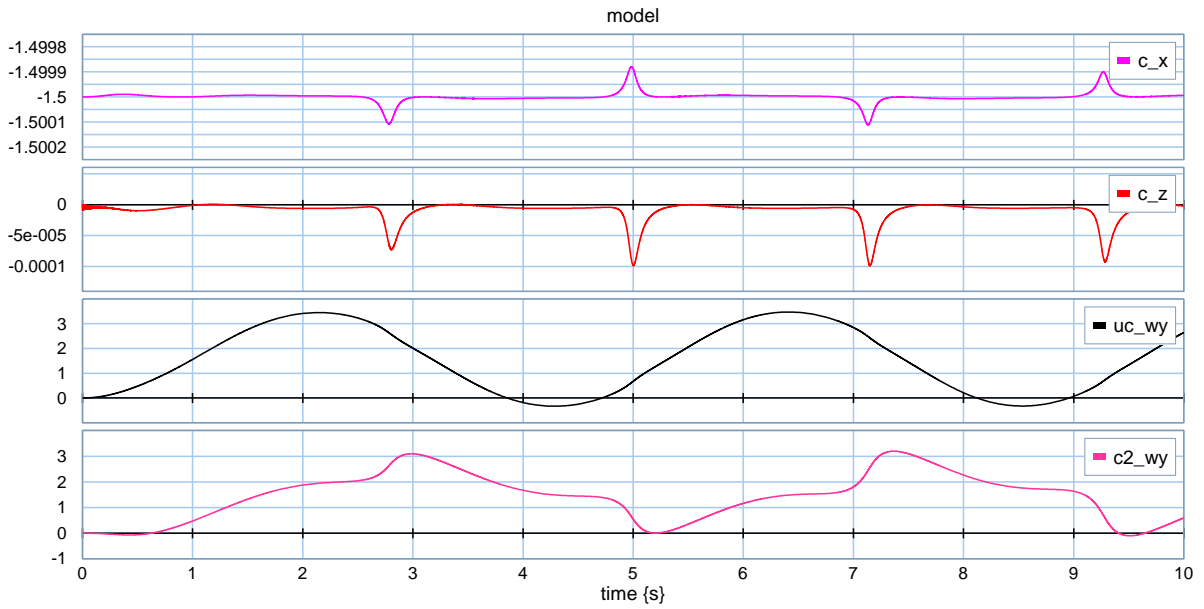
Simulation plot 18: Two link planar arm and spring constant 10^4 and damping



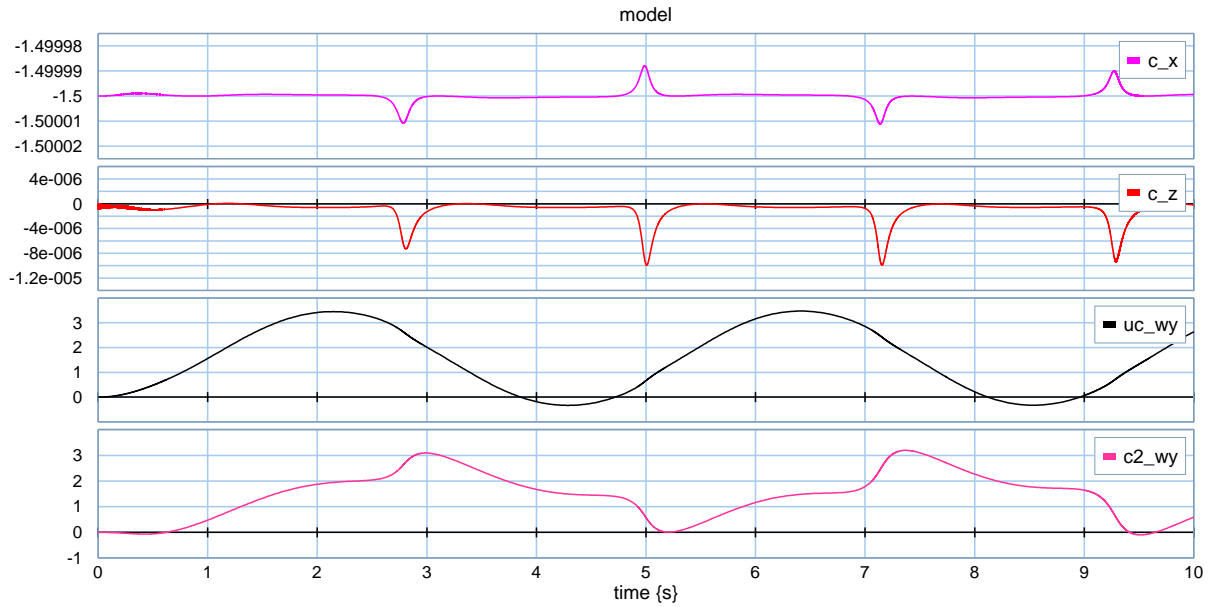
Simulation plot 19: Two link planar arm and spring constant 10^5 and damping



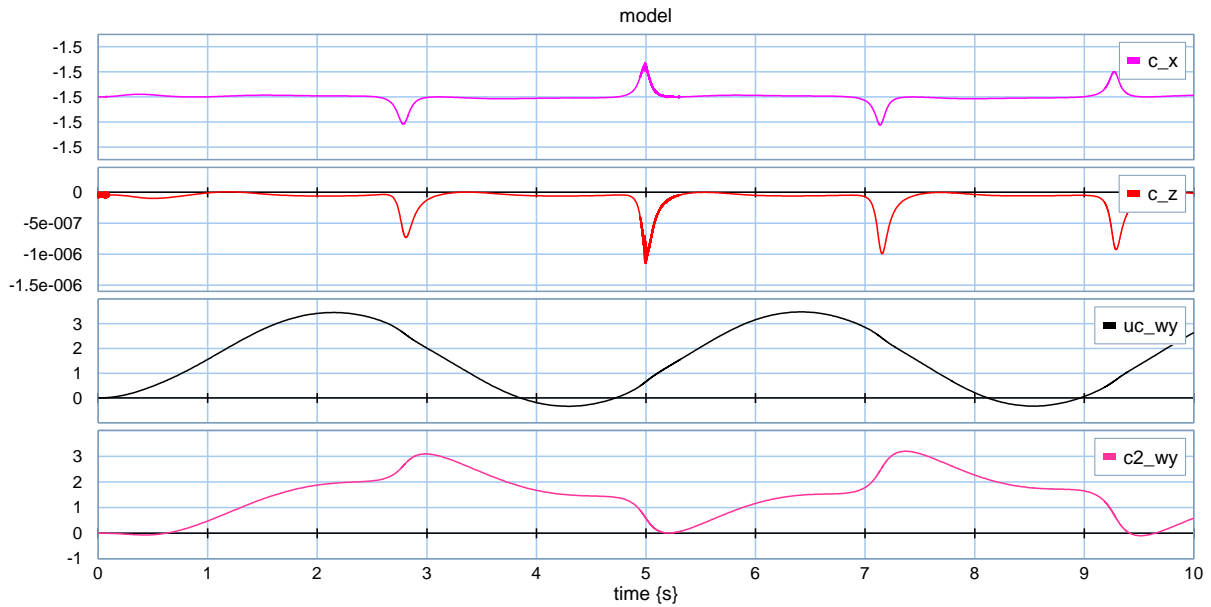
Simulation plot 20: Two link planar arm and spring constant 10^6 and damping



Simulation plot 21: Two link planar arm and spring constant 10^7 and damping



Simulation plot 22: Two link planar arm and spring constant 10^8 and damping



Simulation plot 23: Two link planar arm and spring constant 10^9 and damping

Spring konstant	Simulation time	Model calculations	Output points	Avarage step per second
10^4	1,374	9009	1386	6556
10^5	1,616	18083	3242	11189
10^6	10,722	79212	9064	7387
10^7	21,879	172949	17732	7904
10^8	13,472	169166	17490	12556
10^9	20,728	154792	21066	7467

Table 3: Simulation data with damping in joint

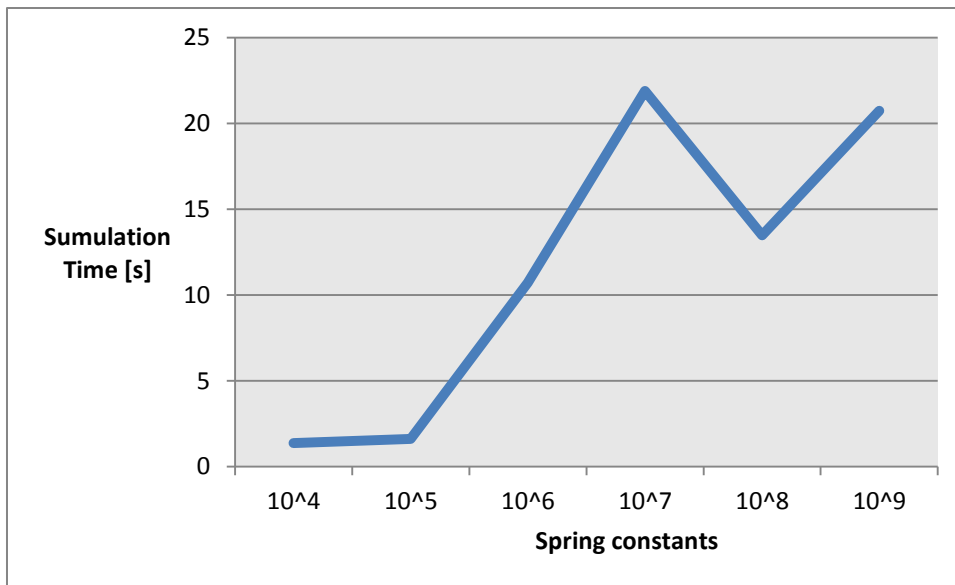


Figure 41: Simulation time vs. spring constant (damping in joint)

It is clear that damping greatly reduces simulation time. Also the models experiences steady results already at $k = 10^4$. Studying the graphs and the animation on the CD we see that acceptable results are achieved somewhere between $k = 10^5$ and $k = 10^6$.

The results above shows a general trend, however there can be many error sources to the data presented; such as available data power at time of simulation and the numerical integration procedure used. Still it is clear that simulation time can be an issue when connecting several rigid body models. Introducing a damping element in the joints will help reduce the simulation time. However there will always be a need for tuning of both k and c for each individual case and for each individual joint in the particular case to achieve acceptable results in a shortest amount of time.

5 Vessel model

The following chapter is written on the basis of material presented in (Fossen, 1994) and (Pedersen, Bond Graph Modelling of Marine Vehicle Dynamics).

5.1 Motion equation

A general rigid body bond graph model has already been developed in this paper. This chapter will focus on extending that model to include the marine vehicle- or vessel- specific characteristics of such a bond graph model. Such specific characteristic may include radiation-induced forces (added mass, hydrodynamic damping and restoring forces), environmental forces (ocean currents, wind and waves) and propulsion forces (propeller/thruster forces and control surface/rudder forces). The general motion equation can be extended to include all of the characteristics above.

$$[\mathbf{M}_{RB} + \mathbf{M}_A]\dot{\mathbf{v}} + [\mathbf{C}_{RB}(\mathbf{v}) + \mathbf{C}_A(\mathbf{v})]\mathbf{v} + \mathbf{D}(\mathbf{v})\mathbf{v} + \mathbf{G}(\boldsymbol{\eta}) = \boldsymbol{\tau} + \boldsymbol{\tau}_H.$$

Where

- $\mathbf{M}_{RB}\dot{\mathbf{v}}$ is the rigid body forces and moments
- $\mathbf{M}_A\dot{\mathbf{v}}$ is the hydrodynamic added mass forces and moments.
- $\mathbf{C}_{RB}(\mathbf{v})\mathbf{v}$ is the rigid body coriolis and centripetal forces and moments
- $\mathbf{C}_A(\mathbf{v})\mathbf{v}$ is the hydrodynamic coriolis and centripetal forces and moments
- $\mathbf{D}(\mathbf{v})\mathbf{v}$ is the combined expression for the hydrodynamic forces and moments which can be denoted further to include radiation-induced potential damping, linear skin friction damping, wave drift damping and vortex shedding damping. $\mathbf{D}(\mathbf{v}) = \mathbf{D}_P(\mathbf{v}) + \mathbf{D}_S(\mathbf{v}) + \mathbf{D}_W(\mathbf{v}) + \mathbf{D}_M(\mathbf{v})$ respective
- $\mathbf{G}(\boldsymbol{\eta})$ is the restoring forces and moments
- $\boldsymbol{\tau}$ is the propulsion forces and moments
- $\boldsymbol{\tau}_H$ is the environmental forces and moments

However in this chapter the goal is to develop a simplified model, i.e. a model which will only give an idea of the possibilities of such a model. Therefore the main focus will be the extension of the 6DOF rigid body bond graph to include simplified radiation- induced forces. Environmental- and propulsion forces will in short be discussed, but merely on a superficial level.

Note that the hydrodynamic coefficients in this chapter use the SNAME notation. Also the general notation for marine vehicle motion is worth listing.

DOF		Forces and moments	Linear and angular vel.	Euler angles
1	motion i x direction (surge)	X	u	x
2	motion i y direction (sway)	Y	v	y
3	motion i z direction (heave)	Z	w	z
4	rotation about x-axis (roll)	K	p	φ
5	rotation about y-axis (pitch)	M	q	ϑ
6	rotation about x-axis (yaw)	N	r	ψ

Table 4: Vessel notation

5.2 Added mass and inertia

The added mass phenomena should according to (Fossen, 1994) be interpreted as *pressure-induced forces and moments due to a forced harmonic motion of the body which are proportional to the acceleration of the body*. The result is that the body feels “heavier” than it really is when trying to move it while it is partly or fully submerged in water, thus the name added- or virtual- mass.

The expression for the added mass can be derived using the expression for fluid kinetic energy

$$T_A = \frac{1}{2} \mathbf{v}^T \mathbf{M}_A \mathbf{v},$$

where $\mathbf{v} = [u, v, w, \omega_x, \omega_y, \omega_z]^T$, i.e the linear and angular velocities of the body. \mathbf{M}_A is the added mass matrix and is defined as

$$\mathbf{M}_A = \begin{bmatrix} A_{11} & A_{12} \\ A_{21} & A_{22} \end{bmatrix} = - \begin{bmatrix} X_{\dot{u}} & X_{\dot{v}} & X_{\dot{w}} & X_{\dot{p}} & X_{\dot{q}} & X_{\dot{r}} \\ Y_{\dot{u}} & Y_{\dot{v}} & Y_{\dot{w}} & Y_{\dot{p}} & Y_{\dot{q}} & Y_{\dot{r}} \\ Z_{\dot{u}} & Z_{\dot{v}} & Z_{\dot{w}} & Z_{\dot{p}} & Z_{\dot{q}} & Z_{\dot{r}} \\ K_{\dot{u}} & K_{\dot{v}} & K_{\dot{w}} & K_{\dot{p}} & K_{\dot{q}} & K_{\dot{r}} \\ M_{\dot{u}} & M_{\dot{v}} & M_{\dot{w}} & M_{\dot{p}} & M_{\dot{q}} & M_{\dot{r}} \\ N_{\dot{u}} & N_{\dot{v}} & N_{\dot{w}} & N_{\dot{p}} & N_{\dot{q}} & N_{\dot{r}} \end{bmatrix}.$$

The hydrodynamic coriolis and centripetal term can be written as

$$\mathbf{C}_A(\mathbf{v}) = \begin{bmatrix} \mathbf{0}_{3 \times 3} & -\mathbf{S}(A_{11}\mathbf{v} + A_{12}\boldsymbol{\omega}) \\ -\mathbf{S}(A_{21}\mathbf{v} + A_{22}\boldsymbol{\omega}) & \mathbf{S}(A_{21}\mathbf{v} + A_{22}\boldsymbol{\omega}) \end{bmatrix}$$

where \mathbf{S} means that the matrix is skew-symmetrical, $\mathbf{v} = [u, v, w]^T$ and $\boldsymbol{\omega} = [\omega_x, \omega_y, \omega_z]^T$.

Implementing this into the rigid body IC-model is done by super positioning the added mass and inertia terms with the rigid body terms.

$$\mathbf{M}_{tot} = \mathbf{M}_{RB} + \mathbf{M}_A$$

$$\mathbf{C}_{tot} = \mathbf{C}_{RB} + \mathbf{C}_A$$

Giving the constitutive relation in the IC-field

$$f = \mathbf{M}_{tot}^{-1} \mathbf{p},$$

$$e = \mathbf{C}_{tot}(\mathbf{v}) \mathbf{v}.$$

5.3 Hydrodynamic damping

As mentioned the hydrodynamic damping forces consist of a number of different physical phenomena and it is logical to assume that the damping matrix would be a 6×6 matrix like the other terms in the motion equation. However giving expressions for most of the terms is difficult. Thus for most applications only values for the diagonal are used. Hens the damping coefficients can be denoted

$$\mathbf{D}(\mathbf{v}) = -diag\{X_u, Y_v, Z_w, K_p, M_q, N_r\}.$$

The damping matrix is understood as power dissipation, hens in bond graph terms it should be implemented in a classic R-element with the constitutive relation

$$\mathbf{e} = \mathbf{D}(\mathbf{v}) \mathbf{f}.$$

The flow input in this element is the angular- and rotational- velocities of the rigid body or vessel meaning it is to be connected to the 1-junction representing the body fixed coordinate system.

5.4 Restoring forces

The restoring forces and momentum for a surface vessel is related to the metacentric stability and buoyancy and can be interpreted as spring forces in a classic mass-damper-spring-system, i.e. forces acting on the body which resist deviation from static equilibrium. There are off course restoring forces associated with directional stability and maneuvering and so on, but here we will only consider the stability forces in heave, pitch and yaw keeping the vessel floating and in an upright position.

The restoring force coefficient matrix in heave, pitch and yaw can be given as

$$\mathbf{G}(\boldsymbol{\eta}) = \begin{bmatrix} 0 & 0 & 0 & 0 & 0 & 0 \\ 0 & 0 & 0 & 0 & 0 & 0 \\ 0 & 0 & Z_z & 0 & Z_\theta & 0 \\ 0 & 0 & 0 & K_\phi & 0 & 0 \\ 0 & 0 & M_z & 0 & M_\theta & 0 \\ 0 & 0 & 0 & 0 & 0 & 0 \end{bmatrix},$$

where

$$Z_z = \rho g A_{wp}$$

$$Z_\theta = M_z = -\rho g \iint_{A_{wp}} x \, dA$$

$$K_{\phi} = \rho g \nabla (z_B - z_G) + \rho g \iint_{A_{wp}} y^2 dA = \rho g \nabla \overline{GM}_T$$

$$M_{\theta} = \rho g \nabla (z_B - z_G) + \rho g \iint_{A_{wp}} x^2 dA = \rho g \nabla \overline{GM}_L$$

ρ = water density [kg/m^3]

z_G = z-coordinate center of gravity [m]

z_B = z-coordinate center of buoyancy [m]

∇ = displaced volume of water [m^3]

A_{wp} = water plane area [m^2]

\overline{GM}_T = transverse metacentric height [m]

\overline{GM}_L = longitudinal metacentric height [m]

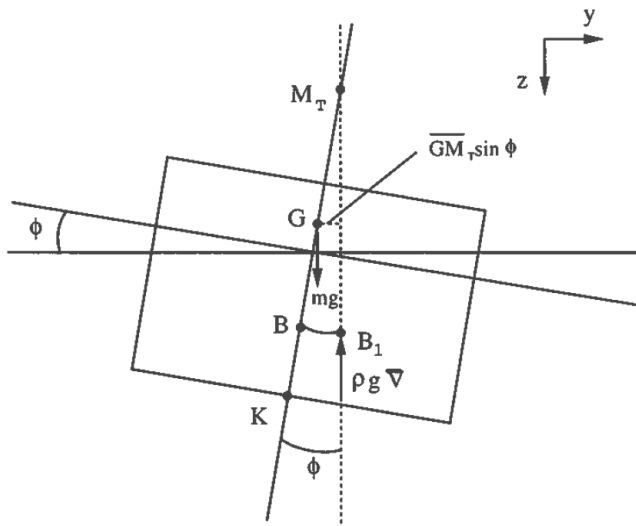


Figure 42: Vessel stability (Fossen, 1994)

The K and M restoring forces are actually a function of the sine function to the respective angle but this can be neglected due to the normal assumption of small angles in conventional initial stability theory.

The restoring forces are implemented in to bond graphs as a C-element following the constitutive relation

$$e = G(\eta) q$$

5.5 Implementation in general rigid body bond graph model

In the actual modeling for this thesis I have chosen to simplify the hydrodynamic added mass matrix and the coriolis and centripetal matrix. This because in practice deriving the values of added mass and inertia coefficients can be an extensive process. The terms are vehicle specific, i.e. they are a function of the vessels characteristics where hull form may be one of the most important parameters. The most accurate results are derived using model test and scaling. But even here some non-linear coupling terms may be ignored because they are difficult to measure. Theoretically determined coefficients are also possible, and can produce sufficient accurate results. Simple static results for the diagonal non-coupled terms can be derived from added mass tables modeling the vehicle as simple geometric shape.

For this reason the vessel model developed I have chosen a simplification where the added mass matrix only has diagonal terms and the terms in the coriolis matrix are simplified to only one parameter for each slot in the matrix. This can be justified by the fact that the off diagonal terms in the added mass matrix tend to be much smaller than the diagonal, thus less impact on the model behavior. The simplifications are actually valid assuming small velocities and that the vehicle has tree planes of symmetry and is according to (Fossen, 1994) a good approximation for many applications.

$$\mathbf{M}_A = -diag\{X_{\dot{u}}, Y_{\dot{v}}, Z_{\dot{w}}, K_{\dot{p}}, M_{\dot{q}}, N_{\dot{r}}\},$$

$$\mathbf{C}_A(\mathbf{v}) = \begin{bmatrix} 0 & 0 & 0 & 0 & -Z_{\dot{w}}w & Y_{\dot{v}}v \\ 0 & 0 & 0 & Z_{\dot{w}}w & 0 & -X_{\dot{u}}u \\ 0 & 0 & 0 & -Y_{\dot{v}}v & X_{\dot{u}}u & 0 \\ 0 & -Z_{\dot{w}}w & Y_{\dot{v}}v & 0 & -N_{\dot{r}}r & M_{\dot{q}}q \\ Z_{\dot{w}}w & 0 & -X_{\dot{u}}u & N_{\dot{r}}r & 0 & -K_{\dot{p}}p \\ -Y_{\dot{v}}v & X_{\dot{u}}u & 0 & -M_{\dot{q}}q & K_{\dot{p}}p & 0 \end{bmatrix}.$$

Connecting the hydrodynamic extensions to the 1-junction representing the body fixed coordinate system in the general rigid body bond graph system gives the almost finished vessel model. To fully complete the model an effort source or Se-element is connected to the 1-junction for the earth fixed coordinate system representing gravity. Also there is an effort source connected to the local 1-junction, this can be used to simulate local forces on the vessel, however only for test purposes. There is also added a port for attaching equipment. This is for attaching the crane at a later stage.

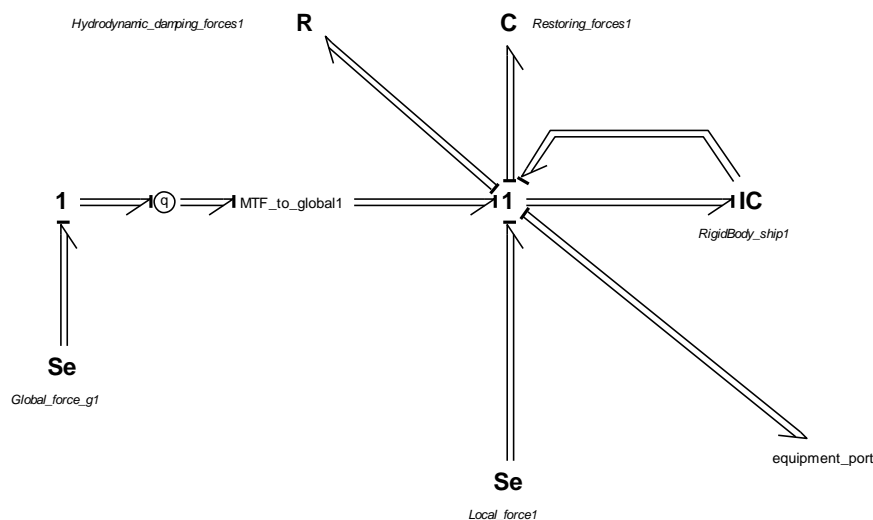


Figure 43: Vessel bond graph

5.6 Simulation demonstration with rigid body vessel model

As with the crane model the center of origin for the local frame is defined in the local mass center, thus the rigid body mass and coriolis centrifugal matrix simplifies to

$$M = \begin{bmatrix} m & 0 & 0 & 0 & 0 & 0 \\ 0 & m & 0 & 0 & 0 & 0 \\ 0 & 0 & m & 0 & 0 & 0 \\ 0 & 0 & 0 & I_x & 0 & 0 \\ 0 & 0 & 0 & 0 & I_y & 0 \\ 0 & 0 & 0 & 0 & 0 & I_z \end{bmatrix},$$

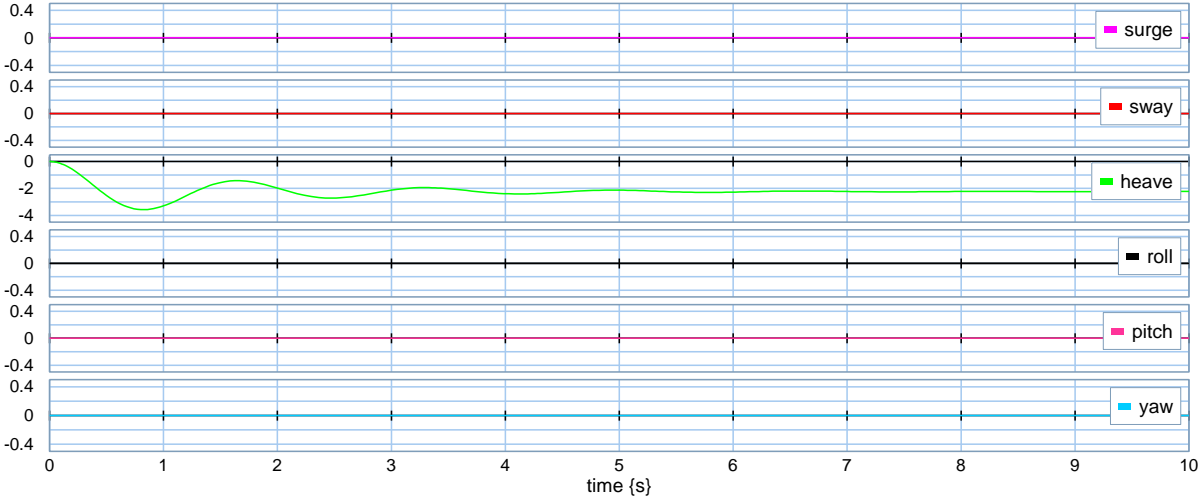
$$C(v) = \begin{bmatrix} 0 & 0 & 0 & 0 & m w & m v \\ 0 & 0 & 0 & -m w & 0 & m u \\ 0 & 0 & 0 & m v & -m u & 0 \\ 0 & -m w & m v & 0 & -I_z \omega_z & -I_z \omega_y \\ m w & 0 & -m u & -I_z \omega_z & 0 & I_x \omega_x \\ m v & m u & 0 & I_z \omega_y & -I_x \omega_x & 0 \end{bmatrix}.$$

For simplification we want to avoid as many off diagonal terms as possible and use the approximation that the vessel has three planes of symmetry and is moving at low speed. This can be justified by the vessel modeled as a square barge and operating as a crane vessel, thus moving with low speed. The hydrodynamic equations will then be as presented earlier. The following barge data is derived from decisions on main dimensions and calculation of simplified parameters for these. The data is only for demonstration and may not be realistic for any barge in existence, but all parameters are tuned in relation to each other.

Barge data		
L	7	[m]
B	5	[m]
H	3	[m]
T	2,2	[m]
Δ	80000	[kg]
Vd	78	[m ³]
Awd	35	[m ²]
GMt	0,55	[m]
GMI	1,45	[m]
Ixx	226667	[kg*m ²]
Iyy	386667	[kg*m ²]
Izz	493333	[kg*m ²]
Xud	30390	[kg]
Yvd	27371	[kg]
Zwd	56409	[kg]
Kpd	29434	[kg*m ²]
Mqd	96644	[kg*m ²]
Nrd	18868	[kg*m ²]

Table 5: Vessel data

The barge data is programmed into the vessel parameters and a simulation is run. Note that the damping parameters are unknown and thus chosen arbitrary.



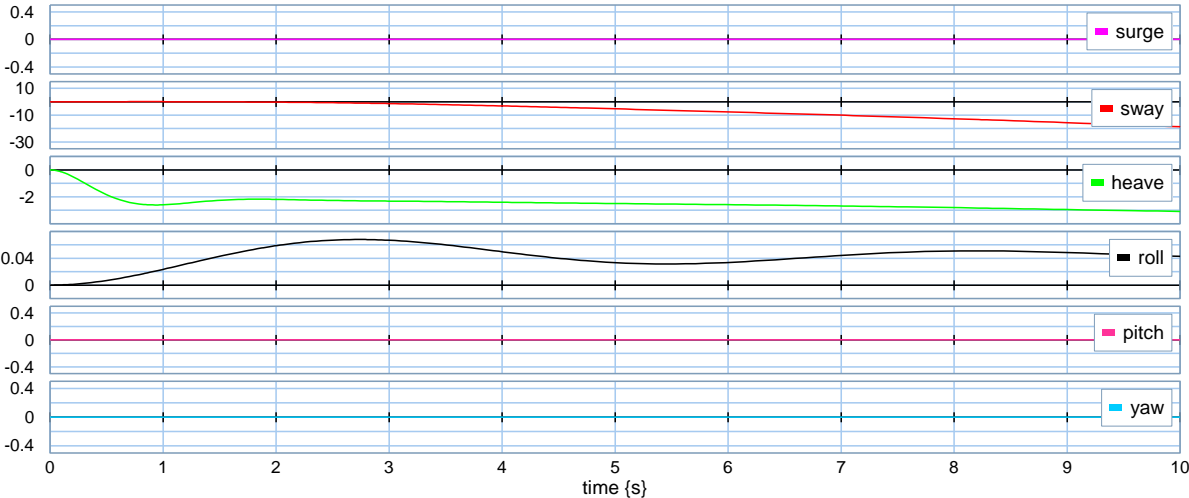
Simulation plot 24: Barge motion

The plot shows the simulation with the initial heave value equal to zero and the barge eventually coming to rest at equilibrium state between gravity- and restoring- force.

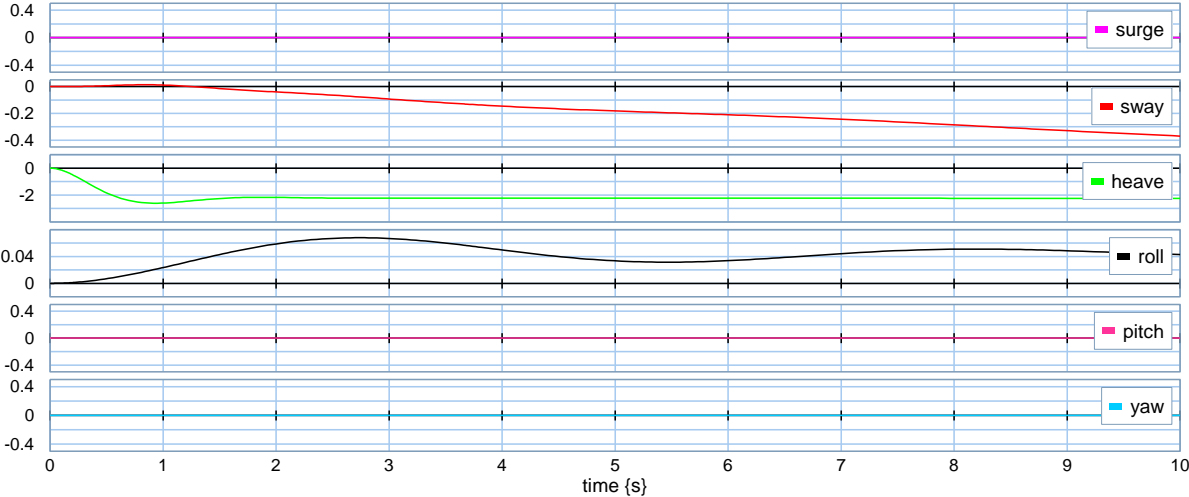
Comment on vessel model

The implementation of vessel characteristics into rigid body bond graph models has proven to be a continuous challenge throughout the work in this thesis. Though the simplified motion equation is relatively straight forward some unexpected result may appear. This is mostly to do with the off diagonal coupled forces in the coriolis centrifugal matrix in relation to the restoring forces. Restoring forces are in the real world the forces which keep a vessel floating with the right side up, but in the modeling world they are in fact spring forces. They are the forces constraining the model in a specific place under the influence of external forces. Inspecting the restoring force matrix note that there are no coefficients in surge, sway and yaw, consistent with the matrix proposed by (Fossen, 1994). This is logical since a vessel should be free to float around at the surface, thus should not be constrained in any other way than the resistance created by water. However in the simplified equations there are off diagonal coupled terms in the coriolis centrifugal matrix which will cause forces in surge, sway and yaw if the model experiences angular forces. For example a bending moment around local x-axis will induce a translational force in sway. The physical interpretation of this is difficult to explain, most people would agree that torque induced on a vessel for example a heavy deck load on the port side would not produce energy and cause the vessel to sway to port. Some of the phenomena may be corrected by not assuming a diagonal inertia tensor, however I find it most convenient to increase the hydrodynamic damping value for the degrees of freedom it concerns. Since the damping value is unknown but probably large, this seems as a ok solution. It is clear that in mathematical modeling of physical phenomena some modifications outside the derived equations may be needed to produce real results.

The next two plots shows the model behavior with an $12 \cdot 10^3$ Nm torque around local x- axis for two cases, one with high damping values and one with excessive low damping values. Example movies can be viewed on CD (“Barge high damping” and “Barge low damping”).



Simulation plot 25: Barge motion with torque and low hydrodynamic damping



Simulation plot 26: Barge motion with torque and high hydrodynamic damping

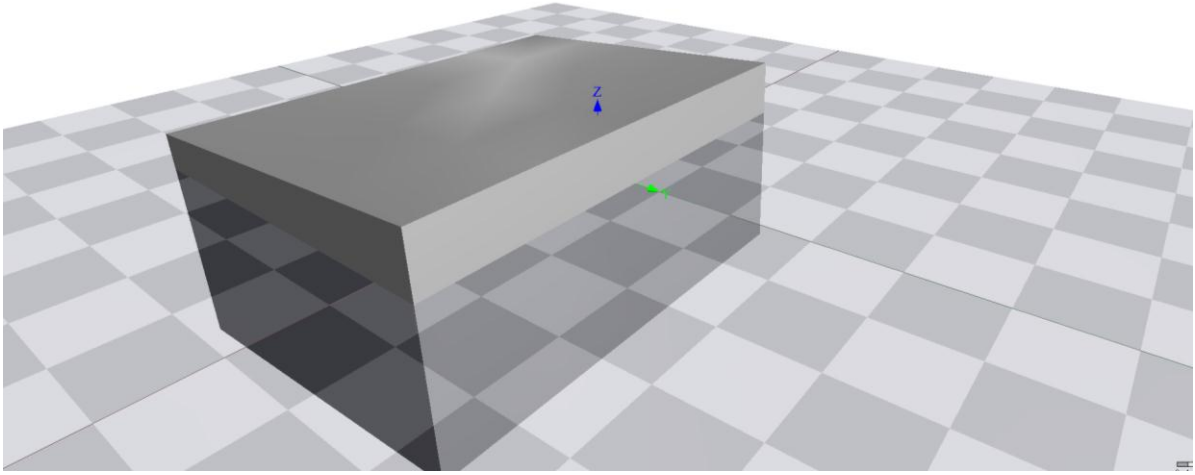


Figure 44: Barge animation

6 Barge with two link planar arm, a complete model

We have developed a vessel model and a two link planar arm with passive control. Now the two models are to be connected to get a complete model of a barge with a crane. The connection is done with relatively ease since the crane model already has a revolute joint in the constrained end. Note the TF- element between the vessel model and the crane sub model. This element denotes the position of the crane on the barge deck, i.e. it transfers the right forces and moments to the barge dependent on the position. The element is similar to the ones used in the crane beam models for transfer of forces and moments from the center of gravity to the arm tip.

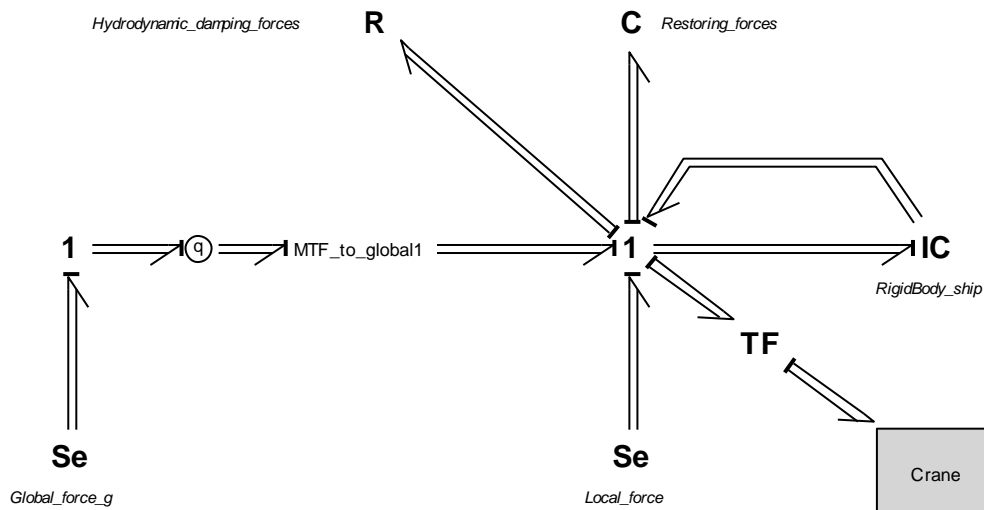


Figure 45: Complete crane barge bond graph

The two link planar arm with passive control is the same one as presented earlier with only one small modification. Since rapid motions of the barge will cause rapid change of position of the two crane arms in the existing model, a global spring and damper has been added to arm one. The goal is to modify the model behavior such that it is possible to get a sense of the crane reaction if it were controlled by hydraulic actuators with internal inertia and resistance of hydraulic fluid. Thus the spring holds the crane arm in place during motions of the barge and the damping element is added to eliminate the oscillating motion created by the spring element.

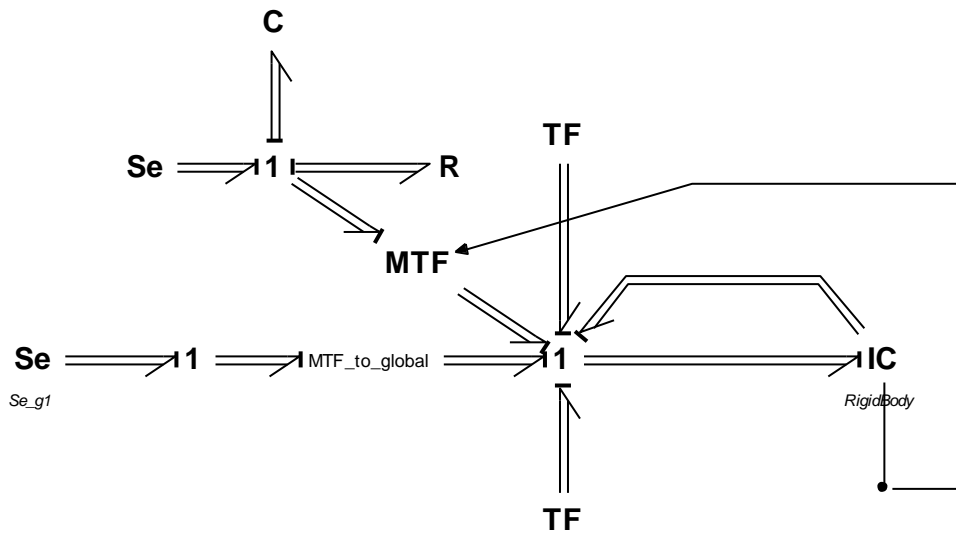
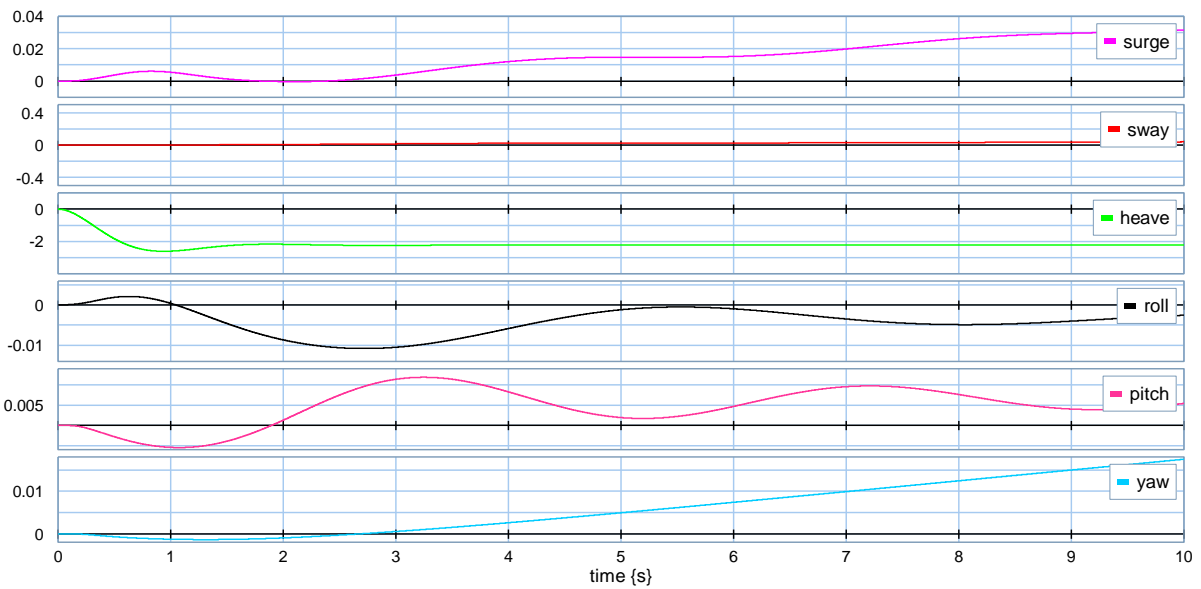


Figure 46: Complete crane bond graph



Simulation plot 27: Barge motion under influence of crane

The plot shows the motion of the barge after being dropped from initial condition to equilibrium condition. The plot shows the crane having an effect on the barge creating a pitching motion which also induces small motion in other direction due to the off diagonal matrix effects discussed earlier. The motion of the crane arm is best demonstrated in the animation “Barge crane demonstration”.

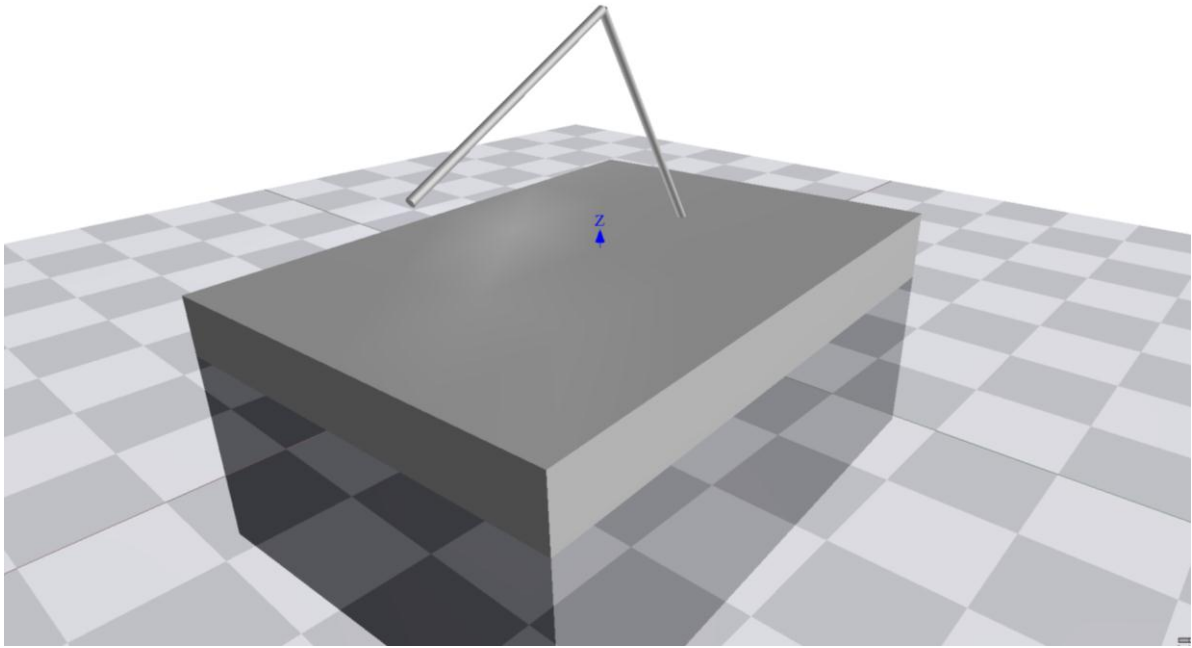
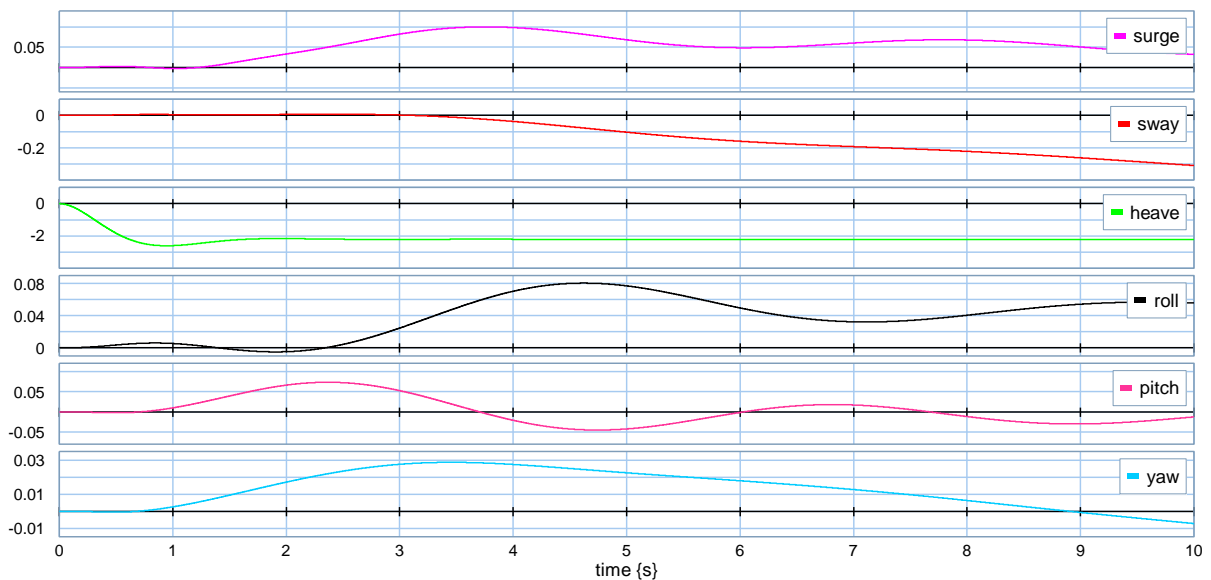


Figure 47: Barge animation under influence of crane

By applying extra force from the global gravity Se-element we can get a sense of the reaction if a heavy load were attached to the crane (see animation “Barge crane with heavy load”). Here the actuators have to be tuned for the extra load. If we however tune the actuator force low, the crane will extend far and the load will create a strong torque and pitching motion (see animation “Barge crane heavy lift heavy pitching”). In this case the animation shows the crane dipping in to the vessel which cannot happen in real life, still it demonstrates the capabilities of the model to simulate load lift and vessel reaction.



Simulation plot 28: Barge motion under influence of crane and load

7 Conclusion and further work

7.1 conclusion

In this report the development of bond graph models for use in larger 6DOF mechanical systems has been research with the aim of utilizing such models for mathematical modeling of vessel dynamics. As often with model development the complexity and ways-of-doing-it for establishing the desired result is diverse. Therefore the focus in this report has been to present tools for the development of highly graphical and easy to understand sub models which can be integrated into larger systems. This has been done with the use of the rigid body bond graph models presented in (Pedersen & Engja, 2008) and with the bond graph joint theory presented in (Filippini, Delarmelina, Pagano, Alianak, Junco, & Nigro, 2007). The rigid body bond graph with the joint bond graph serves as the foundation for larger systems in which the possibilities are large. However the accuracy of the background material and the simplifications made must always be considered when evaluating all types of models. For rigid body bond graph models there are simplifications in the rigid body equations. For example a crane beam may be quite flexible under heavy load, which may cause dynamic behavior far from the one possible to predict with rigid body assumptions.

7.2 Crane model

Perhaps one of the most beneficial uses for a mathematical vessel models is studying ship dynamics under the influence forces caused by “rigidly” connected equipment such as cranes, winches and other. In this thesis it is shown how the rigid body bond graph concept can be used to model a crane beam and be connected to other beams. The functionality of such a crane with two beams has been demonstrated and the control of these discussed. It is clear that such connections of rigid bodies with joints can be done in almost an infinite number of times. However simulation time which is dependent on the computing power and the tuning of the constraining parameters may be a problem, especially if the model is to be used in a simulator controlled live where information needs to be instant.

7.3 Vessel model

It is shown that using the mathematical models presented in (Fossen, 1994) can indeed produce a vessel bond graph using IC-field for rigid body equations, R-elements for hydrodynamic resistance and C-elements for the restoring forces. The model implemented in this thesis was a simplification and the practical use of such a simple model limited. However it is not hard to imagine modifications of such a model to a more realistic level. This may be taking onto account more off diagonal terms in matrixes and adding environmental forces to the model. The 20Sim software actually offers solutions for crating sinusoidal signals, thus it should be possible to model wave force patterns. However the biggest problem for all mathematical vessel models is deriving the hydrodynamic coefficients. In many cases most of them are unknown or approximations which in itself compromises the accuracy of the model.

7.4 The Crane Barge

The model of the crane and barge was fused together to demonstrate the abilities of such models. It was shown that the moment of the crane indeed induced forces and torque on the vessel as in real life. Further extensions as utilizing the prismatic joint on one of the crane beams and a revolute joint to allow the crane to swivel to the side were omitted due to time issues. However both response of the vessel due to the crane and the use of joints were demonstrated, thus these extensions may not have added much value to the findings in this thesis.

7.5 Further work

This thesis has focused on the development of rigid body bond graph models for vessel dynamics and crane operations. The primary building blocks for such models have been developed and the feasibility for modeling larger more accurate real life systems and the integration of other models demonstrated. Such models can be used both for finding dynamic response and force in an operation or maybe be used as a real simulator with live input. However for such applications the level of accuracy in the model has to be raised, models of actuators developed and models of other necessary equipment connected such for example actuators and propulsion. Models of environmental forces may also be desired.

Bibliography

- Berg, T. E. (2007). *Marine Operations: Submarines, AUVs - UUVs and ROVs*. Trondheim, Norway: Department of Marine Technology, Norwegian University of Science and Technology.
- Fagereng, C. (2010). *Project work in marine machinery, Mathematical modeling for marine crane operations*. Trondheim, Norway: Department of Marine Technology, Norwegian University of Science and Technology .
- Filippini, G., Delarmelina, D., Pagano, J., Alianak, J. P., Junco, S., & Nigro, N. (2007). *Dynamics of Multibody Systems with Bond Graphs*. Córdoba, Argentina: Facultad de Ciencias, Ingeniería y Agrimensura, Universidad Nacional de Rosario.
- Fossen, T. I. (1994). *Guidance and Control of Ocean Vehicles* . Chichester West Sussex: John Wiley & Sons Ltd.
- Gilberto, G. A., & Padilla, A. G. (2010). *Steady State of a Planar Robot: A Bond Graph Approach*. SCS.
- Karnopp, D. C., Margolis, D. L., & Rosenberg, R. C. (2006). *System dynamics, Modeling and Simulation of Mechatronic Systems*. John Wiley & Sons, Inc.
- Nielsen, F. G. (2007). *Lecture notes in Marine Operations* . Trondheim, Norway: Department of Marine Hydrodynamics, Faculty of Marine Technology, Norwegian University of Science and Technology.
- Pedersen, E. (2010). ICexampleW3. Trondheim, Norway.
- Pedersen, E. (u.d.). *Bond Graph Modelling of Marine Vehicle Dynamics*. Trondheim, Norway: Department of Marine Technology, Norwegian University of Science and Technology.
- Pedersen, E., & Engja, H. (2008). *Mathematical Modelling and Simulation of Physical Systems*. Trondheim: Department of Marine Technology, Norwegian University of Science and Technology.
- Sciavicco, L., & Siciliano, B. (1999). *Modelling and Control of Robot Manipulators, Second Edition*. Springer.
- Zied, A., & Chung, C.-H. (1992). *Bond Graph Modeling of Multibody Systems: a Library of Three-dimensional Joints*. The Franklin Institute.

Appendix A

Contents of attached CD

- Animations
 - Actuator animations
 - Barge animations
 - Beam animations
 - Spring constant animations

- Demonstration models
 - Actuator demonstrations
 - Barge
 - Barge with two link planar arm
 - One arm revolute y
 - One arm spherical
 - Simulation time models
 - Two link planar arm

- Model component library
 - Example vessel with one crane arm
 - Prismatic joint
 - Revolute joint y
 - Rigid body arm
 - Spherical joint
 - Vessel model

Appendix B

20-sim code

Lagrange/Hamilton IC-field

parameters

real global m, l;

real global c1;

real global c2;

real global c3;

real global c4;

real global J;

variables

real p[2], q[2], f[2], M[2,2];

real p_th1, q_th1, p_th2, q_th2;

real th1, th2, th1d, th2d;

equations

"Relating the angular velocities to the efforts"

p_th1 = int(pl1.e);

q_th1 = int(pC1.f);

p_th2 = int(pl2.e);

q_th2 = int(pC2.f);

p = [p_th1;p_th2];

q = [q_th1;q_th2];

"Flows / Setting upp M matrix"

th1=q_th1;

th2=q_th2;

M=[(0.33)*l^2*(4*m-3*m*(cos(th1))^2+6*(cos(th1))^2), (0.33)*l^2*(-
3*sin(th1)*sin(th2)+3*cos(th1)*cos(th2)); -l^2*sin(th1)*sin(th2)+l^2*cos(th1)*cos(th2), (0.083)*m*l+(0.5)-
(0.5)*(cos(th2))^2+(0.5)*l^2*(cos(th2))^2];

f = inverse(M)*p;

"Programming the efforts"

```

th1d=f[1];

th2d=f[2];

pC1.e=(-0.5*I*(-
2*I*th1d^2*m*sin(th1)*cos(th1)+2*I*th1d*cos(th1)*sin(th2)*th2d+4*I*th1d^2*cos(th1)*sin(th1)+2*I*th1d*si
n(th1)*cos(th2)*th2d+3*m*g_n*cos(th1)));

pC2.e=(-I^2*sin(th1)*cos(th2)*th1d*th2d+0.5*sin(th2)*th2d^2*cos(th2)-I^2*cos(th1)*sin(th2)*th1d*th2d-
0.5*I^2*cos(th2)*th2d^2*sin(th2)-0.5*m*g_n*cos(th2));

"Assigning efforts and flows"

p1.f=f[1];

p2.f=f[2];

"signals"

state1=th1;

state2=th2;

```

Vector IC-field

parameters

```
real global m=150;
```

```
real I=120;
```

variables

```
real M[6,6], Minv[6,6], C[6,6];
```

```
real u, v, w, p, q, r;
```

initialequations

"Setting opp the Mrb (Rigit body inertia matrix)"

```
M=[ m, 0, 0, 0, 0, 0;
```

```
0, m, 0, 0, 0, 0;
```

```
0, 0, m, 0, 0, 0;
```

```
0, 0, 0, I, 0, 0;
```

```
0, 0, 0, 0, I, 0;
```

```
0, 0, 0, 0, 0, I];
```

"Inverting"

```
Minv=inverse(M);
```

Equations

```

pl.f = Minv*int(pl.e);

"Setting up the restoring forces "

u=pl.f[1];

v=pl.f[2];

w=pl.f[3];

p=pl.f[4]; //wx

q=pl.f[5]; //wy

r=pl.f[6]; //wz

C=[ 0 , 0 , 0 , 0 , m*w , m*v ;

    0 , 0 , 0 , -m*w , 0 , m*u ;

    0 , 0 , 0 , m*v , -m*u , 0 ;

    0 , -m*w , m*v , 0 , -l*r , -l*q ;

    m*w , 0 , -m*u , -l*r , 0 , l*p ;

    m*v , m*u , 0 , l*q , -l*p , 0 ];

pC.e =C*(pl.f);

```

Transformer element

parameters

```

real m[6,6];

real Zg=-1.5;//Half lenght of arm/beam.

real Xg=0;

real Yg=0;

```

initialequations

```

m = [ 1.0 , 0.0 , 0.0 , 0.0 , Zg , -Yg ;

      0.0 , 1.0 , 0.0 , -Zg , 0.0 , Xg ;

      0.0 , 0.0 , 1.0 , Yg , -Xg , 0.0 ;

      0.0 , 0.0 , 0.0 , 1.0 , 0.0 , 0.0 ;

      0.0 , 0.0 , 0.0 , 0.0 , 1.0 , 0.0 ;

      0.0 , 0.0 , 0.0 , 0.0 , 0.0 , 1.0 ];

```

equations

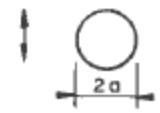
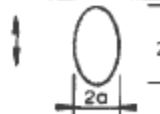
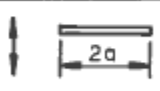
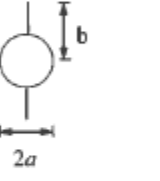
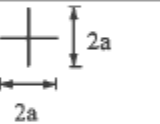
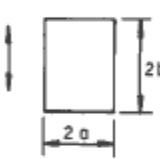
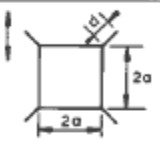
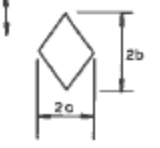
$$p2.e = \text{transpose}(m) * p1.e;$$

$$p1.f = (m) * p2.f;$$

Appendix C

Added mass coefficients, DNV-RP-H103, April 2009

Table A-1 Analytical added mass coefficient for two-dimensional bodies, i.e. long cylinders in infinite fluid (far from boundaries). Added mass (per unit length) is $A_{ij} = \rho C_A A_R$ [kg/m] where A_R [m²] is the reference area

Section through body	Direction of motion	C_A	A_R	Added mass moment of inertia [(kg/m)*m ²]																				
		1.0	πa^2	0																				
	Vertical	1.0	πa^2	$\rho \frac{\pi}{8} (b^2 - a^2)^2$																				
	Horizontal	1.0	πb^2																					
	Vertical	1.0	πa^2	$\rho \frac{\pi}{8} a^4$																				
 Circular cylinder with two fins	Vertical	1.0	πa^2	$\rho a^4 (\csc^4 \alpha f(\alpha) - \pi^2) / 2\pi$ where $f(\alpha) = 2\alpha^2 - \alpha \sin 4\alpha + 0.5 \sin^2 2\alpha$ and $\sin \alpha = 2ab / (a^2 + b^2)$ $\pi/2 < \alpha < \pi$																				
	Horizontal	$1 - \left(\frac{a}{b}\right)^2 + \left(\frac{a}{b}\right)^4$	πb^2																					
	Horizontal or Vertical	1.0	πa^2	$\frac{2}{\pi} \rho a^4$																				
	Vertical	1.0	πa^2	$\beta_1 \rho \pi a^4$ or $\beta_2 \rho \pi b^4$																				
				<table border="1"> <thead> <tr> <th>a/b</th> <th>β_1</th> <th>β_2</th> </tr> </thead> <tbody> <tr><td>0.1</td><td>-</td><td>0.147</td></tr> <tr><td>0.2</td><td>-</td><td>0.15</td></tr> <tr><td>0.5</td><td>-</td><td>0.15</td></tr> <tr><td>1.0</td><td>0.234</td><td>0.234</td></tr> <tr><td>2.0</td><td>0.15</td><td>-</td></tr> <tr><td>5.0</td><td>0.15</td><td>-</td></tr> <tr><td>∞</td><td>0.125</td><td>-</td></tr> </tbody> </table>	a/b	β_1	β_2	0.1	-	0.147	0.2	-	0.15	0.5	-	0.15	1.0	0.234	0.234	2.0	0.15	-	5.0	0.15
a/b	β_1	β_2																						
0.1	-	0.147																						
0.2	-	0.15																						
0.5	-	0.15																						
1.0	0.234	0.234																						
2.0	0.15	-																						
5.0	0.15	-																						
∞	0.125	-																						
	Vertical	1.61 1.72 2.19	πa^2	$\beta \rho \pi a^4$																				
				<table border="1"> <thead> <tr> <th>d/a</th> <th>β</th> </tr> </thead> <tbody> <tr><td>0.05</td><td>0.31</td></tr> <tr><td>0.10</td><td>0.40</td></tr> <tr><td>0.10</td><td>0.69</td></tr> </tbody> </table>	d/a	β	0.05	0.31	0.10	0.40	0.10	0.69												
				d/a	β																			
0.05	0.31																							
0.10	0.40																							
0.10	0.69																							
	Vertical	0.85 0.76 0.67 0.61	πa^2	$0.059 \rho \pi a^4$ for $a = b$ only																				

Appendix D

Project assignment fall 2010

PROJECT WORK IN MARINE MACHINERY
FALL 2010
FOR
STUD. TECHN. CHRISTIAN FAGERENG
MATHEMATICAL MODELLING FOR
MARINE CRANE OPERATIONS

Work description

Mathematical models for marine vessel dynamics including environmental loads is frequently used in many applications. Extending these models to include propulsion machinery, deck machinery, large cranes or other equipment used for marine operations or in operation simulators it is important for efficient model development to have a clear understanding of how the interfaces have to be designed to facilitate connection of models. The bond graph representation or modelling methodology focuses on the model structure and properties required for connecting sub-models into large hybrid model and therefore may serve as a language for analysis of model structure in such a sense.

This representation has been used in the Energy Efficient - All Electric Ship project and in a PhD-thesis where a model library was developed. The work here is a continuation of these attempts and the objective is to increase the number and further develop the models in this library.

Scope of work:

4. Review the modelling and models of Marine Vessel Dynamics. Implement a simplified bond graph template model for a surface vessel for crane operations.
5. Review the modelling and models of large marine cranes for marine operations including typical heave compensation systems, the hydraulic winches and the control of this equipment. Discuss the structure or modular design of these hybrid models and suggest a method or implementation of these model into a modular component model library.
6. Combine the crane model developed and the vessel dynamic model into a complete model of a barge with a large crane for marine operations. Suggest a specific operation and demonstrate the capabilities of the developed model as a software simulator. For demonstration purposes include a Joy-stick for manned operation and develop a simplified animation displaying the motions of the barge and crane.

The report shall be written in English and edited as a research report including literature survey, description of mathematical models, description of control algorithms, simulations results, discussion and conclusion including a proposal for further work. Source code in Matlab/Simulink or equivalent shall be provided on a CD with code listing enclosed in appendix.

It is supposed that Department of Marine Technology, NTNU, can use the results freely in its research work by referring to the students work.

The thesis should be submitted in three copies within _____

Trondheim September 21, 2010

Eilif Pedersen

Associate Professor
